TRANSLATIONAL REPRESSION OF G3BP IN CANCER AND GERM CELLS SUPPRESSES STRESS GRANULES AND ENHANCES STRESS TOLERANCE

APPROVED BY SUPERVISORY COMMITTEE

P. Ryan Potts, Ph.D. (Mentor)

Yuh Min Chook, Ph.D. (Chair)

Nicholas Conrad, Ph.D.

Luke Rice, Ph.D.

Philip Thomas, Ph.D.

DEDICATION

This dissertation is dedicated to my wildly imaginative and amazingly meticulous grandmother. She has all the qualities of an excellent scientist, lacking only in opportunity.

I also dedicate this thesis to my loving parents. Through them, I learned not only the values of diligence and determination, but also the joys of creativity and curiosity. My graduate work is truly a marriage of my parents' passions—medicine and academic research. Without them, I would not have had the courage to pursue and see through this challenging endeavor. For all these things and so much more, I am forever grateful.

I would also like to acknowledge several others to whom I feel a deep sense of gratitude:

Keunwoo Ryu, for his unwavering support over the past seven years, whether that meant being a sounding board for new ideas or a wellspring of encouragement. I am incredibly grateful for his love and to have him by my side.

Joseph Lee, for cheering me on in his signature best-big-brother way, i.e. sending me boxes of hot Cheetos and taking me to Lakers games.

My advisor Ryan Potts, for gambling on me and training me to have not only a wider array of experimental techniques, but also a broader perspective and approach to science.

My thesis committee members Luke Rice, Nick Conrad, Phil Thomas, and Yuh Min Chook for overseeing my progress, sharing scientific insights, and providing encouragement.

Piotr Sliz, for giving me the chance to fall in love with science and pushing me to apply for graduate school.

Members of the Potts Lab, for providing scientific input and creating a fun environment during my graduate training.

And last but not least, my friends. I feel blessed to have people who are always rooting for me and are willing to listen to my nerdy science ramblings (even if they have no idea what I'm talking about).

Thank you all for your support through this long journey. I could not have done it alone.

TRANSLATIONAL REPRESSION OF G3BP IN CANCER AND GERM CELLS SUPPRESSES STRESS GRANULES AND ENHANCES STRESS TOLERANCE

by

ANNA KUNYOUNG LEE

DISSERTATION

Presented to the Faculty of the Graduate School of Biomedical Sciences

The University of Texas Southwestern Medical Center at Dallas

In Partial Fulfillment of the Requirements

For the Degree of

DOCTOR OF PHILOSOPHY

The University of Texas Southwestern Medical Center at Dallas

Dallas, Texas

August, 2020

TRANSLATIONAL REPRESSION OF G3BP IN CANCER AND GERM CELLS SUPPRESSES STRESS GRANULES AND ENHANCES STRESS TOLERANCE

Publication No._____

Anna Kunyoung Lee, Ph.D.

The University of Texas Southwestern Medical Center at Dallas, 2020

Supervising Professor: P. Ryan Potts, Ph.D.

Melanoma antigen (MAGE) genes are conserved in all eukaryotes and encode for proteins sharing a common MAGE homology domain. Although only a single MAGE gene exists in lower eukaryotes, the MAGE family rapidly expanded in eutherians and consists of more than 50 highly conserved genes in humans. A subset of MAGEs initially garnered interest as cancer biomarkers and immunotherapeutic targets due to their antigenic properties and unique expression pattern that is primary restricted to germ cells and aberrantly re-activated in various cancers. However, further investigation revealed that MAGEs not only drive tumorigenesis, but also regulate pathways essential for diverse cellular and developmental processes. Therefore, MAGEs are implicated in a

broad range of diseases including neurodevelopmental, renal, and lung disorders, as well as cancer. Recent biochemical and biophysical studies indicate that MAGEs assemble with E3 RING ubiquitin ligases to form MAGE-RING ligases (MRLs) and act as regulators of ubiquitination by modulating ligase activity, substrate specification, and subcellular localization. Here, we present a comprehensive guide to MAGEs highlighting the molecular mechanisms of MRLs, their physiological roles in germ cell and neural development, oncogenic functions in cancer, and potential as therapeutic targets in disease.

Stress granules (SG) are membrane-less ribonucleoprotein condensates that form in response to various stress stimuli via phase separation. SG act as a protective mechanism to cope with acute stress, but persistent SG have cytotoxic effects that are associated with several age-related diseases. Here, we demonstrate that the testis-specific protein, MAGE-B2, increases cellular stress tolerance by suppressing SG formation through translational inhibition of the key SG nucleator G3BP. MAGE-B2 reduces G3BP protein levels below the critical concentration for phase separation and suppresses SG initiation. Importantly, knockout of the MAGE-B2 mouse ortholog or overexpression of G3BP1 confers hypersensitivity of the male germline to heat stress *in vivo*. Thus, MAGE-B2 provides cytoprotection to maintain mammalian spermatogenesis, a highly thermo-sensitive process that must be preserved throughout reproductive life. These results demonstrate a mechanism that allows for tissue-specific resistance against stress and could aid in the development of male fertility therapies.

TABLE OF CONTENTS

PRIOR PUBLICATIONS

Lee, A.K., Klein, J., Fon Tacer, K., Lord, T., Oatley, M.J., Oatley, J.M., Porter, S.N., Pruett-Miller, S.M., Tikhonova, E.B., Karamyshev, A.L., Wang, Y.-D., Yang, P., Korff, A., Kim, H.J., Taylor, J.P., and Potts, P.R.(2020). Enhanced stress tolerance through reduction of G3BP and suppression of stress granules. bioRxiv 2020.02.03.925677.

Lee, A.K., and Potts, P.R. (2017). A Comprehensive Guide to the MAGE Family of Ubiquitin Ligases. J Mol Biol *429*, 1114-1142.

Wang, L., Nam, Y., Lee, A.K., Yu, C., Roth, K., Chen, C., Ransey, E.M., and Sliz, P. (2017). Lin28 Zinc Knuckle Domain is Required and Sufficient to Induce let-7 Oligouridylation. Cell Reports *18*, 2664-2675.

LIST OF FIGURES

LIST OF TABLES

LIST OF ABBREVIATIONS

AMPK – AMP-activated protein kinase

AR – androgen receptor

ASCI – antigen-specific cancer immunotherapeutic

ASD – autism spectrum disorder

CDS – coding sequence

CLIP-qPCR – cross-linking immunoprecipitation and quantitative polymerase chain reaction

CRL – Cullin-RING ligase

CSC – cancer stem cell

CTA – cancer-testis antigen

CTD – C-terminal domain

CTL – cytotoxic T cell

DNMT – DNA methyltransferase

DUB – deubiquitinating enzyme

F-actin – actin filament

FGFR2 – fibroblast growth factor receptor 2

GTEx – Genome Tissue-Expression

HDAC – histone deacetylase

HLA – human leukocyte antigen

IDR – intrinsically disordered protein

LLPS – liquid-liquid phase separation

MAGE – melanoma antigen

MHD – MAGE homology domain

MRL – MAGE-RING ligase

mTOR – mechanistic target of rapamycin

PGC – primordial germ cell

PWS – Prader-Willi syndrome

Rb – retinoblastoma

RBP – RNA-binding protein

RNP – ribonucleoprotein

SERT – serotonin transporter

SG – stress granule

SHFYNG – Schaaf-Yang syndrome

SMC – structural maintenance of the chromosome

SSC – spermatogonial stem cell

TAP – tandem affinity purification

TCR – T cell receptor

WASH – Wiskott-Aldrich syndrome protein and scar homolog

WH – winged-helix

CHAPTER ONE
INTRODUCTION

OVERVIEW OF THE MAGE FAMILY

Discovery of the MAGEs

During the 1980s, researchers identified a patient, MZ-2, with stage IV amelanotic melanoma of an unknown primary tumor who had strong T cell reactivity against autologous tumor cells in culture (reviewed in (Jager and Knuth, 2012)). Despite surgical intervention and chemotherapy, the patient never achieved a complete remission. However, following multiple vaccinations of patient-derived clones that had been mutagenized *in vitro* and irradiated before being injected intradermally, patient MZ-2 had a remarkable recovery. This dramatic response led researchers to undertake the monumental task of identifying the tumor-associated antigen that allowed for recognition by cytotoxic T cells (CTLs). Through the elegant application of autologous typing and transfection of a cosmid library into the patient-derived MZ2-E cell line, Boon and colleagues discovered and cloned the first human tumor antigen, melanoma antigen-1 (MAGE-1) (van der Bruggen et al., 1991). Subsequent studies and homology searches revealed that MAGE-1, later renamed MAGE-A1, belongs to a larger family of genes that are now known as MAGEs (Chomez et al., 2001).

In humans, the MAGE family consists of about 60 genes (some of which are designated pseudogenes) that are categorized into two classes based on their chromosomal location and expression pattern (Figure 1-1A) (Barker and Salehi, 2002; Chomez et al., 2001). Collectively, the MAGE-A, -B, and -C subfamily members located on the X-chromosome comprise the type I

MAGE cancer testis antigens (CTAs), in that the genes of all three subfamilies are primarily expressed in the testis and are aberrantly expressed in cancers (Chomez et al., 2001). Conversely, the MAGE-D, -E, -F, -G, -H, -L and Necdin genes are classified as type II MAGEs, which are not restricted to the X chromosome and are expressed in a variety of tissues (Chomez et al., 2001).

Chromosome organization

Consistent with their classification as type I MAGEs, the MAGE-A genes are clustered in the q28 region of the X chromosome, the MAGE-B genes at Xp21, and the MAGE-C genes at Xq26-27 (Figure 1-1B) (Dabovic et al., 1995; De Plaen et al., 1994; Lucas et al., 2000; Lucas et al., 1998; Lurquin et al., 1997; Muscatelli et al., 1995; Rogner et al., 1995). This distinct clustering pattern on the X chromosome is not exclusive to the type I MAGE CTAs. In fact, several CTAs, including GAGEs and NY-ESO-1, are also encoded by multi-gene families on the X chromosome (Caballero and Chen, 2009). Interestingly, the X chromosome contains a disproportionately high number of large, highly homologous inverted repeats that predominantly contain genes expressed in the testis (Warburton et al., 2004). It has been estimated that CTA genes constitute approximately 10% of the DNA sequence on the X chromosome, suggesting that these families are the result of gene duplications (Ross et al., 2005).

Aside from the four MAGE-D genes located at Xp11 and the three MAGE-E genes at Xq13, the remaining type II MAGEs are single-copy genes and do not exhibit clustering on the X chromosome (Lucas et al., 1999). Interestingly, MAGE-G1 (15q13.1), MAGE-L2, and Necdin

(15q11.2) cluster together on chromosome 15, while MAGE-F1 is located at 3q13 and MAGE-H1 at Xp11.21.

Evolution of the MAGE genes

The MAGE genes are an ancient protein family that can be evolutionarily traced back to a single gene in protozoa that only recently underwent rapid expansion in placental mammals to create a multi-gene family (Figure 1-2) (Lopez-Sanchez et al., 2007). Katsura and Satta propose that the evolutionary history of the MAGE gene family can be divided into four phases (Katsura and Satta, 2011). In phase I, the ancestral MAGE exists as a single gene, as evidenced by the existence of only a single MAGE homolog in non-mammalian species (Chomez et al., 2001; Katsura and Satta, 2011; Lopez-Sanchez et al., 2007). Phase II is characterized by the emergence of eutherian mammals and LINE elements (Figure 1-2A). It is during this eutherian radiation that the subfamily ancestors were formed via retrotransposition, with the exception of MAGE-C, which was generated by gene duplication of MAGE-A (Chomez et al., 2001; Katsura and Satta, 2011). During phase III, gene duplications occur within the subfamilies and palindromes form in the MAGE-A subfamily (Figure 1-1B) (Chomez et al., 2001; Katsura and Satta, 2011). Finally, in phase IV, the human MAGE-A genes undergo sequence divergence, specifically in epitope-coding regions, to allow for the generation of diverse epitopes that can bind various human leukocyte antigen (HLA) class I molecules (Katsura and Satta, 2011). Intriguingly, this co-evolution of HLA and MAGE epitopes may have promoted functional differentiation whereby MAGEs acquired a novel human-specific role in cancer immunity in addition to their established function in germ cell development.

While the type I MAGEs are composed of three or four exons, with the terminal exon encoding the entire protein, many of the type II MAGEs are characterized by a single exon. The MAGE-D genes, however, have a particularly unique genomic structure. Each MAGE-D gene contains 13 exons with the open reading frame split over 11 exons, thus allowing for alternatively spliced mRNAs. Based on their unique, complex genomic structure, it has been proposed that the MAGE-D genes may be closely related to the ancestral MAGE. In addition, the gene duplication events that generated the MAGE-D genes appear to be much older than the duplication events of other subfamilies. For example, the N- and C-termini of the MAGE-D proteins are highly conserved between human and mouse orthologs, indicating that these genes evolved independently, long before the phylogenic separation of the two species (Chomez et al., 2001). However, it is important to note that the single MAGE genes found in Entamoeba histolytica and Drosophila are encoded by a single exon, and the number of introns in MAGE genes increases in the different animal phyla as they evolve (Lopez-Sanchez et al., 2007). Therefore, the ancestral MAGE gene was likely encoded by a single exon and it acquired introns during the course evolution.

Alternatively, others have suggested that MAGE-G1 is more functionally related to the ancestral MAGE. The yeast MAGE, Nse3, is a component of the SMC5/6 complex, which plays an essential role in homologous recombination (Pebernard et al., 2008; Potts, 2009; Potts et al., 2006). Using proteomics, Taylor et al. identified MAGE-G1 as the human ortholog of yeast Nse3 and determined MAGE-G1 and its cognate RING ligase, NSE1, to be essential components of the human SMC5/6 complex (Taylor et al., 2008). In addition, the Drosophila MAGE protein shows highest sequence identity to MAGE-G1 (Nishimura et al., 2007). Moreover, the chicken MAGE

protein and human MAGE-G1 interact with E2F1 and the p75 neurotrophin receptor (Lopez-Sanchez et al., 2007). Therefore, while genomic architecture points to MAGE-D genes, functional studies suggest that MAGE-G1 may be most related to the ancestral MAGE.

Although it is not entirely clear which specific MAGE is the most evolutionarily ancient, it is clear that type II MAGEs appeared earlier than the type I MAGEs (Figure 1-2B). Overall, type II MAGEs share high homology with their orthologs, with at least 82% nucleotide sequence identity (Zhao et al., 2012). Conversely, the mouse Mage-a and -b genes share much higher sequence conservation within their respective subfamilies than with their human orthologs (Figure 1-2C) (Chomez et al., 2001; De Backer et al., 1995; De Plaen et al., 1994; Osterlund et al., 2000). These discrepancies, in addition to the absence of MAGE-C genes in mice, imply a more recent and rapid evolution of the type I MAGE subfamilies (Chomez et al., 2001).

Zhao et al. attribute the distinct evolution of type I and type II MAGEs to differential selection acting on the two classes of genes (Zhao et al., 2012). Their statistical analyses indicate that type I MAGEs evolved under positive selection while type II MAGEs evolved under purifying or negative selection (Zhao et al., 2012). Where positive selection allows for diversification or the acquisition of additional functions for the redundant type I MAGEs, purifying selection maintains the established essential, non-redundant functions of the type II MAGEs (Zhao et al., 2012).

MAGE homology domain

The MAGE homology domain (MHD) is a feature common to both type I and type II MAGEs (Figure 1-3A). The approximately 170-amino acid domain is highly conserved, such that all human

MHDs share 46% protein sequence identity and most contain a conserved dileucine motif (Figure 1-3B) (Barker and Salehi, 2002; Doyle et al., 2010). The MHDs within specific subfamilies share even higher conservation; for example, the twelve MAGE-A MHDs and the four MAGE-D MHDs are 70% and 75% conserved, respectively (Doyle et al., 2010).

Structural studies have revealed that the MHD consists of two tandem winged-helix (WH) motifs, referred to as WH-A and -B (Figures 1-3C, D) (Doyle et al., 2010; Newman et al., 2016). Each WH features a characteristic helix-turn-helix motif packed against a three-stranded antiparallel β-sheet "wing", however, WH-B also contains additional α-helices (Doyle et al., 2010; Newman et al., 2016). Overall, the MAGE-A3 and -A4 MHD structures share the same relative orientation and both exhibit a peptide extension binding into the conserved cleft between the two WH motifs; however, the C-terminus of MAGE-A4 is more closely associated with the rest of the molecule and forms a longer section of α-helix (Newman et al., 2016).

Despite the sequence and structural similarities shared among MHDs, mounting evidence suggests that MHDs are more versatile and complex than one might expect. Rather than recognizing and binding a common motif, MHDs confer binding specificity to multiple unique interaction motifs (Doyle et al., 2010). In addition, biophysical interrogation of MAGE-A4 by native mass spectrometry revealed a broad charge state distribution, indicating that MAGEs are structurally dynamic proteins (Hagiwara et al., 2016). Therefore, the flexible MHD may undergo conformational changes that allow for interaction with distinct protein domains thereby conferring unique functions to individual MAGEs.

FUNCTION AND MECHANISM OF MAGE-RING LIGASES

Following the initial discovery of MAGEs, the major emphasis, by far, has been on their expression in cancer. While these studies have revealed many valuable aspects regarding the prognostic and therapeutic potential of MAGEs, efforts to characterize their molecular functions in physiology and pathology are limited. However, a growing body of literature has demonstrated that MAGEs assemble with E3 RING ubiquitin ligases to form MAGE-RING ligases (MRLs) that function in a myriad of cellular processes (Figure 1-4A). Interaction studies including targeted and global proteomics have reported more than 50 distinct MRLs, including MAGE-A1-TRIM31, MAGE-A2-TRIM28, MAGE-A3-TRIM28, MAGE-A6-TRIM28, MAGE-B18-LNX1, MAGE-C2-TRIM28, MAGE-D1-PRAJA-1, MAGE-G1-NSE1, and MAGE-L2-TRIM27, that have been studied to various degrees. Within these complexes, MAGEs have been shown to regulate their cognate RING proteins by (1) enhancing ligase activity, (2) specifying novel substrates for ubiquitination, and (3) altering subcellular location. In the sections below, we discuss in detail specific MRL complexes and the mechanisms by which they function.

Ubiquitination and RING ligases

Ubiquitination is the covalent post-translational modification of lysines on substrate proteins with the small 76 amino acid ubiquitin protein and regulates nearly all aspects of cell function. The most well characterized function of ubiquitination is the targeting of proteins for proteasomal degradation; however, ubiquitination also regulates proteasome-independent processes such as endocytosis and lysosomal targeting, nuclear export, DNA repair, and activation of kinases and

transcription factors depending on the specific type of ubiquitin chain linkage (reviewed in (Lorick et al., 1999)). In the ubiquitination cascade, an E1 ubiquitin-activating enzyme activates ubiquitin; this activated ubiquitin is transferred to an E2 ubiquitin-conjugating enzyme, and is subsequently ligated to a substrate via an E3 ubiquitin ligase (Figure 1-4A) (Borden, 2000). Therefore, by providing substrate specificity in the ubiquitin pathway, E3 ligases play a critical regulatory role in various cellular pathways.

The majority of known E3 ubiquitin ligases include the RING domain and RING-like proteins, which mediate substrate recognition and subsequent ubiquitin ligation through activation of the E2 enzyme (Lorick et al., 1999). The RING domain contains a conserved cysteine- and histidine-rich consensus sequence that coordinates two zinc ions via a cross-brace arrangement (Borden, 2000). Interestingly, many RING ligases have been implicated in cancer due to their roles in the maintenance of genomic integrity and cellular homeostasis (reviewed in (Lipkowitz and Weissman, 2011)).

MAGE-RING ligase architecture

Upon determining that MAGE family proteins form complexes with E3 RING ubiquitin ligases, our lab sought to characterize the biochemical and biophysical properties of MRLs. By *in vitro* binding assays, we demonstrated that each MAGE generally binds one specific RING ligase, and highly homologous MAGEs tend to bind the same RING protein (Doyle et al., 2010). Subsequent mapping of the minimal regions required for MRL complex formation revealed that MAGEs bind their cognate RING ligases via the MHD; however, the region on which MAGEs bind RING

ligases varies between different MRLs (Doyle et al., 2010). For example, MAGE-C2 binds the coiled-coil region of TRIM28, MAGE-B18 binds a basic region between the RING and first PDZ domain of LNX1, and MAGE-G1 binds the WH motifs of NSE1 (Doyle et al., 2010). These findings further validate the notion that the MHD is flexible and its conformational plasticity allows for unique and complex interactions with specific RING ligases.

In an effort to gain insights into the structural properties of MRLs, we also determined the crystal structure of MAGE-G1 in complex with its cognate NSE1 RING ligase (Figure 1-4B) (Doyle et al., 2010). Consistent with the *in vitro* domain mapping experiments, MAGE-G1 WH-A interacts with both WH motifs of NSE1 via a series of hydrogen bonds and a large hydrophobic interface that includes the conserved dileucine motif (Doyle et al., 2010). In addition, mutation of the dileucine motif disrupts binding of not only MAGE-G1 and NSE1, but also complex formation of other MRLs, suggesting that these conserved residues play an important role in the binding interface (Doyle et al., 2010).

Intriguingly, while the WH-A and WH-B motifs of NSE1-bound MAGE-G1 and free MAGE-A4 are similar, with rmsd values of 1.05Å and 1.07Å, respectively, their relative orientations are very distinct in the two structures (Figure 1-4C) (Doyle et al., 2010; Newman et al., 2016). The WH motifs in MAGE-G1 are distantly separated, such that WH-B rotates approximately 170° and translates about 30Å relative to WH-A (Doyle et al., 2010; Newman et al., 2016). Moreover, the peptide extension bound between the two WH motifs in the MAGE-A3 and -A4 structures is not present in the MAGE-G1-NSE1 structure (Doyle et al., 2010; Newman et al., 2016). Therefore, the two different conformational states demonstrate that the MHD

undergoes extensive rearrangement for MRL complex formation and the structural changes required to accommodate association with RING ligases may confer binding specificity.

Structurally, MRLs share a number of key features with Cullin-RING ligases (CRLs) (Figure 1-4D). CRLs, the largest family of multi-component E3s, generally consist of four subunits: cullins (CUL1-7), RINGs (Rbx1-2), adaptor proteins, and substrate recognition proteins (reviewed in (Petroski and Deshaies, 2005)). The cullin acts as the core molecular scaffold that binds to an adaptor protein and a substrate receptor protein at the N-terminus and a RING protein at the C-terminus (Zheng et al., 2002). Like MRLs, these modular CRLs can assemble with multiple substrate recognition proteins to recruit various unique substrates (Petroski and Deshaies, 2005). In addition, the cullin C-terminal domain (CTD) shares marked structural similarities to MAGEs, in that two WH motifs contribute to a groove where the RING domain binds (Zheng et al., 2002). Interestingly, this region of the cullin CTD, referred to as the cullin homology region, is conserved in several other proteins including the APC2 subunit of the anaphase-promoting complex/cyclosome (APC/c) E3 ligase, suggesting a conserved function that also extends to MRLs (Grossberger et al., 1999; Yu et al., 1998; Zachariae et al., 1998; Zheng et al., 2002).

MAGEs enhance E3 RING ubiquitin ligase activity

One of the earliest indications that MAGEs form complexes with E3 RING ubiquitin ligases came from the discovery that MAGE-A2, -A3, -A6, and -C2 directly bind and regulate the TRIM28 (also referred to as KAP1) E3 ubiquitin ligase, a multi-functional protein implicated in transcriptional regulation, cellular differentiation, and DNA damage repair (Doyle et al., 2010;

Yang et al., 2007b). Biochemical analysis of TRIM28 ubiquitin ligase activity revealed that these MAGEs stimulate both TRIM28 auto-ubiquitination and ubiquitination of its substrates, the p53 tumor suppressor and ZNF382, *in vitro* and in cells (Doyle et al., 2010; Xiao et al., 2011; Xiao et al., 2014). Moreover, the enhanced ubiquitin ligase activity of MAGE-TRIM28 reduced p53 and ZNF382 protein levels in a proteasome-dependent manner (Doyle et al., 2010; Xiao et al., 2011; Xiao et al., 2014). In addition to MAGEs regulating the TRIM28 ligase, MAGE-A1 has been reported to stimulate the ligase activity of TRIM31 (Kozakova et al., 2015). Furthermore, this ability of MAGEs to enhance E3 ubiquitin ligase activity is not limited to the type I MAGEs. NSE1 normally has weak *in vitro* ubiquitin ligase activity in the presence of the E2 ubiquitin-conjugating enzyme, UbcH13/Mms2; however, upon addition of MAGE-G1, NSE1 activity is significantly enhanced (Doyle et al., 2010; Pebernard et al., 2008). Therefore, the ability to enhance E3 RING ubiquitin ligases is a feature common to both type I and type II MAGEs.

To gain a better understanding of how MAGEs enhance the ligase activity, we tested four possible mechanisms whereby MAGEs (1) induce a conformational change in the E3 RING ligase, thus promoting increased activity, (2) promote substrate binding to the E2-E3 ubiquitin ligase machinery, (3) stimulate charging of the E2 ubiquitin-conjugating enzyme by the ubiquitin E1, or (4) bind and recruit E2 ubiquitin-conjugating enzymes to the E3 substrate complex. However, we found that MAGE-G1 did not alter NSE1 conformation, neither MAGE-A2 nor -C2 enhanced p53 binding to TRIM28, and MAGE-C2 did not affect UbcH2 charging (Doyle et al., 2010). Interestingly, we demonstrated that MAGE-A2/C2 specifically bind the UbcH2 E2 ubiquitin-conjugating enzyme, suggesting that MAGEs may enhance ubiquitin ligase activity by recruiting and/or stabilizing the E2 enzyme at the E3-substrate complex (Doyle et al., 2010).

Depending on whether MAGE-A2/C2 can bind UbcH2 and TRIM28 simultaneously, or if the two binding interactions are mutually exclusive, Feng and colleagues propose two mechanistic models by which these MAGEs facilitate TRIM28 E3 ligase activity (Feng et al., 2011). In the first model, MAGE-A2/C2 binding to TRIM28 and UbcH2 are mutually exclusive. After transferring one ubiquitin to the substrate, UbcH2 is recharged by an E1 ubiquitin-activating enzyme while remaining in close proximity to the TRIM28 machinery via interactions with MAGE-A2/C2. In this way, MAGEs promote the on-site recharging of the E2 enzyme. In the second model, MAGE-A2/C2 binds to TRIM28 and UbcH2 at the same time. Here, two UbcH2 molecules are recruited to the TRIM28 machinery—with one UbcH2 interacting with the TRIM28 RING domain and the other with MAGE-A2/C2—to promote the sequential assembly of a polyubiquitin chain on the substrate (Feng et al., 2011). However, whether MAGE-A2/C2 can bind TRIM28 and UbcH2 simultaneously remains unclear and further work must be done in order to validate these proposed models, as well as determine whether additional MAGEs bind to their cognate E2 enzymes.

Regulation of AMPK by MAGE-A3/6-TRIM28

MAGE-A3 and the highly similar protein MAGE-A6 (referred to as MAGE-A3/6) also bind TRIM28 (Doyle et al., 2010). However, expression of MAGE-A3/6 does not inversely correlate with p53 mutational status, suggesting this MRL may have additional targets relevant to its function in cancer cells (Pineda et al., 2015). In an *in vitro* screen to identify direct substrates of MAGE-A3/6-TRIM28, we found that expression of MAGE-A3/6 enhances ubiquitination of

AMPKα1 (Figure 1-4D) (Pineda et al., 2015). Importantly, MAGE-A3/6 not only promotes ubiquitination and subsequent proteasomal degradation of AMPKα1, but also directly interacts with and specifies AMPKα1 as a substrate for TRIM28 (Pineda et al., 2015). Thus, unlike p53, which can be targeted by TRIM28 in the absence of MAGEs, AMPKα1 is only targeted by TRIM28 in the presence of MAGE-A3/6. Therefore, expression of MAGE-A3/6 in cancer cells reprograms the ubiquitous TRIM28 ubiquitin ligase to degrade a key metabolic regulator and tumor suppressor to enhance tumorigenesis.

AMPKα1 is the catalytic subunit of AMP-activated protein kinase (AMPK) heterotrimer, a crucial energy sensor in cells (Hardie et al., 2012). In response to even modest decreases in ATP production, AMPK is activated and promotes catabolic ATP-generating pathways while also inhibiting anabolic ATP-consuming pathways, such as mTOR signaling to maintain energy homeostasis (Hardie et al., 2012). In this way, AMPK and mTOR signaling play opposing functions in the regulation of autophagy, a degradative process important for balancing energy sources during development and in response to nutrient stress (Hardie et al., 2012). Due to its role as a master regulator of cellular energy, AMPK functions as a critical tumor suppressor to stop cell growth and its activity is often perturbed in various diseases such as cancer.

Further investigation into the functional consequences of AMPK regulation by MAGE-A3/6^{TRIM28} revealed increased glucose consumption and lactate production upon TRIM28 knockdown, suggesting that the inhibition of AMPK by the MRL affects cell metabolism (Pineda et al., 2015). In addition, we found that MAGE-A3/6-TRIM28 is critical for the maintenance of mTOR activity (Pineda et al., 2015). Consistent with the role of MAGE-A3/6 in regulating AMPK

and mTOR signaling, we demonstrated that the MAGE-A3/6-TRIM28 MRL inhibits autophagy (Pineda and Potts, 2015; Pineda et al., 2015).

Taken together, these results suggest that the oncogenic MAGE-A3/6-TRIM28 MRL regulates several cellular metabolic regulatory pathways via ubiquitination and degradation of AMPKα1 (Pineda et al., 2015). Interestingly, breast invasive carcinoma, colon adenocarcinoma, and lung squamous cell carcinoma tumors expressing MAGE-A3/6 have significantly reduced total and active AMPKα protein levels and reduced downstream AMPK signaling, indicating that this regulation of AMPK by MAGE-A3/A6-TRIM28 is relevant in human tumors (Pineda et al., 2015). However, further work will be necessary to examine whether MAGE-A3/6-TRIM28 suppression of autophagy is important for its oncogenic activity and whether MAGE-A3/6-TRIM28 regulates additional AMPK cellular responses. In addition, how this function relates to the physiological role of MAGE-A3/6 in the testis remains unclear. Given that germ cells in the testis change carbon energy sources as they differentiate from spermatogonial stem cells to mature spermatids, it will be intriguing to determine if MAGE-A3/6-mediated AMPK regulation contributes to this metabolic switch during spermatogenesis (Nakamura et al., 1984).

Regulation of WASH-mediated endosomal protein trafficking by MAGE-L2-TRIM27

Endosomal protein trafficking is an essential process that allows for the delivery of membrane components, receptor-associated ligands, and solute molecules to various intracellular destinations such as the lysosome for degradation, the cell surface, or the trans-Golgi network (TGN) (Seaman et al., 2013). The primary function of the retromer complex is to select cargo proteins for

endosome-to-Golgi transport, or retrograde transport. In addition to cargo recognition, the retromer also recruits the WASH complex, which promotes actin filament (F-actin) nucleation by the Arp2/3 complex (Derivery et al., 2009; Gomez and Billadeau, 2009). The formation of actin patches plays a critical role in endosomal sorting by generating discrete domains into which specific proteins are sorted for transport to their respective destinations (Puthenveedu et al., 2010; Seaman et al., 2013).

Our lab found that MAGE-L2 interacts with the TRIM27 E3 RING ubiquitin ligase and localizes to retromer-positive endosomes through interactions between MAGE-L2 and the VPS35 component of the retromer complex (Figure 1-4E) (Hao et al., 2013). Importantly, the ubiquitin ligase activity of MAGE-L2-TRIM27 is required for proper recycling of endosomal proteins through the retromer pathway to the TGN or plasma membrane (Hao et al., 2013). Detailed analysis of the retromer pathway demonstrated that MAGE-L2-TRIM27 is required for WASH-mediated F-actin assembly on endosomes. Additionally, more in-depth studies revealed that MAGE-L2-TRIM27, in conjunction with the Ube2O E2 ubiquitin-conjugating enzyme, facilitates the non-degradative K63-linked ubiquitination of WASH (Hao et al., 2013). Interestingly, additional mechanistic studies revealed that this ubiquitination of WASH on lysine 220 (K220) by MAGE-L2-TRIM27 destabilizes auto-inhibitory contacts in the WASH complex, thus allowing for its activation and F-actin assembly on endosomes and recycling through the retromer pathway (Hao et al., 2013)

In a subsequent study, we made the surprising discovery that the USP7 deubiquitinating enzyme (DUB) is an integral component of the MAGE-L2-TRIM27 MRL complex (Figure 1-4E) (Hao et al., 2015b). Through *in vitro* binding experiments, we found that USP7 directly binds both

MAGE-L2 and TRIM27 to form an intricate and stable protein complex. In the trimeric complex, MAGE-L2 binds the USP7 N-terminal TRAF domain as well as the C-terminal HUBL1-3 regulatory domains, whereas the C-terminal domains of TRIM27 interact with the catalytic domain of USP7 (Hao et al., 2015b). Although previous examples of DUBs regulating ligases have been described, the intricate and obligate nature of USP7 for stable complex formation of MAGE-L2-TRIM27 suggests an important linkage between conjugating (TRIM27) and deconjugating (USP7) enzymes for proper cellular function.

Functional interrogation of the complex demonstrated that USP7 knockdown or disruption of the MAGE-L2-USP7 interaction impaired endosomal actin accumulation and protein recycling, indicating that USP7 acts in concert with MAGE-L2-TRIM27 and is required for regulation of WASH-mediated protein trafficking (Hao et al., 2015b). Interestingly, USP7 performs dual functions in the endosomal protein-recycling pathway: (1) deubiquitination of TRIM27 to protect TRIM27 from auto-ubiquitination-induced degradation and (2) deubiquitination of WASH to precisely regulate WASH activity (Hao et al., 2015b). Through these seemingly opposing activities, USP7 serves as molecular rheostat to fine tune endosomal F-actin levels (Hao et al., 2015b). This buffering capacity of USP7 is critical given that too little or too much F-actin on endosomes can both be detrimental to retromer-mediated recycling (Hao et al., 2015b). Thus, it is no surprise that nature has elegantly linked the conjugation and deconjugation machinery in a single complex to allow precise control of WASH ubiquitination and activity. Additional studies will be necessary to determine if MAGE-L2 regulates TRIM27 and USP7 enzymatic functions in addition to acting as a molecular scaffold in the complex and mediating localization to endosomes. Importantly, these findings open up the exciting possibility that the functional cooperativity

observed between USP7 and MAGE-L2-TRIM27 may be conserved among other MRLs and DUBs.

Regulation of cyclins by MAGEs and SCF

In contrast to the majority of reports on MRLs, recently two MAGEs have been shown to associate with and regulate CRLs. In the first case, MAGE-C2 was identified as a component of the SCF CRL through interactions with Rbx1 E3 RING ubiquitin ligase (Hao et al., 2015a). Interestingly, unlike many of the MRL examples described previously, MAGE-C2 stabilized cyclin E by inhibiting SCF-dependent ubiquitination and subsequent proteasomal degradation (Hao et al., 2015a). This MAGE-C2-mediated stabilization of cyclin E, an essential regulator of cell cycle transition from G1 to S phase, promotes cell cycle progression and cell proliferation (Hao et al., 2015a). Importantly, cyclin E expression positively correlates with MAGE-C2 expression in melanoma tumor samples, suggesting that this newly identified function of MAGE-C2 may be relevant in tumorigenesis (Hao et al., 2015a).

A subsequent study found that MAGE-A11 interacts with Skp2, an F-box domain substrate recognition protein of the SCF CRL (Su et al., 2017). In this case, MAGE-A11 regulates substrate specificity of Skp2, such that MAGE-A11 enhances Skp2-mediated degradation of cyclin A and the retinoblastoma-related protein p130, but inhibits Skp2-mediated degradation of the E2F1 transcription factor (Su et al., 2017). The authors account the differential effects of MAGE-A11 on Skp2 by proposing a competitive relationship between MAGE-A11 and Skp2 in binding cyclin

A (Su et al., 2017). Collectively these data suggest that MAGEs may regulate cell cycle progression by modulating SCF ubiquitin ligase activity and substrate recognition.

Regulation of transcription

Intriguingly, a number of MAGEs have been implicated in the regulation of various transcription factors. Although some of the means by which MRLs regulate p53 and E2F1 are described in earlier sections, here we highlight additional mechanisms of MAGE-mediated transcriptional regulation.

p53

p53 is a transcription factor that responds to a variety of stress signals and coordinates a gene expression program that contributes to tumor suppression. In addition to modulating p53 stability through MAGE-TRIM28-induced ubiquitination and proteasome-dependent degradation, several other roles for MAGEs in regulating p53 have been reported. For example, MAGE-A2 may sterically occlude the p53 DNA-binding domain, recruit histone deacetylases (HDACs), or inhibit the MDM2 E3 ligase to repress p53 transcriptional activity (Marcar et al., 2015; Marcar et al., 2010; Monte et al., 2006).

E2F Transcription Factors

E2F transcription factors are key regulators of cell cycle progression and E2F1 is essential for the transactivation of target genes involved in the G1/S transition (Chen et al., 2009). The

retinoblastoma (Rb) tumor suppressor is a critical regulator of E2F1 transcriptional activity (Chen et al., 2009). During G1 phase, Rb is in a hypophosphorylated state and binds to the transactivating domain of E2F1, thereby repressing E2F1-depedent transcription (Chen et al., 2009). As cell progress toward S phase, cyclin-dependent kinases phosphorylate Rb and E2F1 is released (Chen et al., 2009). E2F1 is then free to transactivate cell cycle progression genes (Chen et al., 2009). In the same way, Necdin and MAGE-G1 bind to the transactivation domain of E2F1 and repress E2F1 transcriptional activity (Kuwako et al., 2004).

In contrast, investigation into the mechanisms of MAGE-A11 function demonstrated that MAGE-A11 stabilizes the retinoblastoma-related protein p107 and promotes p107 binding to E2F1, thus activating E2F1 transcriptional activity (Su et al., 2013). Recent work by Peche et al. also showed that MAGE-B2 interacts with HDAC1, an E2F1 repressor, to enhance E2F1 transactivation (Peche et al., 2015). Therefore, whereas some type II MAGEs target and inhibit E2F function, other type I MAGEs may stimulate E2F activity to promote tumor cell proliferation.

Androgen receptor

The androgen receptor (AR), a member of the nuclear receptor superfamily, is a transcriptional regulator that responds to androgens and is particularly important for the growth and progression of prostate cancer (Wilson, 2010). Therefore, androgen deprivation therapy is often the first-line of treatment for patients with prostate cancer (Wilson, 2010). However, over time, prostate cancer cells can develop resistance to androgen deprivation, this type of relapse is referred to as castration-recurrent prostate cancer and is associated with high mortality (Wilson, 2010).

MAGE-A11 was first identified as an AR coactivator by a yeast two-hybrid screen of a human testis library (Bai et al., 2005). Additional studies revealed that MAGE-A11 binds the AR N-terminal FXXLF motif, thereby recruiting the steroid receptor coactivator (SRC)/p160 coactivators and promoting AR transcriptional activity (Askew et al., 2009). However, by directly interacting with the p160 coactivator transcriptional mediator protein (TIF2) and the transcriptional regulator p300, MAGE-A11 is also able to enhance AR-mediated gene activation (Askew et al., 2010). Subsequent studies demonstrated that epidermal growth factor (EGF), in the presence of dihydrotestosterone, stabilizes the MAGE-A11-AR complex through phosphorylation of MAGE-A11 at threonine 360 and ubiquitination of lysine residues 240 and 245 (Bai and Wilson, 2008). Interestingly, during androgen deprivation therapy, MAGE-A11 levels increase in prostate cancer, suggesting that MAGE-A11 plays a key role in the progression of castration-recurrent prostate cancer by enhancing AR transcriptional activity (Karpf et al., 2009).

Summary of MRL function

Since the discovery that MAGEs function in complex with E3 RING ubiquitin ligases, they have been shown to regulate not only E3 enzymatic activity, but also substrate recognition and cellular localization. These MRLs act on a diverse array of cellular pathways that have clear implications in various pathologies associated with MAGEs, including transcription, metabolism, protein trafficking, and cell proliferation. However, these mechanistic studies are small in number and further work to determine the functions of additional MAGE members as well as their direct contributions to disease will be invaluable in our understanding of the MAGE family of proteins.

In addition, important challenges for the future include identifying the E3 RING ubiquitin ligases that function with orphan MAGEs and discovering the substrates of novel and known MRLs, such as MAGE-A1-TRIM31, MAGE-B18-LNX1, and MAGEG1-NSE1.

PHYSIOLOGICAL EXPRESSION & FUNCTION

Type I MAGEs and germ cell development

Many of the type I MAGEs, consistent with their classification as CTAs, are normally expressed only in germ cells and/or placenta. However, due to the high homology between subfamily members and lack of specific antibodies, determination of the exact spatiotemporal expression profiles of these proteins is not trivial. Initial characterization by RT-PCR revealed that MAGE-A1-A4, -A6, and -A12 are expressed in testis; and MAGE-A4 as well as MAGE-A8-A11 are also expressed in placenta (De Plaen et al., 1994). Like the MAGE-A subfamily, the MAGE-B and MAGE-C genes are also expressed only in testis, with MAGE-B2 expressed in both testis and placenta (Chomez et al., 2001; Li et al., 2003; Lucas et al., 2000; Lurquin et al., 1997). This restricted expression to testis suggests a functional role for type I MAGEs in germ cell development.

In males, the primordial germ cells (PGCs), the progenitor cells of gametogenesis, are surrounded by somatic Sertoli cells and become prospermatogonia, which proliferate for a few days and then arrest at G0/G1 until birth (Figure 1-5) (Gilbert, 2000). At puberty, proliferation resumes to initiate spermatogenesis. Spermatogonia are the germ cells of spermatogenesis that

remain proliferative throughout life to maintain the pool of stem cells, or undergo differentiation to produce spermatozoa. This process occurs through two meiotic divisions, in which tetraploid primary spermatocytes undergo meiosis I to form diploid secondary spermatocytes, which then undergo meiosis II to form haploid spermatids, that develop into spermatozoa.

Early immunohistochemical staining demonstrated MAGE-A1 and -A4 expression in spermatogonia and primary spermatocytes, but not in spermatids or Sertoli cells of adult testes (Takahashi et al., 1995). Subsequent studies using a different antibody that reacts with MAGE-A1, -A3, -A4, -A6, and -A12 detected MAGE-A expression in migrating primordial germ cells in 5-week-old human embryo as well as in the nuclei and cytoplasm of spermatogonia and spermatocytes in adult testes (Gjerstorff et al., 2008; Jungbluth et al., 2000). Like the human MAGE genes, the murine Mage-a genes are expressed in spermatogonia undergoing maturation toward the spermatocyte stage (Chomez et al., 1996; Clotman et al., 2000). These findings indicate that the expression of these proteins is highly regulated and could play an active role in spermatogenesis. Consistent with this notion, a recent mouse model with deletion of Mage-a1, -a2, -a3, -a5, -a6, and -a8 exhibited reduced size of the testes and diameter of seminiferous tubules (Hou et al., 2016b). Furthermore, deletion of the Mage-a cluster led to an increase in apopotic germ cells, primarily in the first wave of testicular apoptosis, as well as activation of p53 and induction of Bax in response to genotoxic stress (Hou et al., 2016b). Moreover, mutations in MAGE-A9B, -C1, and -C3 were identified in a cohort of infertile men (Krausz et al., 2012; Pastuszak, 2015). Collectively, these results support the hypothesis that these proteins play a critical role in germ cell development.

Interestingly, Mage-b4, like Mage-a genes, is preferentially expressed in spermatogonia, whereas Mage-b1 and -b2 are found in postmeiotic spermatids (Chomez et al., 1996; Clotman et al., 2000; Osterlund et al., 2000). In male germ cells, Mage-b4 is preferentially expressed during cell cycle arrest. When cells resume mitosis and enter meiosis, Mage-b4 protein levels decrease and are hardly detectable in pachytene cells, suggesting that Mage-b4 may be important for cell cycle arrest of male germ cells. This differential expression of MAGEs led investigators to hypothesize that Mage-a and Mage-b4 might be involved in germ cell differentiation while Mage-b1 and -b2 regulate spermiogenesis.

In female germ cells, MAGE-A1 is expressed in the human oogonia prenatally and MAGE-A4 is expressed in some migrating PGCs and early oogonia in female human embryos (Gjerstorff et al., 2007; Mollgard et al., 2010). In addition, Mage-b4 is expressed in premeiotic germ cells and during the pachytene and telophase portions of meiosis, suggesting that MAGEs might also function in developing oocytes (Osterlund et al., 2000).

In addition to their role in germ cells, MAGE-A proteins may also be involved in neuronal development. By immunohistochemistry, MAGE-A reactivity was detected in the spinal cord and brain stem of the early developing CNS as well as in peripheral nerves. Investigators also report MAGE-A-positive PGCs in the adrenal cortex of early fetuses (Gjerstorff et al., 2008). Therefore, MAGE-A might also function during embryonic development. However, additional mouse models and mechanistic studies are required to demonstrate the functional relevance of MAGEs in germ cells and to determine how their physiological roles may be co-opted in the context of cancer.

Type II MAGEs and neural development

Type II MAGEs include the MAGE-D, -E, -F, -G, -H, -L and Necdin genes. In contrast to the type I MAGEs, type II MAGE genes are ubiquitously expressed at various levels in many tissues. Intriguingly, a number of these type II MAGEs are enriched in the brain and have been implicated in various neural processes.

MAGE-D1

MAGE-D1, also referred to as NRAGE or Dlxin, is a type II MAGE that has been implicated in multiple pathways including apoptosis, cell cycle progression, and differentiation (Barker and Salehi, 2002). Initial analysis showed that MAGE-D1 is highly expressed in the brain, but is also detected in most embryonic and adult tissues (Chomez et al., 2001). Additional investigation into MAGE-D expression showed that members of this subfamily are widely expressed throughout the human adult brain, with strongest signals in the cerebral cortex and medulla (Bertrand et al., 2004). Based on the widespread distribution of MAGE-D genes in the brain, it is likely that this MAGE subfamily plays a general role in neural differentiation and maintenance. Interestingly, the MAGE-D genes are located in a chromosomal region associated with many monogenic X-linked neurodevelopmental disorders (Chelly and Mandel, 2001). Therefore, the enrichment of MAGE-D in the cerebral cortex and hippocampus—structures involved in higher function—suggests that these genes can be candidates for such disorders.

Consistent with this, Mage-d1 knockout mice demonstrate symptoms of depression such as decreased locomotor activity, social interaction, and reward responsiveness, as well as increased anxiety and immobility time; and treatment with antidepressants attenuated some of these

behavioral changes related to depression (Mouri et al., 2012). Notably, Mage-d1-null mice display decreased extracellular serotonin levels and increased serotonin transporter (SERT) protein levels, suggesting that deficiency in MAGE-D1 induces both behavioral and neurological phenotypes of depression (Mouri et al., 2012). Further investigation revealed that MAGE-D1 regulates ubiquitination and proteasomal degradation of SERT, consistent with previous reports associating MAGE-D1 with PRAJA-1 E3 ligase and modulation of Msx2- and Dlx5-dependent transcription as well as neuronal differentiation (Mouri et al., 2012; Sasaki et al., 2002; Teuber et al., 2013). In an alternative Mage-d1-deficient (hemizygous) mouse model, loss of Mage-d1 results in reduced social interactions, decreased sexual activity leading to infertility in males, reduced motor activity, late-onset obesity associated with hyperphagia, and increased anxiety-like behaviors (Dombret et al., 2012). Several of these phenotypes can be explained by significantly reduced levels of mature oxytocin in the brain of Mage-d1-deficient mice; and suggest that the combined effects of reduced SERT and oxytocin can contribute to an altered serotonergic system as well as the observed phenotypes in the Mage-d1 knockout model (Dombret et al., 2012; Mouri et al., 2012).

Intriguingly, several of the phenotypes reported in the Mage-d1-deficient mice, including hyperphagia and reduced sociability, mimic symptoms of individuals with Prader-Willi Syndrome (PWS) and autism spectrum disorder (ASD). In fact, one of the earliest insights into the physiological function for MAGE genes came from the genetic analysis of PWS, which showed that individuals with PWS bear deletions or mutations within a specific chromosomal region containing NECDIN and MAGEL2 and with MAGE-G1 in close proximity (Cassidy et al., 2012; Chibuk et al., 2001).

Necdin

Necdin mRNA is ubiquitously expressed and is detected in all developing neurons in the central and peripheral nervous systems in early development (Muscatelli et al., 2000; Niinobe et al., 2000). After E13, Necdin is enriched in discrete regions of the nervous system, such as the hypothalamus, thalamus, and pons; suggesting a specific spatial and temporal function therein (Andrieu et al., 2003). Like MAGE-D1, various studies have implicated Necdin in neuronal differentiation and survival (Hayashi et al., 1995; Maruyama et al., 1991; Matsumoto et al., 2001).

In two independent Necdin-deficient mouse models, mutant mice exhibited respiratory distress and death (Gerard et al., 1999; Muscatelli et al., 2000). Strikingly, individuals with PWS exhibit similar breathing defects with irregular rhythm and often manifest sleep apneas (Zanella et al., 2008). Investigation into the observed respiratory failure in mice demonstrated that Necdin is expressed in medullary serotonergic neurons and Necdin deficiency alters the serotonergic metabolism, thereby contributing to abnormal respiratory rhythmogenesis (Ren et al., 2003; Zanella et al., 2008).

Although the surviving Necdin-deficient mice showed a normal growth pattern, the mutant mice exhibited altered behavioral phenotypes reminiscent of PWS patients, such as increased skin scraping and enhanced spatial learning and memory (Muscatelli et al., 2000). In addition, immunohistochemistry revealed a significant decrease in the number of oxytocin- and luteinizing hormone-releasing hormone (LHRH)-producing neurons in the hypothalamus—the primary region of the brain involved in PWS.

MAGE-L2

MAGE-L2 is widely expressed in fetal tissues and is enriched in various parts of the brain (Lee et al., 2000). Unlike its human counterpart, mouse Magel2 is almost exclusively expressed in the hypothalamus and peaks during neurogenesis during E15-17; however, it is also detected in non-neuronal tissues such as the genital tubercle, midgut region, and placenta (Hao et al., 2015b; Lee et al., 2000).

Loss of MAGE-L2 is also implicated in neurodevelopmental disorders and multiple mouse models have been generated to determine its physiological function. Magel2-null mice, generated by lacZ knock-in allele, exhibited 10% postnatal lethality, normal birth weights, and slightly decreased food intake (Kozlov et al., 2007). However, close observation of their growth pattern revealed that the Magel2-deficient mice displayed a two-phase weight curve as seen in PWS patients; such that mutant mice showed delayed growth and decreased weight gain in the first four weeks of life, followed by increased weight gain, higher fat mass, and elevated leptin, insulin, and cholesterol levels (Bischof et al., 2007). It was later discovered that Magel2-null mice have reduced muscle mass and increased expression of atrophy genes, indicating that loss of Magel2 contributes to hypotonia and related musculoskeletal abnormalities such as scoliosis and digital contractures (Kamaludin et al., 2016).

Consistent with PWS phenotypes as well as cellular evidence that MAGE-L2 modulates the activity of circadian rhythm proteins, Magel2-null mice exhibit reduced daytime activity and disrupted circadian regulation (Camfferman et al., 2008; Devos et al., 2011; Kozlov et al., 2007). In addition, the amounts of orexins, the neuropeptides that regulate wakefulness, orexin-positive neurons, and orexin-2 receptors were all reduced in the hypothalamus of Magel2-deficient mice (Kozlov et al., 2007). Taken together, these data suggest that Magel2 is required for proper

hypothalamic function and maintains circadian rhythm potentially though the regulation of orexin levels.

Additional behavioral assays reported increased anxiety-like behavior in Magel2-null mice. MRI analysis found that regions of the brain with moderate to high Magel2, such as the amygdala, hippocampus, and the nucleus accumbens, but not the hypothalamus, were significantly smaller in Magel2-deficient mice (Mercer et al., 2009). In addition to reduced brain volume, the Magel2-mutant mice have reduced serotonin and its metabolite 5-HIAA as well as reduced dopamine. Both serotonergic and dopaminergic pathways are implicated in various neurobehavioral disorders typically seen in PWS patients, including anxiety, depression, and obsessive behavior. Administration of selective serotonin reuptake inhibitors (SSRIs) in PWS mitigates aggressive and compulsive behaviors; further substantiating the notion that altered serotonergic pathway contributes to some of the behavioral aspects of PWS (Hellings and Warnock, 1994; Warnock and Kestenbaum, 1992).

Investigation into the reproductive functions of MAGE-L2 showed early-onset reproductive decline in Magel2-null mice (Mercer and Wevrick, 2009). In males, testosterone, but not luteinizing hormone or follicle-stimulating hormone levels, were reduced; however, despite reduced testosterone, the male reproductive organs and sperm show no overt differences. Interestingly, the male Magel2-deficient mice had altered olfactory preference. Female mice had delayed and lengthened puberty and were infertile by 24 weeks. Although there were no differences in the gross anatomy of ovaries and uteri collected from the infertile 26-week old Magel2-null females, the ovarian histology of these mice showed an absence of corpora lutea, suggestive of normal folliculogenesis with missed ovulations. In fact, Magel2-null females

exhibited abnormal estrous cycles, similar to other circadian mutant female mice and women with PWS.

In a more recent Magel2 mouse model, Magel2-deficient mice exhibited 50% postnatal mortality and the impaired suckling and subsequent feeding deficits seen in PWS newborns (Schaller et al., 2010). In the hypothalamus, Magel2 mutant neonates had reductions in the hypothalamic neuropeptides oxytocin, orexin-A, and arginine-vasopressin. Interestingly, injection of oxytocin just after birth rescued the suckling initiation defects and the neonatal lethality.

These observations from multiple mouse models, as well as complementary cellular studies, draw striking parallels to neurological disorders. Taken together, the data suggest that many type II MAGEs play critical roles in differentiation and neural development, such that loss of function leads to a spectrum of cognitive, behavioral, and developmental deficits.

MAGEs in DISEASE

MAGE-L2 in Prader-Willi and Schaaf-Yang syndromes

Prader-Willi syndrome (PWS, OMIM 176270) is a complex neurodevelopmental disorder that was first described in the medical literature in 1956 (Prader, 1956). It is characterized by infantile hypotonia with poor suck and failure to thrive, often necessitating assisted feeding (Holm et al., 1993). Beginning in early childhood and over time, individuals with PWS exhibit hyperphagia, rapid weight gain, developmental delay, intellectual disability, hypogonadism, and short stature (Holm et al., 1993). In addition to these cardinal features of PWS, a characteristic behavior and

cognitive profile, including reduced activity, obsessive-compulsive traits, and temper outbursts (often associated with food and eating), has also been ascribed to this multi-system syndrome (Holm et al., 1993; Verhoeven and Tuinier, 2006).

The genetic causes of PWS include deletion of paternal 15q11-q13 (65-75% of cases), maternal uniparental disomy (20-30%), and imprinting defects (1-3%) (Cassidy et al., 2012). Although the deletion sizes can be variable, most individuals with PWS lose expression of genes in the PWS locus (15q11-q13), which comprises MKRN, MAGEL2, NDN, NPAP1, SNURF-SNRPN, a family of six small nucleolar RNA (snoRNA) genes, and several lncRNAs (Figure 1-6A) (Cassidy et al., 2012). This locus has also been associated with general neuropsychiatric illness and autism spectrum disorder (ASD) (Cook et al., 1997; Wilkinson et al., 2007). In fact, 10-40% of individuals with PWS meet the criteria for ASD (Dykens et al., 2011). Genotypic and phenotypic correlations have revealed that individuals with PWS caused by maternal uniparental disomy are more commonly affected with ASD (38%) than those with PWS caused by microdeletion (18%) (Fountain and Schaaf, 2015).

Despite the evident importance of genes in the PWS locus, the individual phenotypic contribution of each gene is not entirely clear. Previous reports have shown that individuals with deletions of the SNORD116 snoRNA cluster presented with key characteristics of PWS; however, an individual with paternal deletion of MKRN3, MAGEL2, and NDN exhibited obesity and intellectual disability but not the typical PWS phenotype (de Smith et al., 2009; Duker et al., 2010; Kanber et al., 2009; Sahoo et al., 2008). This indicates that although loss of multiple genes may be required to produce the syndrome, the loss of individual genes could contribute to the various distinct phenotypes of this complex disorder.

Schaaf et al. initially identified four individuals with truncating mutations on the paternal allele of MAGEL2—the first individuals reported as having point mutations in a protein-coding gene within the PWS locus (Figure 1-6B) (Schaaf et al., 2013). All four individuals presented with ASD, intellectual disability, and varying degrees of PWS phenotype. For example, while subject 2 exhibited classic PWS according to the diagnostic criteria established by Holm et al.; the other three subjects did not meet the full clinical criteria (Holm et al., 1993; Schaaf et al., 2013). Due to the phenotypic overlap with PWS, the condition was initially considered a Prader-Willi-like syndrome. However, as the cohort of individuals with truncating MAGEL2 mutations grew, it became more apparent that the clinical condition caused by these mutations manifests specific phenotypes distinct from PWS. For example, hyperphagia and subsequent obesity—hallmarks of PWS—were either absent or only mildly present in individuals with MAGEL2 mutations (Fountain et al., 2016; Schaaf et al., 2013). In addition, ASD was over-represented among individuals with molecularly confirmed mutations in MAGEL2 (Fountain et al., 2016; Schaaf et al., 2013). Moreover, joint contractures, a phenotype rarely reported in PWS, were found in 23 of 28 cases with MAGEL2 mutations (Fountain et al., 2016; Mejlachowicz et al., 2015; Schaaf et al., 2013). To highlight these phenotypic differences, the clinical condition caused by truncating MAGEL2 mutations was renamed Schaaf-Yang syndrome (SHFYNG, OMIM 615547).

In determining the molecular function of MAGE-L2, our lab demonstrated that MAGE-L2, in complex with the TRIM27 E3 RING ubiquitin ligase and USP7 deubiquitinating enzyme, regulates WASH-dependent actin polymerization and protein trafficking (refer to Regulation of WASH-mediated endosomal protein trafficking by MAGE-L2-TRIM27, Figure 1-4F) (Hao et al., 2013; Hao et al., 2015b). These findings, taken together with the characterization of MAGE-L2

truncating mutations in individuals with SHFYNG, led us to hypothesize that similar phenotypes may also present in individuals with USP7 mutations. We identified seven cases with either heterozygous deletion or mutation of USP7 that resulted in phenotypes similar to those seen in SHFYNG and PWS, including intellectual disability, ASD, hypotonia, and hypogonadism (Hao et al., 2015b). Interestingly, these individuals with USP7 haploinsufficiency did not present with the typical PWS phenotypes of infantile feeding difficulties, hyperphagia, excessive weight gain, and characteristic craniofacial features (Hao et al., 2015b). They did however exhibit phenotypes specific to USP7 mutation or deletion, such as seizures and aggressive behavior, suggesting that specific genes in the PWS locus contribute to a spectrum of shared and independent phenotypes (Hao et al., 2015b).

Intriguingly, individuals with mutations in WASH complex components also exhibit neurological pathologies. For example, autosomal dominant mutations in spastic paraplegia (SPG8), the gene encoding Strumpellin, result in hereditary spastic paraplegia (de Bot et al., 2013; Valdmanis et al., 2007). Likewise, recessive mutations in KIAA1033, the gene encoding SWIP, are associated with autosomal recessive intellectual disability and late-onset Alzheimer disease (Ropers et al., 2011; Vardarajan et al., 2012). In addition, TRIM27 has been implicated in ASD and Parkinson disease, suggesting that alterations in protein recycling may contribute to neurological disorders (Liu et al., 2014; St Pourcain et al., 2013).

MAGE-D2 in Bartter syndrome

Polyhydramnios is the excessive accumulation of amniotic fluid caused by an imbalance between production and removal the fluid (Magann et al., 2007). While most cases of polyhydramnios are mild and result from the gradual increase of amniotic fluid, severe polyhydramnios may result in preterm birth and an increased risk of other perinatal complications (Magann et al., 2007). Some of the known causes of polyhydramnios include fetal esophageal atresia and maternal diabetes; however, in 30 to 60% of cases, the cause remains unknown (Dorleijn et al., 2009; Laghmani et al., 2016; Magann et al., 2007). Antenatal Bartter syndrome (OMIM 300971), one of the few Mendelian diseases associated with polyhydramnios, is a rare, often life-threatening autosomal recessive renal tubular disorder characterized by fetal and postnatal polyuria, renal salt wasting, hypercalciuria, hypokalemia (Seyberth et al., 1985).

Previously it was known that mutations in SLC12A1 (encoding NKCC2), KCNJ1, CLCNKA, CLCNKB, or BSND impair the kidneys' ability to reabsorb salt and can cause Bartter syndrome (Jeck et al., 2005). Recently, Laghmani et al. identified mutations in MAGE-D2 that cause X-linked polyhydramnios with prematurity and a transient but severe form of antenatal Bartter syndrome (Figure 1-6C) (Laghmani et al., 2016). These patients initially exhibited a more severe presentation of antenatal Bartter syndrome with earlier onset of polyhydramnios and preterm labor for male offspring (Reinalter et al., 1998). Immediately after birth, the infants developed progressive polyuria and severe hypercalciuria; however, within weeks, clinical symptoms spontaneously resolved (Reinalter et al., 1998). Through genetic sequencing of nine families with transient antenatal Bartter syndrome and idiopathic polyhydramnios, the authors identified seven truncating mutations (two nonsense, two frameshift, and three splice-site

mutations) and two nontruncating mutations (one missense and one in-frame deletion) in MAGE-D2 (Laghmani et al., 2016).

Further investigation revealed that MAGE-D2 promotes the expression and activity of the two crucial sodium chloride cotransporters (NKCC2 and NCC) necessary for proper ion reabsorption in the thick ascending limb of the loop of Henle and distal tubules (Laghmani et al., 2016). Additionally, Laghmani and colleagues demonstrate that MAGE-D2 interacts with HSP40, a cytoplasmic chaperone that interacts with both NKCC2 and NCC and has been shown previously to regulate the biogenesis of NCC (Donnelly et al., 2013; Laghmani et al., 2016). Collectively, these findings indicate that MAGE-D2 plays a key role in fetal renal salt absorption, amniotic fluid homeostasis, and maintenance of normal pregnancy. However, further work will be important to determine how MAGE-D2 regulates NKCC2 and NCC, and if this regulation is dependent on ubiquitin-mediated trafficking.

MAGE-G1 in lung disease immunodeficiency and chromosome breakage syndrome

Members of the structural maintenance of the chromosome complex (SMC) family of proteins form three highly conserved heterodimeric complexes that regulate mitotic proliferation, meiosis, and DNA repair to support genomic stability (Potts, 2009). One such complex, the SMC5/6 complex, consists of SMC5 and SMC6 in addition to non-SMC elements including the MAGE-G1-NSE1 MRL (Pebernard et al., 2008; Taylor et al., 2008). The SMC5/6 complex promotes homologous recombination-mediated DNA repair and is essential for DNA damage response and telomere lengthening by recombination (Potts, 2009; Potts et al., 2006; Potts and Yu, 2007).

Recently, a report associated missense mutations in MAGE-G1 with an autosomal recessive chromosome breakage syndrome that leads to severe lung disease in early childhood (referred to as lung disease immunodeficiency and chromosome breakage syndrome, LICS) (Figure 1-6D) (van der Crabben et al., 2016). Two sisters (subjects A and B) with homozygous MAGE-G1 mutations (c.790C>T) exhibited B and T cell abnormalities, increased infection susceptibility, and eczema. In addition, they experienced feeding difficulties, failure to thrive, weight loss, psychomotor retardation, and axial hypotonia—phenotypes reminiscent of PWS and SHFYNG. After the onset of pediatric acute respiratory distress syndrome (PARDS), these individuals also manifested respiratory complications such as pneumomediastinum, pneumothorax, and subcutaneous emphysema. Following multiple episodes of virus-induced pneumonia, the affected individuals experienced severe progressive irreversible lung damage and died at 12 and 14 months. An affected brother and sister (subjects C and D, respectively) from a second family also developed a similar clinical history of progressive, severe PARDS and infectious pneumonia. Exome sequencing of the second family revealed compound heterozygous mutations in MAGE-G1 with a maternally inherited c.790C>T mutation (identical to the first family), and a paternally inherited c.626C>T mutation (van der Crabben et al., 2016).

In the SMC5/6 complex, MAGE-G1-NSE1 and NSMCE4 form a molecular bridge between SMC5 and SMC6 and are essential for complex formation (Guerineau et al., 2012; Hudson et al., 2011). Interestingly, the two identified variants of MAGE-G1 result in p.Leu264Phe (L264F) and p.Pro209Leu (P209L), and were both shown to disrupt interactions with NSMCE4 and destabilize the SMC5/6 complex (van der Crabben et al., 2016). Consistent with this, SMC5 and SMC6 protein levels were significantly reduced while MAGE-G1 protein was not detectable

in fibroblasts from affected individuals (van der Crabben et al., 2016). Moreover, cells from subject B exhibited increased numbers of micronuclei, a hallmark of genome instability (van der Crabben et al., 2016). These cells also demonstrated hypersensitivity to various DNA damaging agents and defective homologous recombination. In addition, cells from subject B displayed defects in recovery from replication stress, similar to MMS21/NSMCE2-defective cells, and could be rescued by expression of wildtype MAGE-G1 (van der Crabben et al., 2016).

Therefore, the identified mutations in affected individuals alters the stability of the SMC5/6 complex and result in faulty homologous recombination and impaired recovery from replication stress. Although the affected individuals manifest clinical features similar to those seen in Nijmegen breakage and AT chromosomal breakage syndromes, the severe and ultimately fatal pulmonary disease is unique to this novel chromosome breakage syndrome (van der Crabben et al., 2016).

Type I MAGEs in Cancer

In addition to their physiological expression in reproductive tissues, the type I MAGE CTAs are re-activated in a wide variety of tumors (Table 1-1). This aberrant expression of type I MAGEs as well as their prognostic value in various cancers has been extensively documented (Table 1-2).

Given that the MAGE CTAs were originally identified in melanoma cells, it is not surprising that a number of MAGEs are expressed at high frequencies in melanoma. However, it is interesting that MAGE-A1-4, and -C1 expression changes over the course of cancer progression, such that these MAGEs express at higher frequencies in metastases compared to primary

melanoma samples (Barrow et al., 2006; Brasseur et al., 1995; Jungbluth et al., 2002). In addition, expression of these MAGE-A genes associates with thicker tumors and ulcerated melanomas, supporting the notion that high MAGE CTA expression correlates with advanced tumor grade (Barrow et al., 2006; Brasseur et al., 1995).

This trend is not limited to melanoma. For example, MAGE-A3/6 and -C2 expression in breast cancer associates with tumor estrogen receptor- and progesterone receptor-negative status, high histologic grade, as well as worse survival (Ayyoub et al., 2014; Yang et al., 2014). In ovarian cancer, MAGE-A1, -A9, and -A10 expression also correlate with poor survival (Daudi et al., 2014; Xu et al., 2015). Likewise, MAGE-A1, -A2, -A3/6, -A12, -B2, and -C1 are expressed in non-small-cell lung cancer where MAGE-A3/6 and -A9 expression is associated with advanced tumor type and decreased survival (Gure et al., 2005; Jang et al., 2001; Zhang et al., 2015). Similarly, expression of MAGE-A1-6, -B2 and -B6 in patients with head and neck squamous cell carcinoma (HNSCC) correlates with advanced clinical stage of cancer and poor oncologic outcomes (Filho et al., 2009; Noh et al., 2016; Pattani et al., 2012; Zamuner et al., 2015). Furthermore, MAGE-A1, -A6, -A8, -A9, and -A11 are expressed at significantly higher levels at the tumor front of advanced stages of HNSCC, suggesting that these MAGEs contribute to malignancy (Hartmann et al., 2016).

Indeed, a growing body of evidence supports the notion that MAGEs function as oncogenic drivers, rather than simple biomarkers or passengers of global genomic dysregulation. Consistent with this idea, some studies have reported that MAGEs can be turned on early during the process of tumorigenesis even before clinical signs of the disease (Jang et al., 2001). Furthermore, investigation into the oncogenic potential of these genes has demonstrated that MAGE-A3/6 is required for the viability of patient-derived breast, colon, lung cancer and multiple myeloma cells;

whereas MAGE-A3/6 does not significantly alter the viability of MAGE-A3/6-negative cells (Atanackovic et al., 2010; Pineda et al., 2015). This specificity suggests that upon expression of MAGE-A3/6, these cancer cells become dependent on or addicted to MAGE-A3/6 expression for viability (Pineda et al., 2015). Consistent with these findings, MAGE-A3/6 expression drives several hallmarks of cancer such as cell proliferation, cell migration, invasion, and anchorage-independent growth (Figure 1-7A) (Liu et al., 2008; Pineda et al., 2015). Remarkably, expression of MAGE-A3/6 is sufficient to stimulate foci formation in fibroblasts and promote anchorage-independent growth in non-transformed human colonic epithelial cells (Pineda et al., 2015). In an orthotopic xenograft mouse model for thyroid cancer, MAGE-A3/6 expression results in significantly increased tumor growth and larger, more numerous lung metastases (Liu et al., 2008). These results are consistent with a model wherein MAGE-A3/6 functions as a potent driver of tumorigenesis.

While most MAGE-related studies focus on the MAGE-A subfamily and their involvement in cancer, the MAGE-B and -C subfamilies are also associated with tumor growth and progression (Figure 1-7A). For example, knockdown of mouse Mage-b genes reduces cell viability in melanoma and mast cell lines (Yang et al., 2007a; Yang et al., 2007b). Similarly, MAGE-B2 promotes cell proliferation in transformed oral keratinocytes, osteosarcoma, and colon cancer cell lines (Pattani et al., 2012; Peche et al., 2015). Moreover, Mage-b knockdown suppresses growth in a syngeneic mouse model, whereas over-expression of MAGE-B2 enhances tumor growth in mice (Peche et al., 2015; Yang et al., 2007b). Likewise, MAGE-C2 has also been shown to promote cell proliferation in malignant melanoma cells and tumor metastasis *in vivo* by enhancing STAT3 signaling (Hao et al., 2015a; Song et al., 2016). These findings indicate that MAGE CTAs have

oncogenic functions. Additional studies are needed, especially with regard to the MAGE-B and -C subfamilies, to determine the specific activities and mechanisms by which MAGE CTAs promote cancer development.

Interestingly, MAGE CTAs exhibit preferential expression in cancer stem cells (CSCs), a small population of cancer cells that have the ability to self-renew, differentiate, and initiate tumor growth (Reya et al., 2001). Analysis of the MAGE CTA expression profiles in cancer stem-like cells demonstrated that MAGE-A2 and -A3/6 are enriched in the CSC-like side population cells derived from lung and colon adenocarcinoma cells while MAGE-A4 and -B2 are preferentially expressed in the CSC-like side population derived from colon adenocarcinoma cells (Yamada et al., 2013). Additionally, MAGE-A3 exhibits enriched expression in the CSC-like side population in bladder cancer (Yin et al., 2014). Consistent with these findings, MAGE-C1 expresses in stem cells as well as immature B cells (Wienand and Shires, 2015). This preferential expression of MAGE CTAs in CSCs is reminiscent of their physiological enrichment in spermatogonial stem cells. The marked similarities between these cells types, such as immortalization, immune evasion, and induction of specific differentiation pathways has led investigators to speculate that the expression of MAGEs and activation of their physiological functions in cancer initiates a gametogenic program that might contribute to the tumor formation, progression and CSC maintenance (Figure 1-7B).

TRANSCRIPTIONAL REGULATION

Although there is an abundance of evidence for the deregulated expression of type I MAGE CTAs in cancer, the precise mechanisms regulating their aberrant expression is only beginning to be elucidated. While some cancers such as melanoma and lung cancers frequently express MAGEs, others including leukemia and uveal melanoma rarely do. In addition, some tumors tend to express a single or few MAGEs, while others express multiple MAGEs simultaneously (Hofmann et al., 2008). Although the details of how specific MAGE genes get turned on in cancer are not fully understood, it is apparent that epigenetic events, including DNA methylation and histone modifications, contribute to the regulation of MAGE expression in both normal and neoplastic cells (Figure 1-7C).

DNA methylation

DNA methylation of promoter CpG dinucleotides by DNA methyltransferases (DNMTs) exerts a repressive effect on transcription by preventing transcription factor binding and by recruiting methyl-CpG-binding domain proteins (MBDs), which in turn bind chromatin remodeling co-repressor complexes to repress gene expression. A growing body of literature has shown that DNA methylation is the primary regulation of CTA expression in normal and cancer cells. In fact, Weber and colleagues provided the first insights into the transcriptional regulation of MAGEs by demonstrating that 5-aza-2'-deoxycytidine (decitabine), a DNMT inhibitor, induces MAGE-A1 expression in cultured melanoma cells (Weber et al., 1994). Subsequent analysis revealed that expression of several MAGE-A genes correlates with methylation status of its promoter in various types of neoplastic cells (De Smet et al., 1996, Honda, 2004 #267). Importantly, an unmethylated

MAGE-A1 promoter was shown to drive expression of a reporter gene in MAGE-A1 nonexpressing cells, indicating that the methylation status of the MAGE CTA promoter is the leading mechanism for regulating expression (De Smet et al., 1995; Sigalotti et al., 2002). Likewise, downregulation of DNMT1 results in the activation and stable hypomethylation of a methylated MAGE-A1 transgene in melanoma cells (Loriot et al., 2006). Interestingly, Sigalotti et al. reported an association between DNA hypomethylation of CTA promoters and CTA expression in populations of putative melanoma stem cells, suggesting that this form of epigenetic regulation is potentially an important mechanism of CTA gene regulation in cancer stem cells (Sigalotti et al., 2008). Therefore, methylation-specific PCR can be used to evaluate the hypomethylation status of CpG sites in the promoter regions of MAGEs as a method for early cancer detection (Jang et al., 2001). However, while DNA methylation clearly plays an important role in regulating MAGE expression, there is mounting evidence that demethylation is not sufficient to drive expression of all MAGEs and additional nonepigenetic mechanisms are required (Karpf et al., 2004; Suyama et al., 2002; Weber et al., 1994).

Histone modifications

Histone modifications have also been shown to function in the regulation of CTA expression. Histones assemble with DNA into nucleosomes, the basic unit of chromatin. Their flexible N-terminal tails protrude from the nucleosomes and are targeted for post-translation modification, including acetylation and methylation (reviewed in (Chi et al., 2010)). Histone acetylation by histone acetyltransferases (HATs) results in chromatin decompaction and gene transcription.

Conversely, histone deactylases (HDACs) serve the opposite function and promote the compaction of chromatin to prevent the accessibility of DNA to transcription factors and RNA polymerase. In the case of MAGE-A2 and MAGE-A12, treatment with HDAC inhibitors results in up-regulation of transcriptional activity (Wischnewski et al., 2006).

Depending on the lysine residue that is modified, histone methylation is associated with both transcriptional activation and repression. For example, methylation of histone H3 lysine 9 or lysine 27 (H3K9 or H3K27, respectively) are repressive marks whereas methylation of histone H3 lysine 4 (H3K4) is an active mark. In a study from Tachibana et al., knockout of the histone methyltransferases that catalyze H3K9me2, G9a and/or GLP, induced the expression of Mage-a genes in mouse embryonic stem cells (Tachibana et al., 2002). In addition, in G9a- or GLP-null mouse ES cells, Mage-a genes are hypomethylated (Tachibana et al., 2002). These results suggest that histone modifications are also involved in the repression of MAGE CTAs.

Transcription factors

Although less is known about the nonepigenetic mechanisms of MAGE gene regulation, the ETS transcription factor sites have been show to function in the regulation of MAGE-A genes. The ETS protein family is one of the largest families of transcription factors and members of this family are implicated in the development of various tissues as well as cancer progression. Work from de Smet and colleagues revealed that two inverted ETS motifs near the transcriptional start site of MAGE-A1 drive transcriptional activity of the unmethylated promoter (De Smet et al., 1995; Serrano et al., 1996). In cells where the endogenous MAGE-A1 promoter is methylated and inactive, MAGE-

A1 promoter transgenes are highly active and dependent on ETS sequences (De Smet et al., 1995; Serrano et al., 1996). Further studies have shown that methylation of a CpG in the ETS consensus sequence inhibits ETS binding (De Smet et al., 1995; Serrano et al., 1996). Although the identity of the exact ETS factor that drives MAGE-A expression remains unclear, one potential candidate is ETS1, which was shown to activate MAGE-A genes when overexpressed.

BORIS, a paralog of the imprinting regulator and chromatin insulator protein CTCF, has also been implicated in promoting the expression of MAGE-A1. In fact several MAGE-A genes contain BORIS binding sites and the proteins have been shown to coexpress in head and neck cancer (Smith et al., 2009). Moreover, BORIS overexpression in immortalized oral keratinocytes led to MAGE-A induction and DNA hypomethylation (Smith et al., 2009).

Signal transduction pathways

In addition to transcription factors, signal transduction pathways such as activated tyrosine kinases, have been implicated in MAGE CTA expression. The KIT receptor tyrosine kinase is a proto-oncogene that binds to c-kit ligand, also known as steel factor or stem cell factor, to activate its tyrosine kinase activity and signal transduction pathway. Yang et al. reported that treatment of mast cells with the tyrosine kinase inhibitor imatinib results in downregulation of MAGE-A, -B, and -C and potentially alters DNA methylation levels (Yang et al., 2007c). In addition to KIT, others have reported that fibroblast growth factor receptor 2 (FGFR2) activation downregulates MAGE-A3 expression (Kondo et al., 2007). In addition, FGFR2 and MAGE-A3 promoters show reciprocal DNA methylation patterns (Zhu et al., 2008). Therefore, FGFR2 and KIT appear to have

opposing effects of MAGE-A expression. Interestingly, FGFRs are known to play a critical role in a variety of processes including tissue repair and angiogenesis (Powers et al., 2000). Given that MAGE-A1 is expressed during wound healing as well as in the joints of patients with juvenile arthritis, MAGE-A1 may have a role in inflammation (Becker et al., 1994; McCurdy et al., 2002). Furthermore, MAGE-B2 was originally identified as being expressed in patients with systemic lupus erythematosus where MAGE-B2 auto-antibodies can be found (Hoftman et al., 2008; McCurdy et al., 1998). Thus, additional investigation of roles for type I MAGE CTAs in other disease contexts besides cancer is warranted in the future.

THERAPY

Cancer immunotherapy

Since the identification of MAGEs, significant effort has gone into the development of CTA-based immunotherapeutic strategies (Table 1-3). Compared to chemotherapy, which often has limited efficacy in patients with relapsed cancer or advanced disease, immunotherapy has the potential to provide long-lasting responses by modulating the immune response against specific cancer proteins.

From an immunological perspective, MAGE CTAs are ideal target molecules for cancer immunotherapies due to their widespread, prominent expression in various cancers, but restricted normal expression to the immune-privileged testis, thus limiting the possibility of an autoimmune response but maximizing their potential for broad application to large cohorts of patients (Bart et

al., 2002; Fiszer and Kurpisz, 1998; Kalejs and Erenpreisa, 2005). MAGE-A3, which codes for an antigenic nonapeptide that is recognized by CTLs on the HLA-A1 molecule, garnered particular interest as an immunotherapeutic. In a pivotal clinical trial where tumor-bearing HLA-A1-positive patients with metastatic melanoma were treated with subcutaneous injections of MAGE-A3 peptide, seven out of 25 patients displayed significant tumor regression, including three complete responses (Marchand et al., 1999). However, MAGE-A3-specific CTL responses were not detected during the course of vaccinations, even in patients with positive clinical responses (Marchand et al., 1999). Subsequent studies confirmed these immunologic and clinical responses in melanoma patients treated with MAGE-A3-pulsed DCs (Nestle et al., 1998; Thurner et al., 1999)

Additional MAGE CTA-based vaccines have utilized recombinant proteins to (1) induce both CD8+ and CD4+ immune responses thereby magnifying the CTL response, (2) generate responses against multiple epitopes, and (3) avoid specific HLA-type requirements for patients (Marchand et al., 2003). In a phase II clinical trial where 36 patients with stage III or IV M1a melanoma were treated with MAGE-A3 combined with AS15 immunostimulant, three patients exhibited complete responses (Kruit et al., 2013).

Based on these preliminary data, two large clinical trials were set forth—PREDICT and DERMA. PREDICT was a phase II study with the goal evaluating the clinical activity of MAGE-A3 antigen-specific cancer immunotherapeutic (ASCI) in patients with MAGE-A3-positive unresectable metastatic melanoma (Saiag et al., 2016). The goal of DERMA (phase III) was to evaluate the benefit MAGE-A3 antigen-specific cancer immunotherapeutic (ASCI) in melanoma patients after surgical tumor removal. Unfortunately, the objective response rate was lower than in

previous studies (Saiag et al., 2016). Consistent with these findings, DERMA was terminated early following assessment showing lack of efficacy of the treatment.

Similarly, MAGE-A3 ASCI showed promising results in phase II clinical trials of patients with NSCLC and inspired the largest phase III therapeutic trial in lung cancer—MAGRIT (Atanackovic et al., 2004; Brichard and Lejeune, 2007; Tyagi and Mirakhur, 2009; Vansteenkiste et al., 2013). In the case of patients with MAGE-A3-positive surgically resected NSCLC, MAGE-A3 ASCI failed to increase disease-free survival compared with placebo and further development of the MAGE-A3 ASCI was stopped (Vansteenkiste et al., 2016).

More alarming than lack of efficacy, however, are the unexpected deaths associated with MAGE-based immunotherapies. In order to overcome the complications associated with low frequency of cancer antigen-specific cells and low avidity of expanded effector T cells, T cells can be genetically engineered to expressed T cell receptors (TCRs) that have high affinity and specificity. Unfortunately, in a study utilizing anti-MAGE-A3 TCR gene therapy as a treatment for metastatic cancers, one patient developed transient Parkinson-like symptoms, while two patients lapsed into comas and died (Morgan et al., 2006). Further investigation revealed that T cells transduced with the generated TCR also recognized MAGE-A12, which is expressed in the brain (Morgan et al., 2006). Therefore, treatment resulted in neuronal cell destruction that manifested as necrotizing leukoencephalopathy (Morgan et al., 2006). In a separate study using anti-MAGE-A3 TCR therapy, two patients developed progressive cardiogenic shock and died within a week of infusion. In this case, the generated TCR recognized another peptide derived from titin, a component of striated muscle, and the off-target reactivity resulted in severe

myocardial damage with T-cell infiltration (Linette et al., 2013). These studies demonstrate the need for more rigorous studies of MAGE expression and stringent analysis of engineered TCRs.

Combination therapy

In an effort to develop alternative methods to target MAGE-expressing cancers and improve clinical outcomes, investigators are utilizing combinatorial approaches including conventional therapy, immunotherapy, and molecular targeting.

One obstacle to overcome in the development of immunotherapies is T cell recognition of cancer cells expressing MAGE CTAs. In cancer cells, promoter hypermethylation suppresses MHC expression, thereby impeding antigen presentation (Ye et al., 2010). Therefore, several groups have indicated that treatment with demethylating agents such as decitabine, can potentially enhance antigen presentation and cancer cell recognition by upregulating both MHC and MAGE expression (Bao et al., 2011; Serrano et al., 2001; Sigalotti et al., 2003; Weber et al., 1994). In a phase I clinical trial combining dectabine and DC vaccine targeting MAGE-A1 and -A3 for patients with relapsed neuroblastoma demonstrated a response in six of nine patients with complete response in one patient (Krishnadas et al., 2015). Although the preliminary data of this combination therapy looks promising, future trials are needed to better determine the efficacy of this treatment.

A major obstacle to the practical application of cancer immunotherapy is the ability of tumor cells to evade the immune system by promoting an immunosuppressive tumor microenvironment. Therefore, investigators have turned to immune checkpoint therapies, which

target regulatory pathways in T cells to enhance the antitumor immune response. Rather than activating the immune system to directly target tumor cells, immune checkpoint therapies remove inhibitor pathways that block effective anti-tumor T cell responses (reviewed in (Sharma and Allison, 2015)). Therefore, combination approaches with immune checkpoint therapies may be beneficial in the treatment of MAGE-expression cancers and are currently on going (Table 1-3).

In addition to these proposed treatments, molecular targeting of specific protein-protein interactions may prove to be a powerful therapeutic strategy. A prime candidate is targeting specific MRLs. For example, Bhatia and colleagues screened a library of compounds and identified three potential compounds that interfere with MAGE-C2-TRIM28 binding, promote death in MAGE-positive cells, and activate p53 (Bhatia et al., 2011). This data supports the therapeutic value of inhibiting MAGE binding to cognate E3 ligases to block oncogenic functions of MAGE proteins. Furthermore, by knowing the precise cellular targets and functions of MRLS, novel drug susceptibilities can be predicted based on MAGE expression status in individual tumors. For example, considering the interplay between MAGE-A proteins, p53, and HDAC, the use of HDAC inhibitors in combination with other therapeutic approaches could help restore p53 tumor suppressor activity. Furthermore, utilization of AMPK agonists (such as metformin) or mTOR inhibitors may be an effective future treatment for MAGE-A3/6 positive cancers. Future studies validating these approaches in cell and animal models will be important.

DISCUSSION

Since their initial discovery, the MAGEs have gained much attention and interest as cancer biomarkers and targets of cancer immunotherapies. Despite the fact that initial attempts to develop MAGE-based immunotherapies have not been entirely successful, recent studies highlighting a role for MAGEs in the regulation of E3 RING ubiquitin ligases have greatly expanded our understanding of the diverse functions of MAGE family members and their impact on various molecular processes (such as p53 signaling, cell metabolism, and protein trafficking), and have opened up novel avenues for personalized cancer-specific therapies targeting MRLs.

However, many unanswered questions remain. How do the cellular functions attributed to MAGEs contribute to disease progression? How do MAGEs regulate pathways that effect tissue-specific outcomes? What transcriptional programs lead to the aberrant re-expression of type I MAGEs in cancer? Do type I MAGEs have similar functions in their physiological context of germ cells as they do in cancer cells? What are the cellular and physiological functions of the relatively unexplored MAGEs? What are the substrates of many of the uncharacterized MRLs?

Although our understanding of the molecular mechanisms by which MRLs function is still developing, continued identification and characterization of the functional interplay between MAGEs, RING ligases, and deubiquitinating enzymes will provide valuable insights into the role of MAGEs. In addition, structural studies may help us not only to understand the biophysical underpinnings of MRLs, but also design specific MAGE inhibitors for therapeutic purposes. The continued study of MAGEs clearly holds great promise for answering fundamental biological questions and may reveal new ways to target them for the treatment of disease.

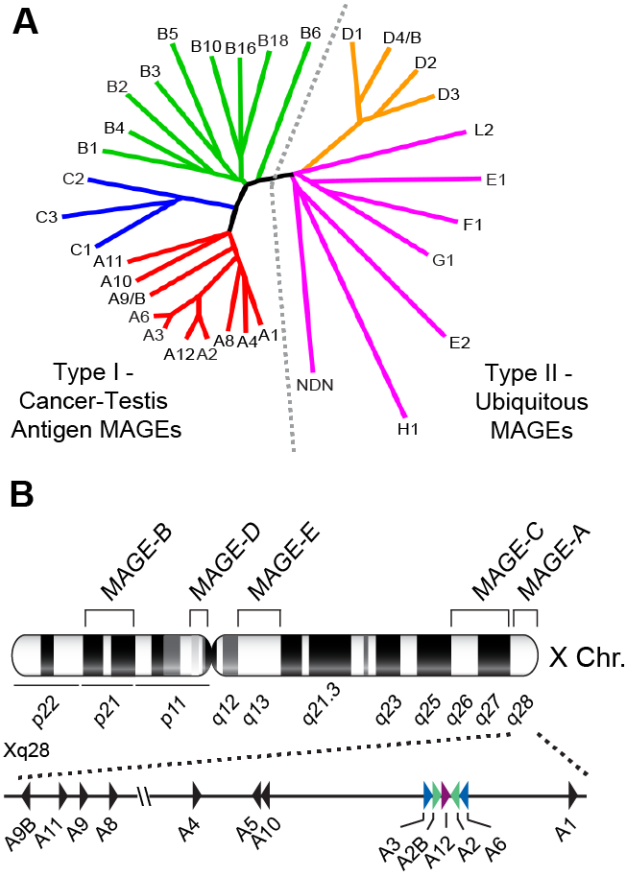

Figure 1-1. The MAGE family

(A) Dendrogram tree of the human MAGE protein family. Type I MAGEs include MAGE-A, -B, and -C subfamilies. Type II MAGEs include MAGE-D, -E, -F, -G, -H, -L2, and Necdin families. (B) Chromosomal locations of MAGE subfamilies on the X chromosome. The MAGE-A genes are clustered in the q28 region of the X chromosome. Triangles indicate gene orientation. Colored triangles represent the palindrome arrangement of MAGE-A genes.

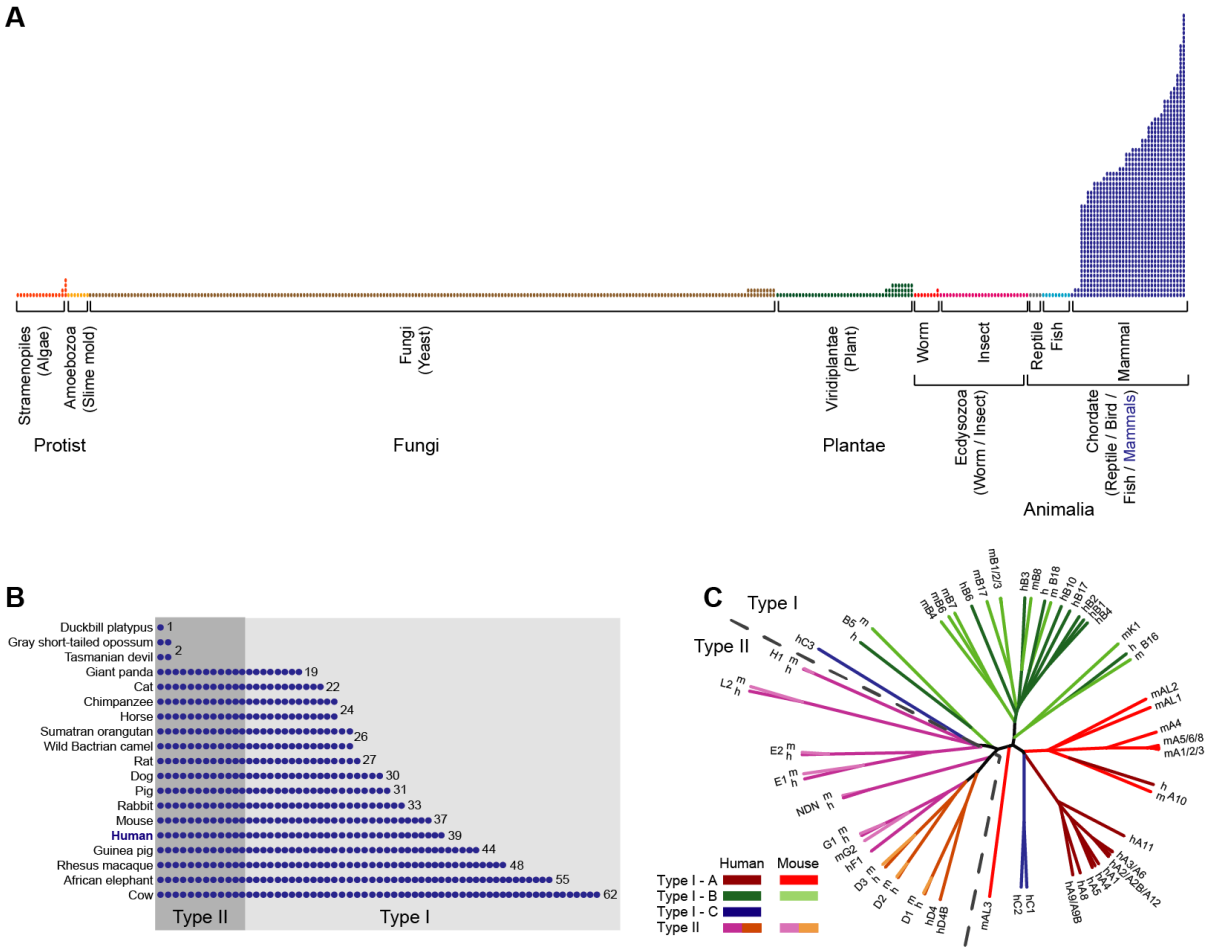

Figure 1-2. Evolution of the MAGE genes

(A) The MAGE family is evolutionarily conserved in all eukaryotes. Following the emergence of eutherian mammals (blue), the MAGE family underwent a rapid and dramatic expansion from a single MAGE in lower eukaryotes to a large multi-gene family. Each column represents an organism with the number of circles denoting the number of MAGE proteins in each organism based on pfam annotation.

(B) A detailed view of the recent expansion of MAGEs in select mammals. The type II MAGEs (designated based on the human MAGEs) are more evolutionarily ancient while the type I MAGEs appear to be the result of recent gene duplications.

(C) The type II MAGEs share high homology with their mouse orthologs whereas type I MAGEs share much higher sequence conservation within their respective subfamilies compared to their mouse orthologs.

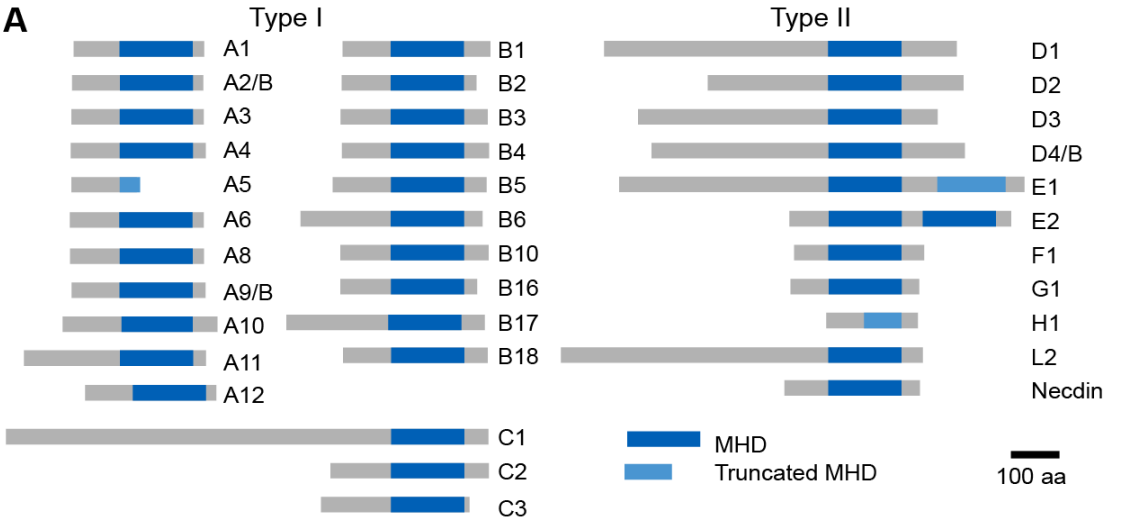

B

MAGE	A1	A2	A3	A4	A6	A8	A9	A10	A11	A12	B1	B2	B3	B4	B5	B6	B10	B16	B18	C1	C2	C3	D1	D2	D3	D4	E1	E2	F1	G1	H1	L2	NDN
A1	100	76	75	80	76	77	71	68	67	77	54	51	55	58	47	49	55	56	53	53	53	55	42	41	42	42	39	30	37	42	21	37	30
A2	76	100	84	71	84	70	65	62	61	91	46	48	45	51	43	42	52	49	48	48	50	51	39	38	38	38	37	28	37	41	22	37	28
A3	75	84	100	69	94	67	64	58	60	84	46	47	45	50	42	43	49	47	47	50	50	51	40	41	40	40	39	29	37	41	25	38	29
A4	80	71	69	100	69	77	72	63	66	71	54	52	53	54	46	48	56	56	51	53	52	49	42	40	42	43	40	29	39	43	23	37	30
A6	76	84	94	69	100	67	63	59	60	84	46	47	45	50	41	42	49	47	47	51	50	51	39	40	40	38	40	30	38	41	25	38	30
A8	77	70	67	77	67	100	75	70	66	71	50	50	52	54	44	47	55	54	53	52	51	57	45	41	43	46	40	31	37	44	22	38	31
A9	71	65	64	72	63	75	100	66	67	64	50	48	53	55	47	46	56	55	52	54	56	56	41	37	41	43	37	29	38	40	20	37	30
A10	68	62	58	63	59	70	66	100	67	61	53	48	54	60	47	46	58	56	53	56	56	57	40	41	40	40	38	31	37	43	22	36	33
A11	67	61	60	66	60	66	67	67	100	60	50	47	54	55	46	47	55	57	54	56	54	51	45	44	45	42	41	33	41	45	24	38	31
A12	77	91	84	71	84	71	64	61	60	100	49	48	47	52	43	44	53	50	47	49	48	49	40	39	40	40	35	30	36	40	23	37	29
B1	54	46	46	54	46	50	50	53	50	49	100	64	59	70	55	59	60	57	58	45	49	41	40	44	44	43	38	33	39	44	23	38	36
B2	51	48	47	52	47	50	48	48	47	48	64	100	57	65	50	51	55	55	55	46	51	44	39	43	44	42	41	36	45	42	25	38	31
B3	55	45	45	53	45	52	53	54	54	47	59	57	100	64	61	56	58	61	57	47	48	41	46	44	47	48	38	35	42	45	25	40	34
B4	58	51	50	54	50	54	55	60	55	52	70	65	64	100	60	57	61	60	58	47	51	48	43	48	48	46	43	33	43	47	25	44	37
B5	47	43	42	46	41	44	47	47	46	43	55	50	61	60	100	52	53	53	51	41	41	34	39	40	44	41	39	28	38	42	23	38	33
B6	49	42	43	48	42	47	46	46	47	44	59	51	56	57	52	100	51	52	53	41	43	40	43	45	47	46	40	34	41	42	26	40	37
B10	55	52	49	56	49	55	56	58	55	53	60	55	58	61	53	51	100	64	63	54	51	45	43	45	47	45	42	35	41	46	25	39	36
B16	56	49	47	56	47	54	55	56	57	50	57	55	61	60	53	52	64	100	63	50	51	44	44	47	47	46	44	36	43	49	25	40	37
B18	53	48	47	51	47	53	52	53	54	47	58	55	57	58	51	53	63	63	100	48	53	44	44	43	44	45	40	34	43	42	25	38	34
C1	53	48	50	53	51	52	54	56	56	49	45	46	47	47	41	41	54	50	48	100	69	66	40	42	43	39	38	31	38	40	25	34	33
C2	53	50	50	52	50	51	56	56	54	48	49	51	48	51	41	43	51	51	53	69	100	64	40	40	39	39	39	30	38	41	26	37	32
C3	55	51	51	49	51	57	56	57	51	49	41	44	41	48	34	40	45	44	44	66	64	100	37	42	39	35	36	25	36	38	12	37	25
D1	42	39	40	42	39	45	41	40	45	40	40	39	46	43	39	43	43	44	44	40	40	37	100	78	76	78	46	38	47	43	25	49	37
D2	41	38	41	40	40	41	37	41	44	39	44	43	44	48	40	45	45	47	43	42	40	42	78	100	79	67	48	34	49	48	30	51	43
D3	42	38	40	42	40	43	41	40	45	40	44	44	47	48	44	47	47	47	44	43	39	39	76	79	100	74	47	34	48	47	30	48	43
D4	42	38	40	43	38	46	43	40	42	40	43	42	48	46	41	46	45	46	45	39	39	35	78	67	74	100	40	38	45	46	25	44	39
E1	39	37	39	40	40	40	37	38	41	35	38	41	38	43	39	40	42	44	40	38	39	36	46	48	47	40	100	38	54	47	29	44	34
E2	30	28	29	29	30	31	29	31	33	30	33	36	35	33	28	34	35	36	34	31	30	25	38	34	34	38	38	100	34	39	25	36	28
F1	37	37	37	39	38	37	38	37	41	36	39	45	42	43	38	41	41	43	43	38	38	36	47	49	48	45	54	34	100	59	27	50	45
G1	42	41	41	43	41	44	40	43	45	40	44	42	45	47	42	42	46	49	42	40	41	38	43	48	47	46	47	39	59	100	27	50	42
H1	21	22	25	23	25	22	20	22	24	23	23	25	25	25	23	26	25	25	25	25	26	12	25	30	30	25	29	25	27	27	100	25	26
L2	37	37	38	37	38	38	37	36	38	37	38	38	40	44	38	40	39	40	38	34	37	37	49	51	48	44	44	36	50	50	25	100	39
NDN	30	28	29	30	30	31	30	33	31	29	36	31	34	37	33	37	36	37	34	33	32	25	37	43	43	39	34	28	45	42	26	39	100

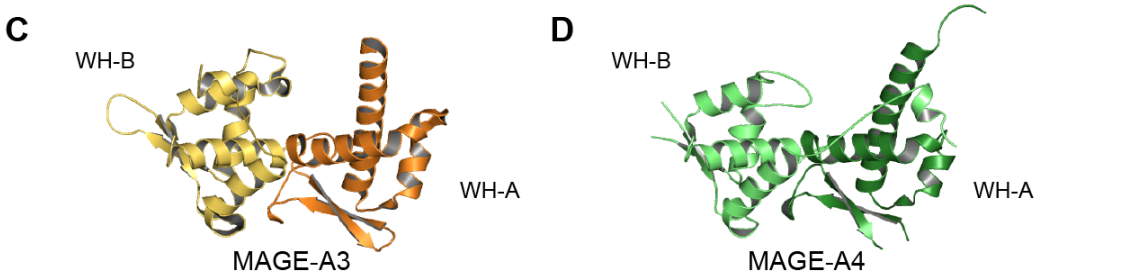

Figure 1-3. The MAGE homology domain
(A) List of human MAGE proteins and their conserved MAGE homology domain (MHD) highlighted in blue.

(B) The percentage of identical amino acids between the various human MHDs is given and colored on a three-color sale (blue = high, gray = medium, red = low).
(C and D) Crystal structures of the MAGE-A3 (C) and MAGE-A4 (D) MHDs. The two winged-helix motifs (WH-A and WH-B) are noted.

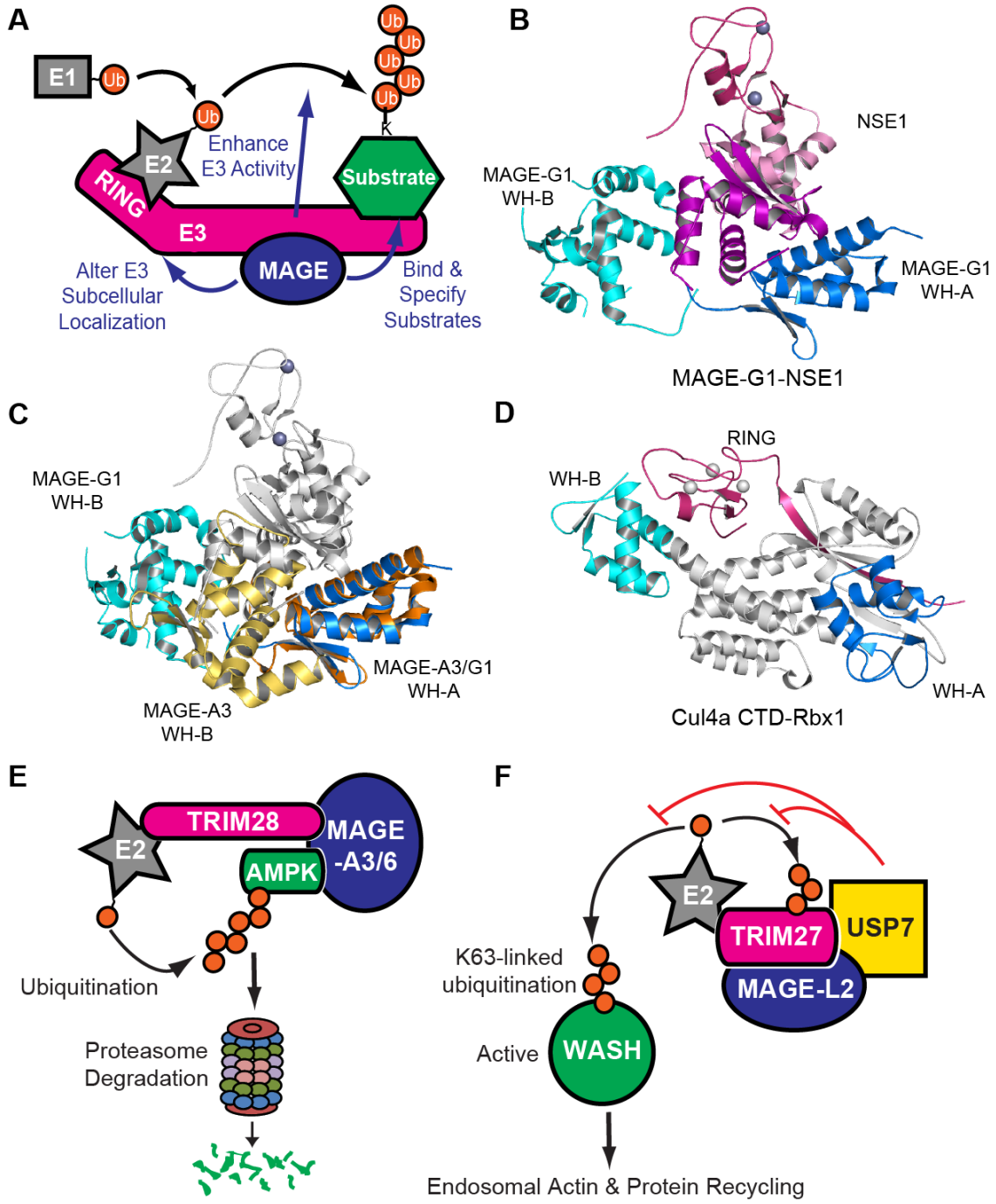

Figure 1-4. Structure and function of MAGE-RING ligases
(A) Schematic representing biochemical and cellular functions of MAGE-RING ligases (MRLs).
(B) Crystal structure of MAGE-G1-NSE1.
(C) Alignment of MAGE-G1-NSE1 and MAGE-A3 based on WH-A. The orientation of the WH motifs differs between unbound MAGE-A3 and NSE1-bound MAGE-G1.

(D) Crystal structure of Cul4A C-terminal domain (CTD)-Rbx1 (PDB: 2HYE) shares structural features similar to MAGE-G1-NSE1.

(E) Model of MAGE-A3/6-TRIM28 ubiquitination and degradation of the AMPK tumor suppressor. MAGE-A3/6 directly bind AMPK and recruit it to the TRIM28 ubiquitin ligase for ubiquitination and subsequent proteasome-mediated degradation.

(F) Model of MAGE-L2-TRIM27, USP7, and K63-ubiquitin regulation of endosomal protein recycling. MAGE-L2-TRIM27-USP7 form stable complex where TRIM27 mediates non-degradative K63-linked ubiquitination of WASH. This ubiquitination events leads to WASH activation, generation of F-actin accumulation, and recycling of proteins through the retromer pathway. USP7 functions to fine-tune WASH ubiquitination to allow for precise levels of endosomal F-actin and stabilize the complex through preventing TRIM27 auto-ubiquitination induced degradation.

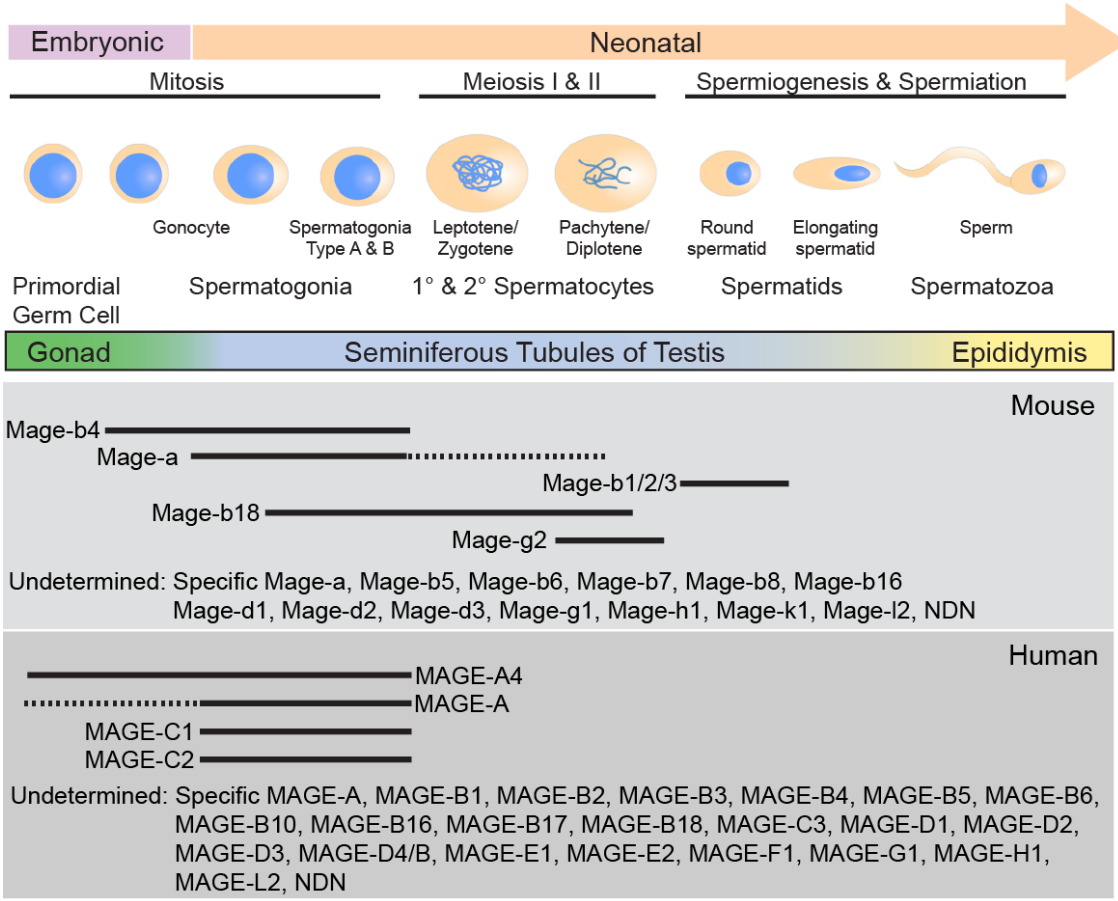

Figure 1-5. MAGEs are differentially expressed during spermatogenesis
Schematic diagram of germ cell development and where specific MAGE genes are expressed. The expression profiles of most MAGE genes are unknown.

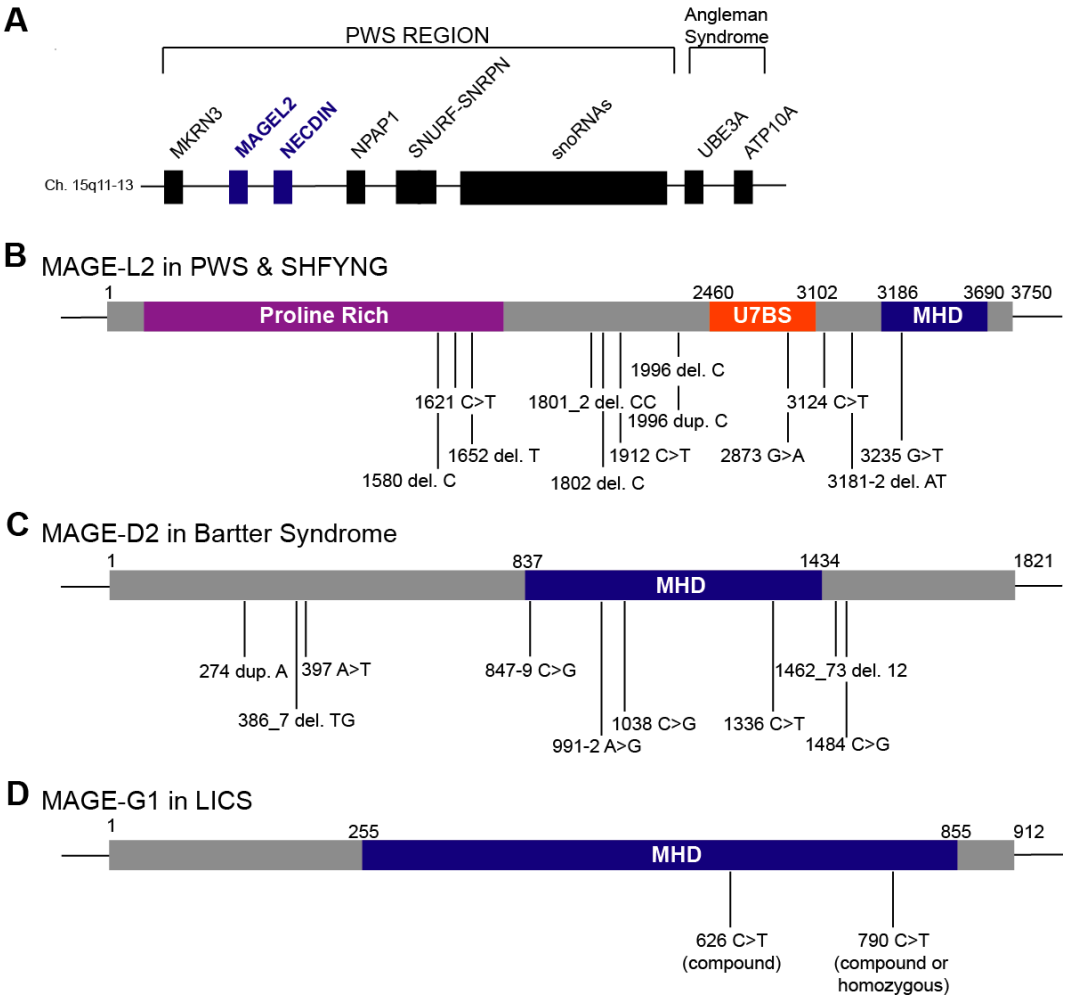

Figure 1-6. Type II MAGEs are associated with various diseases
(A) Schematic representation of the PWS locus.
(B-D) Identified mutations in MAGE-L2 (B), MAGE-D2 (C), and MAGE-G1 (D) associated with PWS and SHFYNG, Bartter syndrome, and LICS, respectively.

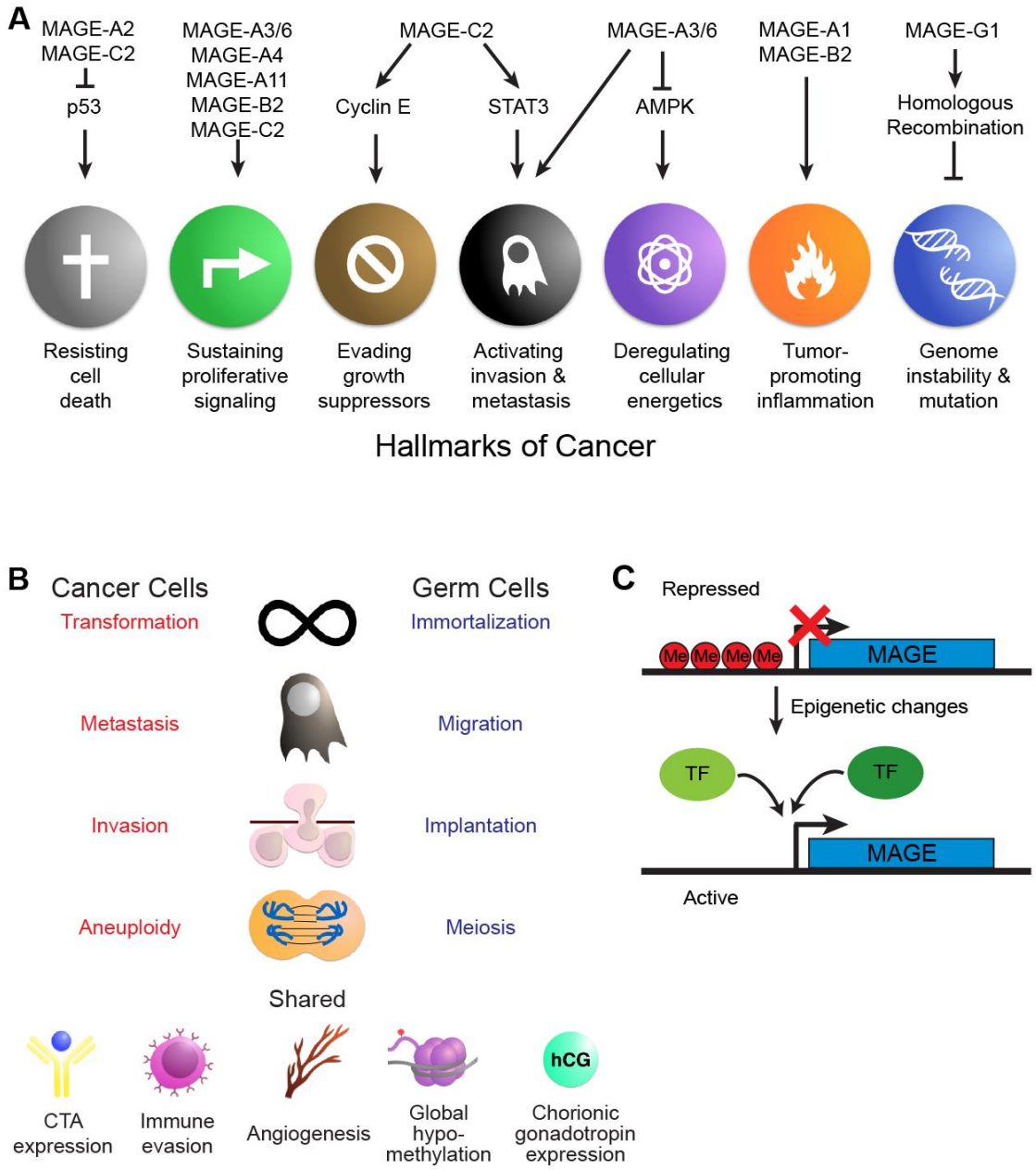

Figure 1-7. Type I MAGEs promote tumorigenesis
(A) Specific functions of several type I MAGEs in driving the hallmarks of cancer is shown.
(B) The shared phenotypes between cancer cells and germ cells suggest that activation of the gametogenic program might contribute to tumorigenesis.
(C) Transcriptional activation of MAGEs. Type I MAGEs are typically silenced but can be activated by epigenetic changes (including DNA CpG demethylation) and specific transcription factors.

Table 1-1. Summary of MAGE expression in select cancer types

	Percent of MAGE-positive patient tumors					
MAGE [a]	**Melanoma**	**Lung**	**Breast**	**Ovarian**	**HNSCC**	**References**
A1	16-61%	24-49%	6%	11-54%	16-23%	(Barrow et al., 2006; Brasseur et al., 1995; Daudi et al., 2014; Gure et al., 2005; Noh et al., 2016; Tajima et al., 2003; Zhang et al., 2015)
A2	44-84%	40%	20%	3%	20-31%	(Brasseur et al., 1995; Noh et al., 2016)
A3	48-80%	38-55%	10-26%	3-37%	29-41%	(Ayyoub et al., 2014; Brasseur et al., 1995; Daudi et al., 2014; Filho et al., 2009; Noh et al., 2016; Pineda et al., 2015; Tajima et al., 2003; Zamuner et al., 2015; Zhang et al., 2015)
A4	9-34%	19-65%	13-19%	32-47%	23-47%	(Barrow et al., 2006; Brasseur et al., 1995; Daudi et al., 2014; Noh et al., 2016; Tajima et al., 2003; Zhang et al., 2015)
A6	48-82%	26-50%	28%	5%	31-43%	(Ayyoub et al., 2014; Filho et al., 2009; Noh et al., 2016; Pineda et al., 2015; Zamuner et al., 2015)
A8	4-9%	7%	4%	3%	1-3%	(Yao et al., 2014)
A9	8-23%	69%	16-45%	25-37%	25-33%	(Tajima et al., 2003; Xu et al., 2015)
A10	13-61%	43%	8%	19-52%	13-19%	(Tajima et al., 2003; Zhang et al., 2015)
A11	15-41%	61%	8-67%	33%	18-38%	(Yao et al., 2014)
A12	45-77%	27%	9-15%	5%	13-28%	(Yao et al., 2014)
B1	4-23%	9%	25%	8%	0-7%	(Yao et al., 2014)
B2	10-27%	41%	3%	8%	19-35%	(Pattani et al., 2012)
B3	0%	0%	1%	5%	1%	(Yao et al., 2014)
B4	0%	0%	3%	0%	0%	(Yao et al., 2014)
B6	18-25%	55%	1%	5%	20-27%	(Zamuner et al., 2015)
B16	6-21%	6%	21%	1%	1-4%	(Yao et al., 2014)
B18	9-20%	9%	4%	18%	1-5%	(Yao et al., 2014)
C1	24-62%	28%	5-38%	16-35%	9-13%	(Atanackovic et al., 2010; Brasseur et al., 1995; Daudi et al., 2014; Hou et al., 2016a; Jungbluth et al., 2002; Tajima et al., 2003)
C2	33-67%	21%	8-58%	13%	4-13%	(Hou et al., 2016a; Yang et al., 2014)

a MAGE expression correlates with DNA methylation status (green)

Table 1-2. Correlation between MAGE expression and overall survival in select cancer types

Cancer type	MAGE	Overall survival			References
		HR	CI (95%)	P-value	
Lung	A3	3.226	1.446-7.918	0.004	(Chen, 2017; Gure et al., 2005; Pineda et al., 2015)
	A9	2.334	1.664-3.274	0.001	(Zhang et al., 2015)
	C2	1.909	0.954-3.821	0.068	(Chen, 2017)
Breast	A1	2.285	0.910-5.732	0.078	(Balafoutas et al., 2013)
	A3	3.446	1.00-11.77	0.049	(Balafoutas et al., 2013)
	A9	3.702	1.392-9.845	0.009	(Xu et al., 2014)
	C2	3.07	1.47-12.01	0.003	(Yang et al., 2014)
Ovarian	A9	2.271	1.372-3.761	0.001	(Xu et al., 2015)
Colorectal	A9	2.376	1.380-4.089	0.002	(Zhan et al., 2016)
LSCC	A9	3.57	1.457-8.762	0.005	(Han et al., 2014)
HCC	A9	2.17	1.121-4.205	0.022	(Gu et al., 2014)
ESCC	A11	2.689	1.434-5.040	0.002	(Sang et al., 2016)
Gastric	A12	1.78	1.23-2.58	0.002	(Wu et al., 2017)

HR, hazard ratio; CI, confidence interval

Table 1-3. Clinical trials with MAGEs

MAGE	Tumor type	Phase	Intervention	Identifier	Status
A3	Melanoma	I/II	MAGE-A3.A1 peptide and CpG7909	NCT00145145	Terminated
A3	Melanoma	II	GSK1203486A recombinant MAGE-A3 ASCI	NCT00706238	Terminated
A3	Melanoma	II	GSK2132231A, dacarbazine	NCT00849875	Terminated
A3	Melanoma	III	GSK 2132231A	NCT00796445	Terminated
A3	Lung	I	GSK1572932A, cisplatin, vinorelbine, radiotherapy	NCT00455572	Terminated
A3	Lung	III	GSK1572932A	NCT00480025	Terminated
A3, A12	Metastatic	I/II	anti-MAGE-A3/12 TCR, aldesleukin, cyclophosphamide, fludarabine	NCT01273181	Terminated
A3	Melanoma	I/II	Enhanced TCR Transduced Autologous T Cells	NCT01350401	Ongoing
A3	Multiple myeloma	I/II	Enhanced TCR Transduced Autologous T Cells	NCT01352286	Ongoing
A3, C2	Melanoma	II	TriMix-DC and ipilimumab	NCT01302496	Ongoing
A3, C1	Multiple myeloma	I	CT7, MAGE-A3, and WT1 mRNA-electroporated Langerhans cells (LCs)	NCT01995708	Recruiting
A3	Metastatic	I/II	Anti-MAGE-A3-DP4 TCR, cyclophosphamide, fludarabine, aldesleukin	NCT02111850	Recruiting
A3	Metastatic	I/II	MG1MA3 (MG1 Maraba/MAGE-A3 adenovirus vaccine)	NCT02285816	Recruiting
A10	Urinary bladder, head and neck, melanoma	I	Autologous genetically modified MAGE A10^{c796}T cells	NCT02989064	Recruiting
A10	Lung	I/II	Autologous genetically modified MAGE A10^{c796}T cells	NCT02592577	Recruiting
A3	Lung	I/II	Ad-MAGEA3, MG1-MAGEA3, pembrolizumab	NCT02879760	Recruiting

CHAPTER TWO
Enhanced Stress Tolerance through Reduction of G3BP and Suppression of Stress Granules

INTRODUCTION

Cells regularly encounter a variety of stresses, therefore, one of their largest challenges lies in their ability to respond to and defend against changing conditions. In addition to sensing different insults, cells must select an appropriate course of action in order to engage the proper pathways to ultimately repair, reprogram, or undergo cell death, depending on the type and severity of the damage. Exposure to various stressors, such as oxidative or heat stress, initiate highly coordinated cellular stress response pathways that result in the inhibition of translation, disassembly of polysomes, and reorganization of mRNAs and proteins into stress granules (SG) (Anderson et al., 2015; Kedersha and Anderson, 2002).

SG are conserved, highly dynamic ribonucleoprotein (RNP) condensates that, like other RNP granules, are thought to form through liquid-liquid phase separation (LLPS) via the collective behavior of protein-protein, protein-RNA, and RNA-RNA interactions (Protter and Parker, 2016; Van Treeck and Parker, 2018). A growing body of evidence has linked mutations that increase SG formation or decrease SG clearance to various age-related neurodegenerative diseases (Dobra et al., 2018; Kim et al., 2013; Mackenzie et al., 2017; Molliex et al., 2015; Nedelsky and Taylor, 2019; Patel et al., 2015). Yet, it remains unclear what role SG play during the stress response and how disturbances in SG dynamics might promote disease progression. In fact, SG have been proposed to have both pro-survival and pro-death functions depending on the type and duration of stress; however, the exposure of cells to either acute or chronic stress has been suggested as a determinant between the assembly of protective or harmful SG, respectively (Arimoto et al., 2008;

Reineke and Neilson, 2019; Zhang et al., 2019). Therefore, cells with long lifespans, such as stem cells and neurons, may be especially prone to repeated episodes of stress, and thus, particularly susceptible to the potentially toxic effects associated with SG formation. Intriguingly, the male germline in mammals is extremely vulnerable to heat stress, such that minor increases in testicular temperature result in reduced spermatogenesis and increased risk of infertility (Reid et al., 1981; Rockett et al., 2001; Yin et al., 1997). However, whether these and other stress-prone cells or tissues have acquired mechanisms to modulate their sensitivity to stress and SG dynamics remains unclear.

Recent efforts have focused largely on deciphering the principles that drive SG assembly as well as identifying the protein and RNA constituents of SG (Jain et al., 2016; Khong et al., 2017; Markmiller et al., 2018; Namkoong et al., 2018; Souquere et al., 2009; Wheeler et al., 2016). G3BP1 and its paralog, G3BP2, (collectively referred to as G3BP) are the best characterized SG nucleating proteins and have been shown to be critical for SG assembly, where overexpression induces SG formation in the absence of stress and deletion ablates SG in response to arsenite (Kedersha et al., 2016; Reineke et al., 2012; Zhang et al., 2019). Although the formation of biomolecular condensates is thought to be highly dependent on factors that drive LLPS, such as protein concentrations of key nucleators, whether G3BP protein levels dictate the set point for SG assembly and the cellular stress threshold have not been determined. Moreover, the molecular mechanisms regulating G3BP concentration and whether different cell types or disease states fine-tune G3BP concentration to alter stress tolerance remain unknown.

Melanoma antigen (MAGE) genes encode a family of proteins sharing a common MAGE homology domain (MHD) (Lee and Potts, 2017). Following the emergence of eutherian mammals,

the MAGE family underwent a rapid expansion from a single *MAGE* in lower eukaryotes to more than 50 genes in humans (Lopez-Sanchez et al., 2007). Most MAGEs, including *MAGE-B2*, are located on the X-chromosome and are classified as cancer-testis antigens (CTAs) given that they are primarily expressed in the testis but are aberrantly expressed in cancers (Chomez et al., 2001; Fon Tacer et al., 2019; Weon and Potts, 2015). While the precise mechanisms regulating MAGE expression are not fully understood, a growing body of studies has revealed that MAGEs assemble with E3 RING ubiquitin ligases to form MAGE-RING ligases (MRLs) and act as regulators of ubiquitination in diverse cellular and developmental processes (Doyle et al., 2010; Lee and Potts, 2017). However, the functions of most MAGEs, including MAGE-B2, have not been fully elucidated and their study has been primarily restricted to cancer cells (Peche et al., 2015).

Here, we identify MAGE-B2 as a regulator of the cellular stress response. We demonstrate that MAGE-B2 inhibits SG formation by reducing protein levels of the concentration-dependent SG nucleator, G3BP. Intriguingly, in an unanticipated deviation from prototypical MRLs, MAGE-B2 functions as an RNA binding protein (RBP) that directly binds to the G3BP transcript and inhibits its translation. MAGE-B2 suppresses G3BP translation by displacing the DDX5 RNA helicase which promotes G3BP translation. Importantly, MAGE-B2 expression is restricted to the testis where it maintains stemness of spermatogonial stem cells (SSC). Moreover, mice lacking the MAGE-B2 ortholog exhibit increased sensitivity to heat stress *in vivo* as measured by increased SG assembly, significantly damaged testis histology, and mouse infertility. Together, these results establish that MAGE-B2 protects the highly thermo-sensitive germline from heat stress, suggesting that calibration of G3BP levels and SG formation by MAGE-B2 enhances the cellular stress threshold.

RESULTS

MAGE-B2 regulates stress granule dynamics

To investigate the molecular function of MAGE-B2, we first identified MAGE-B2 interactors by tandem affinity purification (TAP) coupled to mass spectrometry (TAP-MS) using HEK293 cells stably expressing either the TAP empty vector or TAP-MAGE-B2. Analysis of the proteins that were present in the TAP-MAGE-B2 purification but absent in the control TAP vector alone, revealed an enrichment for RBPs, particularly those localizing to SG (Figure 2-1A). Intriguingly, a previous report characterizing the human RNA-binding proteome identified MAGE-B2 as an RBP (Trendel et al., 2019). Therefore, we examined whether MAGE-B2 localizes to SG in U2OS cells. Although MAGE-B2 did not co-localize with the critical SG factor, G3BP1, within SG (Figure 2-2A), depletion of MAGE-B2 by three independent siRNAs resulted in significantly increased SG formation in response to the oxidative stressor, sodium arsenite (Figures 2-1B and 2-2B-D). This enhanced SG phenotype was not the result of spontaneous SG formation (Figure 2-1C) and was not restricted to U2OS cells, as depletion of MAGE-B2 in HCT116 cells also led to increased SG numbers (Figures 2-1D and E). Furthermore, these results were not specific to oxidative stress, as knockdown of MAGE-B2 led to increased SG formation upon ER stress (thapsigargin), heat stress (Figures 2-1B and 2-2D), and translation inhibition (rocaglamide A) in a dose-dependent manner (Figures 2-2E-G). Consistent with transient MAGE-B2 knockdown, MAGE-B2 knockout by CRISPR-Cas9 also resulted in increased SG formation (Figure 2-1F) that

could be rescued by re-expression of MAGE-B2 (Figures 2-1G and 2-2H). Furthermore, overexpression of MAGE-B2 reduced G3BP1 expression and SG formation in cells treated with 500 μM sodium arsenite (Figures 2-1H and 2-2I). We next examined the impact of MAGE-B2 depletion on SG dynamics by live-cell imaging of U2OS cells stably expressing G3BP1-GFP. Knockdown of MAGE-B2 both enhanced SG assembly and delayed SG disassembly (Figures 2-1I-L and 2-2J). Given the observed changes on SG assembly, we also determined whether P-bodies, which are RNA granules closely related to SG, are affected by MAGE-B2 depletion; yet P-body assembly was not significantly altered upon MAGE-B2 depletion (Figure 2-1M).

To determine whether MAGE-B2 regulation of SG dynamics has a functional outcome on cells, we measured the viability of wildtype and MAGE-B2 knockout U2OS cells in response to sodium arsenite. MAGE-B2 knockout cells exhibited hypersensitivity to prolonged low dose sodium arsenite as measured by reduced cell viability that could be rescued by re-expression of MAGE-B2 (Figure 2-2K). Importantly, wildtype and MAGE-B2 knockout cells grew at similar rates in the absence of stress (Figure 2-1N). Together, these results suggest that MAGE-B2 inhibits SG formation in response to multiple stressors and that this activity is important for protecting cells against prolonged stress.

MAGE-B2 modulates SG formation through regulation of G3BP protein levels

Given that MAGE-B2 overexpression led to reduced overall G3BP1 signal by immunostaining (Figure 2-1H), we hypothesized that MAGE-B2 modulates SG formation by regulating G3BP protein levels. Indeed, depletion of MAGE-B2 by knockdown (Figures 2-3A and B) or knockout

(Figures 2-3C and D) resulted in increased G3BP protein expression. Conversely, overexpression of MAGE-B2 reduced G3BP and re-expression of MAGE-B2 in MAGE-B2 knockout cells rescued G3BP protein levels (Figures 2-3E and F). Importantly, these changes in protein expression were specific to G3BP, such that other SG-associated RBPs were unaffected by MAGE-B2 knockout (Figure 2-4A). To determine whether MAGE-B2-mediated regulation of G3BP protein levels is responsible for altering SG formation, we rescued G3BP expression in MAGE-B2 depleted cells by concomitantly knocking down G3BP to similar levels as control cells (Figures 2-3G-H and 2-4B). Rescue of G3BP protein back to control levels in MAGE-B2 depleted cells not only rescued the SG phenotype (Figures 2-3I and 2-4C), but also cell viability under prolonged stress (Figure 2-3J). These results suggest that G3BP protein levels are suppressed by MAGE-B2 and this alters the tolerance of cells to stress conditions.

Cellular SG assembly dynamics is dependent on G3BP concentration

Like many other membrane-less organelles, SG are thought to form via LLPS, a biophysical process driven by weak multivalent protein-protein, protein-nucleic acid, and nuclei acid-nucleic acid interactions to create discrete cytoplasmic foci. The crucial molecular features of phase separating proteins include multivalency (tandem arrays of modular domains) and intrinsically disordered regions (IDR), like those found in G3BP (Figure 2-4D). These proteins phase separate into liquid droplets *in vitro* when their total concentration exceeds a critical threshold, and they return back to a one-phase state once the total concentration drops below the threshold.

Because our results suggest that G3BP protein levels dictate SG dynamics and G3BP has been shown to be a key scaffold for SG assembly, we hypothesized that even modest alterations in G3BP protein levels would contribute to significant changes in SG formation. In order to precisely determine the correlation between G3BP expression and SG initiation time, we transfected G3BP knockout U2OS cells with varying levels of GFP-G3BP1 and determined SG initiation time. Interestingly, the relationship between G3BP1 protein levels and SG kinetics was not linear. Rather, the relationship was switch-like, such that cells expressing G3BP1 beyond the critical threshold exhibited enhanced SG assembly (Figures 2-3K and 2-4E), which is consistent with the concept that phase separation is dictated by a critical threshold concentration. Examination of endogenous G3BP1 protein concentrations in wildtype cells revealed that G3BP1 levels are normally maintained just below the threshold (Figures 2-3L and 2-4F). However, MAGE-B2 knockout significantly increased G3BP1 beyond the threshold (Figures 2-3L and 2-4F). In line with these findings, overexpression of G3BP1 was sufficient to increase SG formation similarly to MAGE-B2 knockout (Figures 2-3M and 2-4G). Furthermore, *in vitro* phase separation assays confirmed that small (two-fold) changes in G3BP1 concentration, similar to those observed upon MAGE-B2 knockout, have dramatic effects on G3BP1 LLPS (Figures 2-3N and 2-4H). Together, these results suggest that similar to *in vitro* findings, biomolecular condensates in cells are highly dependent on protein concentration; moreover, cells have evolved mechanisms to precisely modulate condensate assembly by directly controlling the key proteins that drive their formation.

MAGE-B2 downregulates G3BP by translational repression

To determine the mechanism by which MAGE-B2 decreases G3BP protein levels, we tested three potential modes of regulation: transcription, protein stability, and translation. We found that MAGE-B2 did not affect *G3BP1* transcript levels in U2OS, HCT116, or HeLa cells (Figures 2-5A, 2-6A and B). Our lab and others have previously demonstrated that MAGEs assemble with E3 RING ubiquitin ligases to form MAGE-RING ligases (MRLs) and act as regulators of ubiquitination by modulating ligase activity, substrate specificity, or subcellular localization (Doyle et al., 2010; Hao et al., 2013; Lee and Potts, 2017; Pineda et al., 2015). Therefore, we hypothesized that MAGE-B2 might promote degradation of G3BP. Unexpectedly, G3BP1 protein half-life as measured by ^{35}S-methionine/cysteine pulse-chase was unaffected by MAGE-B2 knockout (Figure 2-5B). In addition, proteasomal inhibition by MG132 in U2OS or HeLa cells did not alter G3BP1 protein levels (Figures 2-6C and D, respectively), consistent with its relatively long protein half-life (~12 hrs; Figure 2-5B). Together, these data suggest that MAGE-B2 does not regulate G3BP1 protein levels via the ubiquitin-proteasome system.

Although the G3BP1 protein half-life was unchanged by MAGE-B2, the relative amounts of ^{35}S-labeled G3BP1 immediately after 1 hr pulse labeling indicated that G3BP1 protein synthesis was enhanced in MAGE-B2 knockout U2OS cells (Figure 2-5B, inset). Indeed, ^{35}S-methionine/cysteine incorporation assays revealed significantly increased G3BP1 translation in MAGE-B2 knockout cells (Figure 2-5C). Consistent with our finding that the protein levels of other SG-associated RBPs were unaffected by MAGE-B2 knockout (Figure 2-4A), MAGE-B2-mediated regulation of G3BP1 translation is specific and not the result of altered global translation as determined by global ^{35}S-methionine/cysteine incorporation assays or polysome profiling

(Figures 2-5D and 2-6E). Together, our results suggest that MAGE-B2 regulates cellular G3BP protein concentrations by downregulating its translation.

DDX5 mediates MAGE-B2-dependent regulation of G3BP and SG formation

To determine how MAGE-B2 regulates G3BP translation, we hypothesized that MAGE-B2 might affect RBPs bound to *G3BP* UTRs, either by recruiting a translational inhibitor or displacing a translational activator. Therefore, we utilized RNA pulldowns and mass spectrometry to unbiasedly identify proteins differentially bound to *G3BP1* mRNA upon knockout of MAGE-B2. RNA pulldowns from wildtype or MAGE-B2 knockout U2OS cells using biotinylated RNAs consisting of the Luciferase coding sequence (*Luc* CDS) flanked by the *G3BP1* UTRs (bait RNA) or the *Luc* CDS alone (control RNA) were performed and analyzed by mass spectrometry. Interestingly, five RBPs (DDX5, DDX17, DHX30, HNRNPC, and SAFB) bound specifically to the bait RNA in MAGE-B2 knockout cells, but not in wildtype cells or to the control *Luc* CDS RNA (Figure 2-5E). Notably, a previously described regulator of G3BP1 translation, YB1, was not identified in any RNA pulldowns and its depletion did not affect G3BP1 levels (Figure 2-6F). However, knockdown of the five candidate RBPs, in wildtype or MAGE-B2 knockout U2OS cells revealed that DDX5 depletion specifically decreased G3BP protein levels in MAGE-B2 knockout cells, but not wildtype cells (Figures 2-5F-H and 2-6G). Additionally, DDX5 protein levels were similar in MAGE-B2 wildtype and knockout cells (Figure 2-5G). DDX5, also referred to as p68, is a DEAD-box RNA helicase that has been shown to have a number of functions including microRNA processing (Dardenne et al., 2014); however knockdown of AGO2 did not alter G3BP1

protein levels (Figure 2-6H), suggesting that DDX5-mediated regulation of G3BP1 is independent of its role in microRNA processing. Importantly, knockdown of DDX5 in MAGE-B2 knockout U2OS cells returned both G3BP1 translation (Figures 2-5I and J) and SG formation (Figures 2-5K and L) to the wildtype phenotype without affecting global translation (Figure 2-6I) or *G3BP1* transcript levels (Figure 2-6J). These data suggest that DDX5 mediates the enhanced G3BP translation and SG phenotypes observed in MAGE-B2-depleted cells.

MAGE-B2 and DDX5 have opposing roles in the regulation of G3BP1 translation

We found that MAGE-B2 represses G3BP1 translation and in its absence DDX5 promotes G3BP1 translation, suggesting that MAGE-B2 and DDX5 may have opposing, competing roles. To experimentally determine whether MAGE-B2 and DDX5 bind *G3BP1* mRNA in an opposing fashion, we performed CLIP-qPCR. We found that MAGE-B2 and DDX5 interact with the *G3BP1* transcript (Figure 2-7A-C). However, DDX5 interaction inversely correlated with MAGE-B2 expression, such that expression of MAGE-B2 decreases DDX5 binding to *G3BP1* transcript (Figure 2-7B), whereas MAGE-B2 knockout increases DDX5 interaction with *G3BP1* transcript (Figure 2-7C). Furthermore, using RNA pulldown experiments, we found that MAGE-B2 bound *in vitro* transcribed bait *Luc* CDS with *G3BP1* UTRs, but not control *Luc* CDS alone RNA (Figure 2-7D). Importantly, DDX5 only bound the *G3BP1* RNA in the absence of MAGE-B2 (Figure 2-7D). Thus, MAGE-B2 and DDX5 bind to the *G3BP1* transcript in an opposing fashion.

To further characterize the mechanism by which MAGE-B2 and DDX5 regulate G3BP1 translation, we performed *in vitro* translation assays using a luciferase reporter in which the *G3BP1*

5' UTR, 3' UTR, both, or neither were included. We found that recombinant MAGE-B2 had no effect on translation of the reporters (Figures 2-7E and 2-8A). However, recombinant DDX5 promoted translation of the reporter (Figures 2-7E and 2-8A). Furthermore, this activity was dependent on the 5' UTR of *G3BP1* (Figures 2-7E and 2-8A-C). In addition, the helicase activity of DDX5 was required for enhanced translation *in vitro*, as addition of DDX5 K144N had minimal effect on translation in comparison to wildtype DDX5 (Figure 2-7F). Previous reports have identified DDX5 binding motif consensus sequences (Lee et al., 2018). Scanning of the *G3BP1* 5' UTR revealed a putative 10 nucleotide DDX5 recognition sequence (Figure 2-7G). Deletion of the putative DDX5-binding motif within the *G3BP1* 5' UTR ablated DDX5's ability to increase translation (Figure 2-7G) and bind to the *G3BP1* 5' UTR (Figure 2-7H). Interestingly, deletion of the DDX5 recognition sequence also inhibited MAGE-B2 binding to the *G3BP1* 5' UTR, suggesting that MAGE-B2 and DDX5 compete for the same region of the *G3BP1* 5' UTR (Figure 2-7H).

Therefore, we utilized the *in vitro* translation system to test for competition between MAGE-B2 and DDX5. Indeed, titrating increasing amounts of MAGE-B2 could inhibit DDX5's ability to promote translation (Figures 2-7I and 2-8D-F). Consistent with a competition model, we did not observe binding between MAGE-B2 and DDX5 (Figures 2-8G-J). These results suggest that DDX5 is a key factor in determining G3BP1 translation and that this can be modulated by MAGE-B2 competition for *G3BP1* 5' UTR binding. Interestingly, when comparing the basal translation of our reporter constructs, we found that the *G3BP1* 5' UTR had a suppressive effect on translation (Figure 2-7J), which might suggest that the 5' UTR contains a structural element that must be unwound by DDX5 for efficient translation. Overall, these findings suggest that

MAGE-B2 and DDX5 act as key regulators of G3BP concentration to fine-tune the cellular stress response through controlling SG assembly dynamics (Figure 2-7K).

The mouse ortholog of human MAGE-B2 (Mage-b4) regulates stemness of spermatogonial stem cells

Given our findings that MAGE-B2 regulates the SG response in cells, we sought to determine how this mechanism relates to normal physiology. To examine the expression pattern of *MAGE-B2*, we analyzed a panel of 26 human tissues by RT-qPCR and found that human *MAGE-B2* is restricted to expression in the testis (Figure 2-9A), which was consistent with *MAGE-B2* expression data from the Genome Tissue-Expression (GTEx) dataset of 53 disease-free human tissues (Figure 2-10A). We extended these analyses to characterize its expression profile in two mouse strains (BALB/C and C57BL/6) by RT-qPCR and found that the mouse ortholog of human *MAGE-B2*, *Mage-b4*, is predominantly expressed in the testis (Figures 2-9B and 2-10B). Notably, we found that *Mage-b4* underwent a gene duplication event in the mouse that resulted in a second copy (paralog), *Mage-b10*, which is 100% identical to *Mage-b4* within the MHD and only varies in the number of repetitive C-terminal elements that results in an 88 amino acid deletion (Figure 2-10C). Consistently, *Mage-b10* was also largely restricted to expression in the testis (Figure 2-10D). Given their high sequence identities and similar expression profiles, we refer to these two genes simply as *Mage-b4* herein.

We next sought to determine in which cell type MAGE-B2 and its ortholog are expressed in the testis. Immunohistochemistry staining of human testis sections revealed that MAGE-B2

protein is enriched in spermatogonia (Figure 2-9C). Likewise, immunohistochemistry analysis of the mouse testis revealed that Mage-b4 co-localized with PLZF, a marker for undifferentiated spermatogonia including spermatogonial stem cells (SSC) (Figure 2-9D) (Osterlund et al., 2000). These findings are consistent with previous work from our lab demonstrating that Mage-b4 is enriched in spermatogonia based on developmental timing, cell sorting, and $Kitl^{Sl}/Kitl^{Sl\text{-}d}$ (steel) mice lacking spermatocytes (Fon Tacer et al., 2019). Furthermore, previously published single cell RNA-sequencing data also suggest that Mage-b4 is primarily expressed in spermatogonia (Figure 2-9E) (Lukassen et al., 2018). Additionally, single cell RNA-sequencing results identified Mage-b4, along with PLZF, as a unique marker of undifferentiated mouse spermatogonia (Jung et al., 2019). MAGE-B2 was also shown to be enriched in spermatogonia in human testis by single cell RNA-sequencing (Guo et al., 2018; Sohni et al., 2019; Xia et al., 2020).

To determine whether Mage-b4 expression is important for SSC maintenance, we utilized primary cultures of undifferentiated spermatogonia from mice expressing an Id4-eGFP reporter transgene (Chan et al., 2014). Previous work described cells exhibiting high levels of reporter expression ($EGFP^{Bright}$) as stem cells, whereas cells with low levels of reporter expression ($EGFP^{Dim}$) include progenitor fractions (Chan et al., 2014). Knockdown of Mage-b4 decreased the fraction of $EGFP^{Bright}$ SSCs and increased the fraction of $EGFP^{Dim}$ progenitor cells to a similar degree as a known regulator of SSC maintenance, Rb1 (Figure 2-9F) (Yang et al., 2013). Knockdown of Id4 was included as a positive control that increases the $EGFP^{Bright}$ cell population due to a compensatory up-regulation of Id4-eGFP (Oatley et al., 2011). To determine whether Mage-b4 affects stem cell function *in vivo*, we performed spermatogonial transplantation assays (Brinster and Zimmermann, 1994) in which we depleted Mage-b4 in primary cultures of

spermatogonia expressing a Rosa26-LacZ transgene before transplantation into the testes of recipient males lacking germ cells. The efficiency of the transplanted cells to repopulate the recipient males' testes was determined by counting the number of LacZ-positive colonies clonally derived from a single transplanted SSC. Knockdown of Mage-b4 resulted in a significantly reduced ability to repopulate testes after transplantation into mice (Figure 2-9G and H), demonstrating a key role for Mage-b4 in regulating SSC function both *in vitro* and *in vivo*.

The MAGE-B2 ortholog in mouse regulates G3BP1 and SG formation

Given our results that MAGE-B2 regulates the stress response through repression of G3BP translation and SG, we reasoned that MAGE-B2 and its ortholog Mage-b4 may be important for controlling SG dynamics in SSC. Therefore, we utilized CRISPR-Cas9 to generate mice deficient in Mage-b4 and its paralog Mage-b10 (Figure 2-11A) and test their role *in vivo*. To confirm that Mage-b4 is the functional ortholog of human MAGE-B2, we measured G3BP1 protein levels and SG formation in primary cell cultures of undifferentiated spermatogonia from wildtype or Mage-b4 knockout mice. Consistent with human MAGE-B2 function, we found that Mage-b4 knockout SSC exhibited increased G3BP1 protein levels (Figures 2-11B and C) and enhanced SG formation when treated with sodium arsenite (Figures 2-11D and E).

Next, we investigated whether Mage-b4 regulates G3BP1 and SG assembly *in vivo*. Because Mage-b4 is only expressed in a small subpopulation of cells within the testis, we utilized immunofluorescent staining of G3BP1 to quantify the intensity of G3BP1 specifically in spermatogonia where Mage-b4 is expressed. In line with our findings from cancer cell and primary

cell cultures, Mage-b4 KO mice exhibited increased levels of G3BP1 (Figures 2-11F and G). To induce SG *in vivo,* wildtype or Mage-b4 knockout mice were partially submerged in a control (33 °C) or heated water bath (38 °C or 42 °C) for 15 minutes to heat stress their lower extremities, including the testes. SG formation was analyzed by G3BP1 immunostaining of the testes. Consistent with the enhanced SG induction seen in Mage-b4 knockout primary cell culture, we found that the Mage-b4 knockout mice exhibited increased SG formation in response to heat, specifically in spermatogonia that normally express Mage-b4 (Figures 2-11H and I).

The MAGE-B2 ortholog in mouse protects the male germline from heat stress

General characterization of the Mage-b4 knockout mouse revealed a modest reduction in testis weight (Figure 2-12A) whereas various other tissues were unaffected (Figures 2-12B-G). Fertility tests including pregnancy rate, litter size, sperm counts, and sperm motility revealed no significant defects in the fertility of male Mage-b4 knockout mice under standard laboratory conditions (Figures 2-12H-K and 2-13A). These data suggest that Mage-b4 is not required for male fertility under non-stressed conditions. This finding may not be surprising given the recent evolution of Mage-b4 in eutherian mammals (Katsura and Satta, 2011; Lee and Potts, 2017).

Spermatogenesis is a highly thermo-sensitive process such that maintenance of the testes at a temperature 4-5 °C lower than core body temperature is required for proper sperm production (Widlak and Vydra, 2017). Even modest increases in temperature can lead to apoptosis of germ cells, impaired spermatogenesis, and reduced testes weight (Reid et al., 1981; Rockett et al., 2001; Yin et al., 1997). Intriguingly, previous studies suggest that the early stages of spermatogenesis,

which includes less differentiated cell types such as spermatogonia, exhibit a higher threshold of heat stress tolerance than later stages (Reid et al., 1981; Rockett et al., 2001; Yin et al., 1997). Therefore, we speculated that Mage-b4 may have evolved in mammals to protect the male germline from mild heat stresses. Given that MAGE-B2 inhibition of SG formation is important for protecting cells against prolonged stress (Figures 2-2K and 2-3J), we determined whether Mage-b4 is important for spermatogenesis after heat stress. The testis of wildtype and Mage-b4 knockout mice were heat stressed for 15 min at 42 °C and were analyzed 2, 4, or 6 weeks later to allow enough time for two rounds of spermatogenesis. Strikingly, heat stress caused significantly greater reduction in the testis weight of Mage-b4 knockout mice compared to wildtype mice (Figure 2-12L). Histological analysis of testis from heat stressed mice revealed an increased number of damaged seminiferous tubules in Mage-b4 knockout mice compared to wildtype mice (Figures 2-12M-N and 2-13B-C). Moreover, Mage-b4 knockout mice had reduced fertility after heat stress compared to wildtype mice (Figure 2-13D). Interestingly, Mage-b4 knockout mice treated with the genotoxic agent busulfan did not significantly differ from wildtype mice in terms of testis weight (Figure 2-12O) or testis histology (Figures 2-12P and Q), suggesting that SSC in Mage-b4 knockout mice are not generally more sensitive to all types of stress.

We then sought to establish whether the phenotypes observed in Mage-b4 knockout mice are mediated through changes in G3BP1 levels. Due to the embryonic lethality of G3BP1 knockout mice (Martin et al., 2013), we utilized mice expressing a G3BP1-GFP transgene (Tg-G3BP1), thereby effectively mimicking the excess G3BP1 seen in Mage-b4 knockout mice (Figure 2-12R). Upon exposure to heat stress, the Tg-G3BP1 mice not only exhibited enhanced SG formation (Figures 2-12S and T), but also an increased number of damaged seminiferous tubules (Figures 2-

13E and F). These *in vivo* findings in conjunction with our *in vitro* data support the notion that Mage-b4-mediated suppression of G3BP1 protein levels results in reduced SG assembly and altered stress tolerance.

Given the striking disparity in the ability of wildtype and Mage-b4 knockout mice to cope with heat stress, we utilized RNA-sequencing to investigate transcriptional differences that occur 72 hr after a 20 min exposure to heat stress. Control treated mice did not display any significant differences in their global gene expression; however, following heat stress, Mage-b4 knockout and wildtype mice exhibited remarkably distinct gene profiles (Figure 2-13G and 2-14A). Interestingly, transcripts previously identified to be enriched in SG (Jain et al., 2016; Khong et al., 2017; Markmiller et al., 2018; Namkoong et al., 2018; Souquere et al., 2009; Wheeler et al., 2016) were overrepresented (χ^2, $p<0.000001$) in Cluster 1 of heat stress-induced transcripts that were differentially expressed between wildtype and Mage-b4 knockout mice (Figure 2-13H). Moreover, unbiased gene ontology analysis of Cluster 1 revealed a significant enrichment of lysosomal genes (Figure 2-14B and C). Genes encoding components of lysosomes were dramatically upregulated upon heat stress in testis of wildtype mice, but this response was significantly blunted in Mage-b4 knockout testis (Figure 2-13I). Lysosomes are not only key facilitators of cellular waste clearance (such as protein aggregation and organelle damage), but are also essential for integrating environmental cues. Lysosomal clearance of misfolded proteins is critical for cellular adaptation and survival in response to various stressors (Kaushik and Cuervo, 2018; Raben and Puertollano, 2016). Our findings suggest that Mage-b4 allows for a greater capacity of stress-induced cellular damage.

Finally, we investigated the effect of heat stress on spermatogenesis markers and discovered that early stage spermatogenesis markers were significantly upregulated in wildtype heat stressed samples relative to Mage-b4 knockout samples (Figure 2-13J). Collectively, these data suggest that Mage-b4 evolved to maintain the highly sensitive process of spermatogenesis in the face of fluctuating environmental temperatures by protecting germline cells in the testis.

DISCUSSION

In this study, we identify a testis-specific factor, MAGE-B2, as a previously unknown regulator of the cellular stress response. Unlike previously characterized MAGE proteins, MAGE-B2 is an RBP that functions as a translational repressor of the essential SG nucleator, G3BP. Mechanistically, MAGE-B2 inhibits G3BP translation by competing with the translational activator, DDX5. Importantly, the fine-tuned suppression of SG that results from reduced G3BP protein levels increases the cellular stress threshold such that expression of MAGE-B2 allows for protection of the male germline from heat stress.

SG assembly is a multi-step process that typically begins with phosphorylation of the eukaryotic initiation factor 2α by a stress-sensing kinase to inhibit global translation (Sonenberg and Hinnebusch, 2009). The reduction of available 48S pre-initiation complex leads to polysome disassembly and the accumulation of untranslating mRNAs in the cytoplasm that can associate with G3BP and coalesce into SG cores (Kedersha and Anderson, 2002). These SG cores can then recruit additional IDR-containing RBPs, which mediate the assembly of additional proteins to form the mature SG consisting of a core and shell (Jain et al., 2016; Wheeler et al., 2016). As a highly

coordinated biological process, SG can be regulated at multiple stages. Although knowledge of the biophysical drivers underlying SG formation (Kato et al., 2012; Molliex et al., 2015; Protter and Parker, 2016) and the RNA and protein composition of assembled SG is rapidly growing (Banani et al., 2016; Khong et al., 2017; Markmiller et al., 2018; Namkoong et al., 2018), our understanding of their regulation in typical physiological conditions is relatively limited. We find that MAGE-B2 modulates the stress response by directly regulating G3BP protein levels to suppress SG formation, thereby enhancing the tolerance to stress.

Like other RNP granules, SG are thought to form through the biophysical process of LLPS (Alberti et al., 2017; Protter and Parker, 2016). Phase separating proteins coalesce into liquid droplets *in vitro* when their concentration exceeds a critical threshold (Alberti, 2017). We demonstrate that this holds true for the key driver of SG phase separation, G3BP1. Moreover, we extend these *in vitro* studies to demonstrate the switch-like behavior between G3BP1 protein levels and SG initiation in cells and find that although MAGE-B2 has a modest effect on G3BP protein levels (two-fold), this change can have significant impact on SG formation.

What is the result of suppressed SG formation? Evidence supporting both pro-survival and pro-death functions of SG have been reported (Reineke and Neilson, 2019). However, a growing body of evidence suggests that disturbances in SG dynamics drives several age-related neurodegenerative diseases including amyotrophic lateral sclerosis, frontotemporal dementia, and inclusion body myopathy (Hackman et al., 2013; Mackenzie et al., 2017; Patel et al., 2015; Ramaswami et al., 2013). A number of disease-causing mutations affect SG disassembly and clearance and have been suggested to evolve into the aggregate pathology due to the increased risk of uncontrolled protein aggregation that accompanies high local concentrations of intrinsically

disordered proteins. While it is not clear how the formation of these stable aggregates leads to the associated diseases, one model proposes that the increased predisposition to aggregate promotes promiscuous interactions within SG and increases the likelihood of SG to accumulate misfolded proteins, thereby impairing SG function. Likewise, disrupted SG clearance could compromise the function of RBPs that become trapped within aggregating SG and inhibit the synthesis of proteins essential for cell adaptation. Therefore, the suppression of SG and enhanced SG disassembly via regulation of G3BP protein levels by MAGE-B2 could reduce the risk of pathological aggregation, especially under chronic or repeated stress exposures that is common for the unique environment of SSC in the testis.

Recent biochemical and biophysical studies have demonstrated that MAGEs assemble with E3 RING ubiquitin ligases to form MAGE-RING ligases (MRLs) and function as regulators of ubiquitination in a multitude of cellular processes (Lee and Potts, 2017). The finding that MAGE-B2 regulates G3BP protein levels through translational regulation rather than ubiquitination was unprecedented. Approximately two thirds of MAGE-B2's protein sequence consists of the highly conserved MHD that is shared among all human MAGEs. While it is possible that MAGE-B2's MHD confers this unexpected function, it is likely that the N-terminal region outside the MHD contains an RNA recognition motif. In fact, the N-terminal region of MAGE-B2 (and mouse Mage-b4) includes a conserved 20 amino acid region enriched with basic residues (pI = 12.5), suggesting a potential interface for RNA binding. Whether other MAGEs, particularly those in the MAGE-B subfamily, share the capacity to bind RNA and the identification of other potential targets for translational repression will require further investigation.

DDX5, like other members of the DEAD box family of RNA helicases, is a multifunctional protein with roles in transcription as well as RNA and miRNA processing. Consistent with its functions in mediating various steps of gene expression, our results ascribe DDX5 with a role in translational regulation. *In vitro* translation assays revealed that DDX5 helicase activity was required for the enhanced translation of G3BP1 (Figure 4G). One possibility is that DDX5 unwinds and remodels a structural element within *G3BP1* 5' UTR to allow for efficient translation. Interestingly, DDX5 was recently implicated as an inhibitor of translation (Hoch-Kraft et al., 2018). Further interrogation into how DDX5 achieves these opposing functions and the factors that dictate whether DDX5 activates or represses translation will provide informative insights into DDX5 mechanism of action.

Spermatogenesis is an intricate developmental process that depends on proper SSC maintenance to allow for the continuous production of sperm (de Rooij, 2017). In most mammals, testes are located in the scrotum outside the body, which allows spermatogenesis to occur at optimal temperatures substantially lower (4-5 °C) than the core body temperature (Widlak and Vydra, 2017). Spermatogenesis is highly thermo-sensitive such that elevated testicular temperature results in germ cell apoptosis, compromised sperm quality, and increased risk for infertility (Reid et al., 1981; Rockett et al., 2001; Yin et al., 1997). Although the detrimental effects of increased testicular temperature on spermatogenesis in mammals has been established for many years, the reasons why most mammals have evolved to maintain their testes at low temperatures remain unclear. Moreover, little is known about molecular mechanisms that have evolved to protect spermatogenesis from unstable temperature fluctuations, but regulation of SGs and mRNPs is an emerging concept for controlling germline stem cell homeostasis (Zhou et al., 2017). Given our

findings that MAGE-B2-mediated modulation of G3BP and the stress response allowed for enhanced survival of cultured U2OS cells in the presence of oxidative stress (Figures 1L and 2G), we postulate that within the testis, SSC endogenously expressing MAGE-B2 utilize this function to allow for preservation of spermatogenesis in the presence of heat stress. Unfortunately, due to the embryonic lethality of G3BP1 knockout mice (Martin et al., 2013), precise determination of whether Mage-b4 protects germline cells through modulation of G3BP will not be trivial. Nonetheless, these findings suggest possible new routes for development of male fertility therapies through modulation of MAGE-B2, G3BP, and SG.

MAGEs are an evolutionarily ancient protein family, however, the type I MAGE CTAs only recently evolved in eutherians through a rapid expansion. Recent work from our lab revealed that the MAGE-A subfamily of MAGE CTAs evolved to protect primary spermatocytes against nutrient and genotoxic stress (Fon Tacer et al., 2019). Here, we propose that MAGE-B2 protects spermatogonial cells against heat stress through modulation of SG dynamics. Given the recent evolution of MAGE CTAs, it is perhaps not surprising that MAGE-B2 does not appear to impact basal spermatogenesis. Rather, MAGE-B2 serves as a mechanism to fine-tune the heat stress response in SSCs. This raises the question of whether such a mechanism might allow for the transmission of potentially damaged genetic material. Interestingly, it has been reported that heat stress does not induce pro-survival pathways via activation of heat shock transcription factors (HSFs) in meiotic and post-meiotic cells germ cells; rather, these cells undergo apoptosis, presumably to mitigate such unfavorable outcomes (Kus-Liskiewicz et al., 2013; Widlak and Vydra, 2017). Therefore, it is conceivable that the elevated heat stress threshold of SSC allows these select cells to survive and restore spermatogenesis, thereby preventing permanent

azoospermia. Although most models of cellular stress management view each cell as autonomous sensory units, it is likely that this coordinated response provides a more systemic survival program to preserve fertility of the organism as a whole.

In summary, our work demonstrates that MAGE-B2 attenuates SG formation through translational inhibition of the SG nucleator, G3BP. Moreover, we provide evidence that the selective expression of MAGE-B2 in testis provides germline cells with an enhanced stress tolerance to maintain fertility in the face of stressful heat conditions, suggesting that the MAGE family evolved specifically to protect the male germline in eutherian mammals during times of stress.

EXPERIMENTAL PROCEDURES

Animals

Mage-b4/Mage-b10 knockout mice and G3BP1-GFP transgenic mice were generated by the transgenic/gene knockout shared resource facility at St. Jude Children's Research Hospital. Mage-b4/Mage-b10 knockout mice were generated by injecting sgRNA (targeting both *Mage-b4* and *Mage-b10*) and Cas9 protein in the pronucleus and cytoplasm of C57BL/6 zygote. G3BP1-GFP transgenic mice were generated by injecting a digested fragment of pSF-CAG-hG3BP1-GFP vector into the pronucleus of FVB/NJ zygotes. All animals were crossed at least six generations before experimentation. Animals were group housed under standard conditions. All studies were

approved by the St. Jude Children's Research Hospital institutional review committee on animal safety.

Cell lines

All cell lines were maintained at 37 °C with 5% CO_2 and passaged when reaching 70-90% confluency. U2OS, HCT116, HeLa, and HEK293 cells were grown in DMEM supplemented with 10% fetal bovine serum (FBS), 2 mM L-glutamine, 100 units/mL penicillin, 100 mg/mL streptomycin, and 0.25 mg/mL Amphotericin B. G3BP KO (both G3BP1 and G3BP2) U2OS cells and U2OS cells stably expressing G3BP1-GFP have been previously described (Figley et al., 2014; Zhang et al., 2018). Cell lines were authenticated by STR analysis. Sex of cells used: Female, HEK293, U2OS, HeLa; Male, HCT116.

Microbe strains

DH5α (Thermo Fisher Scientific, #18265017) and XL1-blue (Agilent,#200130) competent cells were used for molecular cloning and plasmid amplification. One shot Stbl3 competent cells (Life Technologies, #C7373-03) were used for lentiviral plasmids. BL21-codon plus (DE3)-RILP competent cells (Agilent Technologies, #230280) were used for recombinant protein production and purification. Bacteria were cultured under laboratory standard conditions at 37 °C, 225 rpm.

Transfections and siRNA sequences

siRNA and plasmid transfections were performed using Lipofectamine RNAiMAX (Invitrogen) and Effectene (QIAGEN), respectively, according to the manufacturers' instructions. siRNAs were purchased from Sigma. Sequences of siRNAs: control: Sigma MISSION siRNA Universal Negative Control #1, MAGE-B2 #1: 5'-CGUUACAAAGGGAGAAAUG-3', MAGE-B2 #2: 5'-GGCAGAUUCUUUACUUUGU-3', MAGE-B2 #3: 5'-GUGGUCAAUUCUUGGUUUA-3', G3BP1 #1: 5'-CAAAUCAGAGCUUAAAGAU-3', G3BP1 #2: 5'-CUGAUGAUUCUGGAACUUU-3', G3BP2 #1: 5'-CUCUGAACCAGUUCAGAGA-3', G3BP2 #2: 5'-GAGCUAAAGGAAUUCUUCA-3', DDX5 #1: 5'-CUGAUAGGCAAACUCUAAU-3', DDX5 #2: 5'-CUACCUUGUCCUUGAUGAA-3', DDX17 #1: 5'-GCCAAUACACCUAUGGUCA-3', DDX17 #2: 5'-CCAAUACACCUAUGGUCAA-3', DHX30 #1: 5'-GACAUCUUGCCCUUGGGCA-3', DHX30 #2: 5'-CCUAUCACAGGCAAGCCCU-3', HNRNPC #1: 5'-GAUGAAGAAUGAUAAGUCA-3', HNRNPC #2: 5'-CUCAUUUAGUUGAGUAGCU-3', SAFB #1: 5'-GAUGAUAAAUGUGACAGAA-3', SAFB #2: 5'-GUAAUCCUGACGAAAUUGA-3', ID4 #1: 5'-CAACAAGAAAGUCAGCAAA-3', ID4 #2: 5'-GAGAUCCUGCAGCACGUUA-3', ID4 #3: 5'-GCGAUAUGAACGACUGCUA-3', ID4 #4: 5'-CCGUGAACAAGCAGGGUGA-3', RB1 #1: 5'-GGAGUUUGAUUCCAUUAUA-3', RB1 #2: 5'-GCAUAUCUCCGACUAAAUA-3', RB1 #3: 5'-UCGAAGCCCUUACAAGUUU-3', RB1 #4: 5'-UGCGUUAUCUACUGAAAUA-3', Mage-b4 #1: 5'-AAGGAAGACAGGAATGCTGATG-3', Mage-b4 #2: 5'-AGTCACACTTGTGGACTCTTGCA-3', Mage-b4 #3: 5'-TGAGAATCCACAGAATGATCTT-3', YB1 #1: 5'-CCUAUGGGCGUCGACCACA-3', YB1 #2: 5'-

GUUCCAGUUCAAGGCAGUA-3', YB1 #3: 5'-GAAGUACCUUCGCAGUGUA-3', AGO2 #1: 5'-GGUCUAAAGGUGGAGAUAA-3', AGO2 #2: 5'-GGAUUCACGAGACCAGCUA-3', and AGO2 #3: 5'-CCAUGUUCCGGCACCUGAA-3'.

Antibodies

Rabbit polyclonal anti-MAGE-B2 antibody was produced by immunization of rabbits (Cocalico Biologicals) with recombinant full-length human MAGE-B2 protein produced in bacteria (described below) and affinity purified from serum. Antibody recognizing mouse Mage-b4 was previously described (Osterlund et al., 2000) and generously provided by Katarina Nordqvist. Commercial antibodies used in this study are as follows:

anti-Actin (Abcam, ab6276), anti-CAPRIN1 (Proteintech, 15512-1-AP), anti-DDX3 (Abcam, ab128206), anti-DDX5 (Abcam, ab126730), anti-eIF2α (Cell Signaling Technology, 5324), anti-eIF4G (Santa Cruz Biotechnology, sc-11373), anti-FLAG (Sigma, F3165), anti-G3BP1 (Abcam, ab181149), anti-G3BP1 (BD Biosciences, 611126), anti-G3BP1 (mouse tissue, BioRad, VPA00492), anti-G3BP2 (Bethyl Laboratories, A302-040A), anti-GST (Potts and Yu, 2005), anti-HA (Sigma, A2095), anti-Myc (Santa Cruz Biotechnology, sc-40), anti-PABP-C1 (Abcam, ab21060), anti-PLZF (R&D Systems, AF2944), anti-TIA1 (Santa Cruz Biotechnology, sc-166247), anti-TIAR (BD Biosciences, 610352), anti-TRIM25 (Abcam, ab167154), anti-TRIM28 (Abcam, ab22553), anti-Tubulin (Sigma, T9026), anti-USP10 (Proteintech, 19374-1-AP), anti-YB1 (Abcam, ab12148), anti-YTHDF1 (Proteintech, 17479-1-AP), anti-YTHDF2 (Proteintech,

24744-1-AP), anti-YTHDF3 (Santa Cruz Biotechnology, sc-377119), normal mouse IgG (Santa Cruz Biotechnology, sc-2025), and normal rabbit IgG (Santa Cruz Biotechnology, sc-2027).

Generation of MAGE-B2 KO cells

MAGE-B2 knockout U2OS cells were generated using CRISPR-Cas9 technology. Briefly, two sgRNAs were used to delete the entire ORF (upstream sgRNA – 5'-GAAUAGAUGGUUAGUAUACC-3', downstream sgRNA – 5'-UUUGGGAGAUUGAUUGGCUA-3'). 400,000 cells were transiently co-transfected with 200 ng of each gRNA expression plasmid (cloned into Addgene plasmid #43860), 500 ng Cas9 expression plasmid (Addgene plasmid #43945), and 200 ng of pMaxGFP via nucleofection (Lonza, 4D-Nucleofector X-unit) using solution P3, program CM-104 in small cuvettes according to the manufacturer's recommended protocol. Five days post-nucleofection, cells were single-cell sorted by FACs for transfected cells based on pMaxGFP expression into 96-well plates. After sorting, cells were clonally expanded and screened for the desired modification using PCR-based assays. Knockout of MAGE-B2 was further verified by immunoblotting. Knockout lines with deletions were established. The sequences are indicated below:

Clone #1: 5'–TCACAGATCTCATTCTCCCATCTCCAGGTA---deletion---ATCAATCTCCCAAAGCCAAGTTTACCTGCTGTT-3'

Clone #2: 5'–TCACAGATCTCATTCTCCCATCTCCA-----deletion--------ATCAATCTCCCAAAGCCAAGTTTACCTGCTGTT-3'.

Immunostaining and stress granule analysis

Cells were washed with PBS, fixed in methanol for 10 min at -20 °C, permeabilized with blocking solution (PBS containing 0.2% (v/v) Triton X-100 and 3% (w/v) bovine serum albumin (BSA)) for 20 min at 4 °C, and incubated overnight at 4 °C with primary antibodies. The next day, cells were incubated with secondary antibodies conjugated with Alexa Fluor 488 or 568 for 30 min and nuclei were stained with DAPI. Stained cells were then mounted with Aqua-Poly/Mount (Polysciences) and imaged using a Leica SP8 TCS STED 3X confocal microscope with a 63x/1.4NA oil objective. Stress granules were manually quantified using the indicated markers. At least 50-100 cells were counted for each condition in each experiment. For testis tissue sections, stress granules were quantified per seminiferous tubule using automated software. G3BP1 puncta were identified and segmented using IgorPro software. Segmented images were then counted using CellProfilerPro and the number of G3BP1 puncta (stress granules) was normalized to tubule size. 10-20 tubules were counted per mouse testis with at least four mice per genotype analyzed.

Live-cell imaging and analysis

Live-cell imaging experiments were performed using either a Marianas 2 spinning disk confocal microscope or Bruker Opterra II Swept Field confocal microscope. Images were acquired using a 63x/1.4 Plan Apochromat objective with Definite focus or 60x Plan Apo 1.4NA oil objective with Perfect focus, respectively. During imaging, cells were maintained at 37 °C and supplied with 5% CO_2 with an environmental control chamber and imaged at 40 s intervals with a 100 ms exposure

time. For experiments measuring stress granule assembly and disassembly in response to heat stress, an objective heater and temperature-controlled flow chamber (Bioptechs) was utilized. For experiments correlating G3BP1 expression to stress granule initiation time, G3BP KO U2OS cells were transfected with GFP-G3BP1. 48 hr post-transfection, cells were treated with either 62 μM or 500 μM sodium arsenite. GFP intensity at t = 0 was measured as a readout of GFP-G3BP1 expression.

To determine if the relative amounts of G3BP1 in either WT or MAGE-B2 KO U2OS cells, G3BP KO U2OS cells were transfected with GFP-G3BP1. The following day, either WT or MAGE-B2 KO U2OS cells were seeded with the GFP-G3BP1 transfected cells. 48 hr post-transfection, cells were imaged to measure GFP intensity as a readout of GFP-G3BP1 expression. Cells were subsequently fixed and stained with a G3BP1 antibody as described above. Each cell that was previously imaged for GFP, was then imaged to measure G3BP1 intensity as a readout of G3BP1 expression. Linear regression analysis was applied to model the relationship between GFP-G3BP1 intensity and G3BP1 intensity in the G3BP KO cells transfected with GFP-G3BP1 (R^2= 0.86). The calculated linear regression line (y=0.5308x + 640.28) was then used to determine the GFP-G3BP1 equivalent of the average measured endogenous G3BP1 intensity in WT or MAGE-B2 KO cells (8.0 or 13.4 RFU, respectively).

Tandem affinity purification and mass spectrometry

Tandem affinity purification (TAP) was performed as described in previously (Doyle et al., 2010). Briefly, 15 15 cm^2 dishes of HEK293 stably expressing TAP-Vector or TAP-MAGE-B2 were

lysed, bound to IgG sepharose beads (GE Amersham), cleaved off the beads with TEV protease, collected on calmodulin sepharose beads (GE Amersham), eluted with SDS sample buffer (4X SDS sample buffer: 0.5 M SDS, 165 mM Tris base, 60% glycerol, 3 mM bromophenol blue, and 0.2 M DTT), separated by SDS-PAGE and stained with colloidal Coomassie blue (Pierce). Total protein bands were excised, in-gel proteolyzed, and identified by LC/MS-MS.

Cell viability

Cells were seeded in 6-well plates and allowed to adhere for at least 4 hr before being treated with 4 μM sodium arsenite for 72 hr. Cells were trypsinized and the number of viable cells was determined using a Beckman Coulter Vi-Cell XR automated cell counting system.

Preparation of cell lysates and immunoblotting

Cells were washed with PBS, collected by scraping, and pelleted by centrifugation. Cell pellets were lysed in NP-40 lysis buffer (50 mM Tris-HCl pH 7.5, 150 mM NaCl, 0.5% (v/v) IGEPAL CA-630 (Sigma-Aldrich), 1 mM DTT, and 1X protease inhibitor cocktail (Sigma-Aldrich)) for 30 min on ice and centrifuged to clarify. The Micro BCA Protein Assay Kit (Thermo Scientific) was used to quantify total protein concentration of lysates. Lysates were prepared in SDS sample buffer, resolved on SDS-PAGE gels, and transferred to nitrocellulose membranes. Membranes were blocked with 5% BSA in TBST (25 mM Tris pH 8.0, 2.7 mM KCl, 137 mM NaCl, 0.05% (v/v) Tween-20) and incubated with primary antibodies. After three washes with TBST,

membranes were incubated with secondary antibodies, washed an additional three times, and detected via chemiluminescence or near-infrared fluorescence.

Protein disorder prediction

Intrinsically disordered regions were calculated using IUPred2A global structure disorder prediction (long disorder, default option). G3BP1 protein sequence was used as the input and the IUPred server returned a disorder tendency score between 0 and 1 for each residue with higher values corresponding to a higher probability of disorder.

Recombinant protein purification

GST-MAGE-B2, GST-DDX5 (wildtype or K144N), or GST alone were produced in BL21-CodonPlus (DE3)-RIPL cells by overnight induction at 16 °C with 0.5 mM Isopropyl b-D-1-thiogalactopyranoside (IPTG). GST-G3BP1 was produced in BL21-CodonPlus (DE3)-RIPL cells using the ZYM-5052 complex auto-inducing medium for induction by lactose (Studier, 2014). Bacterial pellets were solubilized with 50 mM Tris-HCl pH 7.7, 150 mM KCl, 1 mM dithiothreitol (DTT), and 1X protease inhibitor cocktail (Sigma) for GST and GST-MAGE-B2; 50 mM Tris-HCl pH 7.4, 300 mM KCl, 10% (v/v) glycerol, 1 mM DTT, and 1X protease inhibitor cocktail for GST-DDX5; and 50 mM Tris-HCl pH 8.0, 300 mM NaCl, 10% (v/v) glycerol, 1 mM DTT, and 1X protease inhibitor cocktail for GST-G3BP1. GST-tagged proteins were purified from bacterial lysates with glutathione Sepharose (GE Amersham) and eluted with 10 mM glutathione. In some

cases, the GST tag was cleaved by on column digest overnight at 4 °C with PreScission Protease. Purified proteins were immediately used for all assays prior to freezing.

In vitro phase separation assay

Samples were prepared by combining the indicated concentrations of purified recombinant G3BP1 and NaCl in a buffer containing 50 mM Tris-HCl pH 8.0 and 100 mg/mL Ficoll 400 (Sigma-Aldrich). Samples were sandwiched between a hydrophobic coverslip and microscope slide using an adhesive imaging spacer prior to imaging on a Lecia SP8 Widefield microscope.

RT-qPCR

RT-qPCR analysis was performed as described previously (Pineda et al., 2015). RNA was extracted using either RNAStat60 (TelTest) or Trizol Reagent (Invitrogen) according to the manufacturers' instructions, treated with DNase I (Roche), and converted to cDNA using the High Capacity cDNA Reverse Transcription kit (Life Technologies). cDNA was subjected to qPCR and gene expression was measured using SYBR Green (Applied Biosystems). Data were analyzed by ΔΔCt method normalizing to *18S* rRNA. qPCR primers used: *G3BP1* Forward: 5'-TGAGGTCTTTGGTGGGTTTG-3', *G3BP1* Reverse: 5'-TGCTGTCTTTCTTCAGGTTCC-3', *18S* rRNA Forward: 5'-ACCGCAGCTAGGAATAATGGA-3', *18S* rRNA Reverse: 5'-GCCTCAGTTCCGAAAACCA-3', *RPLP0* Forward: 5'-TCTACAACCCTGAAGTGCTTGAT-3', *RPLP0* Reverse: 5'-CAATCTGCAGACAGACACTGG-3', *Mage-b4* Forward: 5'-

TGAGCAAGCACCCATTACTTTG-3', and *Mage-b4* Reverse: 5'-TGACGGTTTACACATTTCTCTTTGT-3'.

^{35}S metabolic labeling

^{35}S labeling experiments were performed as described previously (Bonifacino, 2001). Briefly, U2OS Cells were washed with PBS and incubated with labeling media (methionine- and cystine-free DMEM supplemented with 10% dialyzed FBS, 2 mM L-glutamine, 100 units/mL penicillin, 100 mg/mL streptomycin, and 0.25 mg/mL Amphotericin B) for 30 min at 37 °C. Cells were then labeled with 0.1 mCi/mL EasyTag EXPRESS ^{35}S Protein Labeling Mix (Perkin Elmer) diluted in labeling media. For G3BP1 half-life experiments, cells were pulse labeled for 1 h at 37 °C, chased with complete media (DMEM supplemented with 10% FBS, 2 mM L-glutamine, 100 units/mL penicillin, 100 mg/mL streptomycin, and 0.25 mg/mL Amphotericin B), and harvested at the indicated time points. For G3BP1 translation experiments, cells were labeled and harvested at the indicated time points. Cells were lysed in RIPA lysis buffer (50 mM Tris-HCl pH 7.5, 150 mM NaCl, 1% (v/v) IGEPAL CA-630, 0.5% (w/v) sodium deoxycholate, 0.5% (w/v) SDS, 1 mM DTT, and 1X protease inhibitor cocktail) for 30 min on ice and centrifuged to clarify. Supernatants were pre-cleared with control IgG for 1 hr at 4 °C and Protein A/G Plus-Agarose beads (Santa Cruz Biotechnology) for 30 min at 4 °C before incubation with primary antibody overnight at 4 °C. The next day, samples were incubated with beads for 4 hr at 4 °C, washed with RIPA lysis buffer, and eluted with SDS sample buffer. Samples were resolved on SDS-PAGE gels, and either transferred to nitrocellulose membranes for immunoblotting, or fixed and dried for phosphorimaging. For

global translation experiments, cells were labeled and harvested at the indicated time points. 10 µL of the labeled cell suspension were added to 0.1 mL of BSA/NaN_3 (1 mg/mL BSA containing 0.02% (w/v) NaN_3) and precipitated by the addition of 1 mL 10% (w/v) trichloroacetic acid (TCA). Samples were vortexed and incubated for 30 min on ice before filtration onto glass microfiber disks. Disks were washed with 10% (w/v) TCA and ethanol. 10 µL of the labeled cell suspension was spotted onto another glass microfiber disk to measure the total amount of radiolabeled amino acid. Disks were transferred to vials with scintillation fluid for scintillation counting.

Co-immunoprecipitation

Cells were washed with PBS, collected by scraping, and pelleted by centrifugation. Cell pellets were lysed in NP-40 lysis buffer (50 mM Tris-HCl pH 7.5, 150 mM NaCl, 0.5% (v/v) NP-40, 1 mM DTT, and 1X protease inhibitor cocktail (Sigma-Aldrich)) for 30 min on ice and centrifuged to clarify. Soluble lysates were incubated with myc-conjugated Protein A beads for 2 hr at 4 °C. Beads were washed with NP-40 lysis buffer, eluted with SDS sample buffer, and resolved on SDS-PAGE for subsequent immunoblotting.

Polysome profiling

Polysomal profiling in U2OS WT and MAGE-B2 KO cells was done as described previously (Karamysheva et al., 2018) with minor modifications specific to cell culture. Cells were seeded in 20 mL of the DMEM medium (Sigma-Aldrich) supplied with 10% FBS and

penicillin/streptomycin mixture (100 units and 100 µg/mL correspondingly) (Sigma-Aldrich) with initial cell count of $0.5x10^5$ cells/mL. Cells were grown at 37 ˚C and 5% CO_2 for 5 days. To arrest the ribosome on translated mRNAs cells were treated with 100 µg/mL cycloheximide (CHX) (Sigma-Aldrich) for 10 min at 37 ˚C and 5% CO_2. After incubation with CHX cells were washed twice with cold PBS (Sigma-Aldrich) supplied with 100 µg/mL CHX, and immediately lysed on ice with 500 µl of 20 mM HEPES-KOH (pH 7.4), 100 mM KCl, 5 mM $MgCl_2$, 1 mM DTT, 0.5% NP-40, 1x protease inhibitor cocktail (EDTA-free), 100 µg/mL CHX, and 1 mg/mL heparin (Sigma-Aldrich). Cells were scraped from the plate, and concentrations of $MgCl_2$ and NP-40 were adjusted for increased sample volume. The cell lysates were passed through a 22-gauge needle 6 times and then clarified by centrifugation at 11,200 x g and 4 ˚C for 8 min. To evaluate the amount of starting material for polysome fractionation, absorbance at 260 nm was measured in cell lysates and adjusted to have equal input for all samples. 500 µl of cell lysate was used for fractionation. Linear sucrose gradients were prepared using Gradient Master 108 (BioComp) with 10% and 50% sucrose containing 20 mM HEPES-KOH (pH 7.4), 100 mM KCl, 10 mM $MgCl_2$, 1 mM DTT, 0.5% NP-40, 1x protease inhibitor cocktail (EDTA-free), and 1 mg/mL heparin in Polyclear centrifuge tube (Seton). Lysates were loaded on the top of the gradient and centrifuged at 260,000 x g and 4 ˚C for 2 h using SW 41 rotor (Beckman). Collection of polysomal fractions were done using Piston Gradient Fractionator (BioComp). Absorbance at 260 nm and 280 nm was recorded during each run of fractionation.

Affinity pulldown of biotinylated RNA

Affinity pulldown of biotinylated RNA for detection of protein-RNA complexes was performed as previously described (Panda et al., 2016). Briefly, pCS2-luciferase CDS or pCS2-luciferase with G3BP1 5'UTR and 3'UTR were linearized with Sal I (New England Biolabs) and gel purified (Qiagen). Biotinylated transcripts were produced from the linearized DNA *in vitro* using the MEGAscript kit (Life Technologies) and biotin-UTP (Sigma) according to the manufacturer's instructions and purified by the MEGAclear spin columns (Life Technologies) according to the manufacturer's instructions. Integrity of the transcripts were confirmed by non-denaturing agarose gel electrophoresis.

The purified control Luciferase CDS RNA or Luciferase CDS with *G3BP1* UTR RNA (10 µg) were added to cell lysate supernatants (approximately 1 mg) prepared from U2OS parental or MAGE-B2 KO cells in NP-40 lysis buffer (50 mM Tris-HCl pH 7.5, 150 mM KCl, 0.5% (v/v) NP-40, 1 mM DTT, 1X protease inhibitor cocktail (Sigma), and Ribolock RNase inhibitor (Thermo Fisher)). RNA was incubated in cell lysates for 45 min at room temperature followed by addition of 50 µL streptavidin Dynabeads M-280 (Invitrogen) for 45 additional minutes at room temperature. Beads were separated on a magnetic stand and washed 4 times with NP-40 lysis buffer. Proteins were eluted in 1X SDS-sample buffer and analyzed by liquid chromatography with tandem mass spectrometry (LC-MS/MS) or immunoblotting using the following antibodies: anti-DDX5 (Abcam, ab126730), anti-MAGE-B2 (described above), and anti-TRIM28 (Abcam, ab22553).

CLIP-qPCR

Cross-linking immunoprecipitation and QPCR (CLIP-QPCR) was carried out as previously described (Yoon and Gorospe, 2016). Briefly, HEK293/TAP-Vector, HEK293/TAP-MAGE-B2, U2OS parental, or U2OS MAGE-B2 KO cells (10-15 15 cm^2 dishes) were washed in ice-cold, magnesium-free PBS and irradiated on ice with 150 mJ/cm^2 of UVC (254 nm) in a Stratalinker 2400 (Agilent). Cells were collected in ice-cold PBS, pelleted, lysed in NP-40 lysis buffer (50 mM Tris-HCl pH 7.5, 150 mM KCl, 0.5% (v/v) NP-40), and centrifuged for 15 min at 10,000 xg at 4 °C. Supernatants were collected and subjected to immunoprecipitation. HEK293 cell lysates were incubated with 20 µL IgG Sepharose (GE Healthcare) or as a control Sepharose without IgG (GE Healthcare) for 3 hr at 4 °C rotating. U2OS cell lysates were incubated with 20 µL pre-coupled antibody-protein A/G PLUS-agarose beads (Santa Cruz Biotechnology) for 3 hr at 4 °C rotating. Antibodies (10 µg) used were as follows: normal rabbit IgG control (Santa Cruz, sc-2027) and anti-DDX5 (Abcam, ab126730). Beads were then washed three times in NP-40 lysis buffer, treated with 20 units of RNase-free DNase I for 15 min at 37 °C, and proteins degraded by treatment with 0.5 mg/mL proteinase K (Invitrogen) in 0.5% SDS at 55 °C for 15 min. RNA was then separated by phenol:chloroform extraction, followed by ethanol precipitation. RNA was then converted to cDNA using the High Capacity cDNA reverse transcriptase kit (Invitrogen) according to manufacturer's instructions. qPCR analysis was performed on cDNA using PowerUp SYBR Green master mix (Applied Biosystems) according to manufacturer's instructions using the following primers: *G3BP1* F 5'-TGAGGTCTTTGGTGGGTTTG-3', *G3BP1* R 5'-TGCTGTCTTTCTTCAGGTTCC-3', *RPLP0* F 5'-TCTACAACCCTGAAGTGCTTGAT-3', *RPLP0* R 5'-CAATCTGCAGACAGACACTGG-3'. Data were analyzed by ΔΔCt method normalizing to *RPLP0* and control pulldowns (normal IgG (U2OS) or non-IgG beads (HEK293)).

In vitro translation assays

In vitro translation assays monitoring luciferase enzyme production in rabbit reticulocyte lysate were carried out as follows. Purified proteins, GST, GST-MAGE-B2, DDX5 WT, or DDX5 K144N, were added alone or in combination at the indicated concentrations (0.25-4 pmol) to *in vitro* translation reactions (Promega SP6-TNT Quick rabbit reticulocyte lysate system) containing firefly luciferase coding sequence (CDS) alone or luciferase CDS with *G3BP1* 5' UTR and/or *G3BP1* 3' UTR sequences. Reactions were incubated at 30 °C for 1.5 hr. Samples were diluted in passive lysis buffer (Promega) before analysis of luciferase protein levels using Dual-Glo luciferase assay system (Promega) and an EnSpire multimode plate reader (Perkin-Elmer).

In vitro binding assays

In vitro binding assays were performed as described previously (Doyle et al., 2010; Hao et al., 2013). 15 µg of purified GST-tagged proteins were bound to glutathione Sepharose beads in binding buffer (25 mM Tris pH 8.0, 2.7 mM KCl, 137 mM NaCl, 0.05% (v/v) Tween-20, and 10 mM 2-mercaptoethanol) for 1 hr and then blocked for 1 hr in binding buffer containing 5% (w/v) milk powder. *In vitro* translated proteins (Promega SP6-TNT Quick rabbit reticulocyte lysate system) were then incubated with the bound beads for 1 hr, extensively washed in binding buffer, eluted with 2X SDS-sample buffer, boiled, subjected to SDS-PAGE, and immunoblotting.

Animals and tissue collection

Human tissues were obtained from commercially available sources and mouse tissues were collected as described previously (Fon Tacer et al., 2019). All procedures and use of mice were approved by the Institutional Animal Care and Use Committee of St. Jude Children's Research Hospital.

Spermatogonial cultures, ID4-eGFP flow cytometry and transplantation analyses

Spermatogonia cultures were established as previously described (Fon Tacer et al., 2019). Briefly, primary cultures of undifferentiated spermatogonia were generated from the double-transgenic *Id4-eGFP;Rosa26-LacZ* hybrid mice that express the LacZ transgene in all germ cells, but express the EGFP transgene only in ID4+ spermatogonial stem cells (Chan et al., 2014; Helsel et al., 2017b) or Mage-b4 knockout mice (described below). Primary cultures were established from the magnetic-activated cell sorting (MACS)-sorted THY1+ fraction of testis homogenates of P6–8 mice (Oatley and Brinster, 2006). Spermatogonial cultures were maintained on mitotically inactivated SIM mouse embryo-derived thioguanine- and ouabain-resistant feeder monolayers (STOs) in mouse serum-free medium (mSFM), devoid of fatty acids and supplemented with the growth factors GDNF (20 ng/mL; Peprotech, NJ, USA) and FGF2 (1 ng/mL; Peprotech). Cultures were kept in glycolysis-optimized conditions in humidified incubators at 37 °C, 10% O_2 and 5% CO_2 in air (Helsel et al., 2017a). Culture media was replaced every other day, and passaging onto fresh feeders was performed every 6–8 days.

For siRNA transfection, cultured spermatogonial clumps were separated from feeders by gentle pipetting and a single-cell suspension was generated by trypsin-EDTA digestion. $1x10^5$ or $2x10^4$ cells were plated in 24 or 96 well plates, respectively, without STO feeder cells in mSFM with GDNF and FGF2. Cells were transfected with either non-targeting control (Dharmacon, D-001810-10-05) or Mage-b4/10 siRNA oligonucleotides by Lipofectamine 3000 (Invitrogen) as follows: 2 µL Lipofectamine 3000 in 100 µL OptiMem and 75 pmol siRNA in 100 µL OptiMem per $1x10^5$ cells. 16 hrs after transfection, cells were washed with HBSS and fresh mSFM with GDNF and FGF2 was added. To assess ID4-eGFP expression level, cells were analyzed by flow cytometry 6 days after transfection. Single-cell suspensions were generated by trypsin-EDTA digestion as described previously and analyzed using an Attune NxT Flow Cytometer (Thermo Scientific, MA, USA). Identification and gating of the ID4-eGFPbright and ID4-eGFPdim populations from cultures was done as described previously (Chan et al., 2014; Helsel et al., 2017b).

To compare the regenerative capacity of spermatogonial culture populations after siRNA transfection, transplantation analysis was performed (Oatley and Brinster, 2006). Six days after siRNA transfection spermatogonial clumps were separated from feeders by gentle pipetting, single-cell suspension generated by trypsin-EDTA digestion and cells suspended in mouse serum-free medium at $1x10^6$ cells/ml. 10 µl (10,000 cells) was microinjected into each recipient testis. Recipient testes were evaluated for colonies of donor-derived spermatogenesis 2 months later.

Generation and genotyping of *Mage-b4* knockout mouse models

Mouse lines were generated by injecting sgRNAs and Cas9 protein in the pronucleus and cytoplasm of C57BL/6 zygote. A single sgRNA targeting both *Mage-b4* and *Mage-b10* (TCCAGAATCCTGATTAGAGC) was prepared by *in vitro* trascription (MEGAshortscript T7 Kit, Ambion) and purified by MEGAclear™ Transcription Clean-Up Kit (Ambion). The progeny was screened for frameshift mutations by Cel-1 assay and Sanger sequencing. Animals were genotyped as previously described (Fon Tacer et al., 2019). Briefly, tail snips (1-2 mm) were collected at weaning (~21 days old) and again when animals were euthanized for organ collection. Genomic DNA (gDNA) was prepared by incubating tails in 200 µl of 50 mM NaOH at 95 °C for 35 min, allowed to cool for a 3 min, and neutralized by addition of 20 µl 1 M Tris (pH 8.0). PCR was performed using KAPA2G Robust Hotstart PCR kit (KAPA Biosystems, #KK5518), following the manufacturer's protocol. Buffer A, Enhancer, and 1 µl of gDNA was used. Primers used were as follows: *Mage-b4* forward – 5'-TTCCTCAATCCCGGTACAAG-3', *Mage-b4* reverse – 5'-TGTGCACCTTCCCATCATAA-3', *Mage-b10* forward – 5'-TACTAAGCTAGCTCTAGCGG-3', *Mage-b10* reverse – 5'-AAAGTACCAGAGGTCCAAGGGAGGA-3'. The *Mage-b4* locus was genotyped by PCR alone. The *Mage-b10* locus was amplified by PCR and then amplicons were digested with BslI enzyme (NEB) at 55°C for 1 hour in NEB Cutsmart buffer; KO animals displayed a unique banding pattern compared to WT.

Generation and genotyping of *G3BP1-GFP* transgenic mouse models

Human G3BP1 cDNA in frame with GFP was inserted into the pSF-CAG-Kan vector (Cat# OG505, Oxford Genetics) between HindIII and XbaI sites. This plasmid contains the mammalian CAG promoter which is a synthetic composite of the CMV immediate early enhancer followed by the CBA promoter and the rabbit beta globin intron. The expression cassette containing the promoter, G3BP1-GFP coding sequence, and polyA tail was cut out by AsiSI+PacI enzyme. The insert was gel-purified and injected into FVB/NJ donor zygotes by the St Jude Children's Research Hospital Transgenic/Gene Knockout Shared Resource. Offspring were genotyped by PCR and founders bred to wild type FVB/NJ mice to confirm transmission of the transgene and generate F1 mice for testing of transgene expression. Of the 3 potential founder lines identified, only 1 expressed detectable levels of G3BP1-GFP by western blot in the tissues tested (brain, spinal cord and skeletal muscle). Hemizygous transgenic mice from this line (#16) were bred to wildtype FVB/NJ mice to maintain the FVB/NJ background and were used for experiments.

Tissue weights and fertility evaluation

To assess the effect of Mage-b4 depletion on organ weights, wildtype and KO mice were sacrificed and organ weights measured immediately after dissection. To test the fertility in males, wildtype females were paired with individually housed wildtype or KO males and checked for vaginal plugs for up to 4 days. Females were then removed, and males were allowed two days to recover before addition of a new female. This process was then repeated for a total of 3 females per male. Females that were successfully plugged were then monitored for pregnancy. We recorded successful pregnancies, number of pups born, and average pup weight at birth. Sperm was prepared from

cauda epididymis. Cauda epididymal sperm were allowed to swim out and were incubated for 15 min at 37 °C in DPBS (Dulbecco's' PBS with 0.1% FBS, 10 mM HEPES, 10 mM sodium pyruvate, glucose (1 mg/mL), and penicillin/streptomycin (1 mg/mL)). Sperm number and motility were quantified using a computer-assisted semen analysis system (Hamilton Thorne Research) and by manual counting using a hemocytometer. We used 6 males per genotype for fertility and organ weight measurement.

Heat stress and busulfan treatments

To evaluate spermatogenesis recovery after heat stress 10-12 week old mice were anesthetized and placed in a polystyrene float in a water bath so that their lower third was submerged. Mice were anesthetized by intraperitoneal injection of ketamine:xylazine (100 mg/kg:10 mg/kg body weight). Water baths were maintained at 33 °C for control or 38 °C or 42 °C for heat stress. Animals were incubated for 15 or 20 minutes, removed, dried, and (when appropriate) monitored for recovery. For monitoring stress granules, mice were sacrificed immediately after heat stress and processed for G3BP1 immunostaining as described below. At sacrifice (immediately or 2, 4, or 6 week post-stress), testes were weighed and fixed in 4% PFA for 24 hr. For busulfan treatment, 4 month old wildtype and KO mice were intraperitoneally injected with 20 mg/kg body weight of busulfan (Sigma) dissolved in 1:1 volume ratio of DMSO and water. Eight weeks after treatment, mice were sacrificed and analyzed similarly as heat stressed mice above.

Immunohistochemistry (IHC) and immunofluorescence (IF) tissue staining

Testes were fixed for 24 hr at 4 ^{o}C in 0.1 M sodium phosphate buffer, pH 7.2, containing 4% (w/v) paraformaldehyde (PFA). Fixed testes were paraffin embedded for H&E staining and IHC. IHC-based labeling was performed after de-paraffinization using a Discovery XT autostainer (Ventana Medical Systems) with anti-Mage-b4 antibody. All slides were counterstained with hematoxylin. Bright-field images were taken with an upright Eclipse Ni (Nikon) or constructed from digitized images using Aperio ImageScope (Leica Biosystems). The percentage of damaged tubules showing vacuolization and reduced germ cell layers (<4) was determined in a blinded manner in which >200 tubules from 2-6 mice per genotype per experiment were analyzed.

For IF, fixed testes were incubated in a 10% sucrose solution (w/v, dissolved in 1x PBS) at 4 ^{o}C until equilibrated, and then in 30% sucrose overnight at 4 ^{o}C. Once equilibrated, testes were embedded in tissue freezing medium (Electron Microscopy Sciences) and frozen using a Shandon Lipshaw cryobath. Tissues were cut into 6 µm sections. Prior to labeling, sections were equilibrated in air to room temperature for 8 min, hydrated for 8 min in PBS at room temperature, heat-treated at 80 °C for 8 min in 10 mM sodium citrate (pH 6.0) and then incubated for 1 hour at room temperature in blocking buffer (3% (w/v) BSA or 1% (v/v) Roche Blocking Reagent, diluted in 0.1 M sodium phosphate buffer, containing 0.2% (v/v) Triton X-100. Sections were then treated for 18-24 hr at 4 ^{o}C with antibody diluted in blocking buffer. Antibodies used were as follows: anti-Mage-b4 (Nordqvist lab, 1:100), anti-PLZF (R&D Systems AF2944, 1:50), and anti-G3BP1 (BioRad VPA00492, 1:100). After treatment with primary antibodies, sections were washed 3 times for 10 min per wash in PBS containing 0.02% (v/v) Triton X-100 and then incubated for 1 hr at room temperature with Alexa-flour secondary antibodies (Molecular Probes) diluted to 4

μg/mL in blocking buffer. After treatment with secondary antibodies, sections were washed two times in PBS containing 0.02% (v/v) Triton X-100. Samples were then incubated in DAPI diluted to 1 μg/ml in PBS for 5 minutes at room temperature, washed once in PBS containing 0.02% (v/v) Triton X-100, once in PBS, and cover-slipped for viewing using Fluorogel mounting medium (Electron Microscopy Sciences).

RNA-sequencing

Total RNA was extracted from mouse whole testes, and four or more biological replicates were prepared for RNA-seq with the TruSeq stranded mRNA library preparation kit (Illumina) and sequenced on the Illumina HiSeq 4000 platform. The 100 bp paired-end reads were trimmed against quality (Phred-like Q20 or greater) and aligned to a mouse reference sequence GRCm38 (UCSC mm10), with the STAR aligner (version 2.5.3a). For gene expression comparisons, the transcript per million (TPM) counts were calculated. A total of 15781 genes with TPM count greater than one in at least one sample were included in the principal component analysis (PCA) and the gene expression analysis was performed using the non-parametric anova applying the Kruskal-Wallis and Dunn's tests on log-transformed TPM counts among at least four biological replicates of all experimental groups, implemented in Partek Genomics Suite v7.0 software (Partek Inc.). The expression of a gene was considered significantly different if the adjusted P-value was less than 0.005 and the expression change was more than two folds between wild type and knockout groups. The z-scores of 2767 significantly differential expressed genes were calculated and hierarchical clustered in a heat map, using correlation distance measure, implemented in

Spotfire v7.5.0 software (TIBCO). The gene sets were analyzed by DAVID (v6.8, www.david.ncifcrf.gov) and Gene Set Enrichment Analysis (GSEA, www.gsea-msigdb.org) to identify enriched functional classes of genes. The RNA-Seq data discussed in this publication have been deposited in the NCBI's Gene Expression Omnibus and are accessible through GEO Series accession number GSE149802.

Quantification and statistical analysis

All data were analyzed by Prism 7 (GraphPad). Statistical details of experiments can be found in figure legends. Unless noted otherwise, data are representative of at least three biologically independent experiments. Single time-point datasets were analyzed by *t* test. Multiple comparison (>3 groups) was performed using one-way Anova with Dunnett's post-hoc test as indicated. Multiple time-point datasets were analyzed by two-way ANOVA unless otherwise stated. For all statistical analyses: * = $p \leq 0.05$, ** = $p \leq 0.01$, *** = $p \leq 0.001$, **** = $p \leq 0.0001$, n.s. = not significant.

A

GO Biological Process	Fold Enrichment	P value
Protein localization to cytoplasmic stress granule	>100	8.97E-05
Ribosomal small subunit assembly	64.94	4.59E-08
ncRNA export from nucleus	64.94	1.21E-02
SRP-dependent cotranslational protein targeting to membrane	43.69	9.85E-33

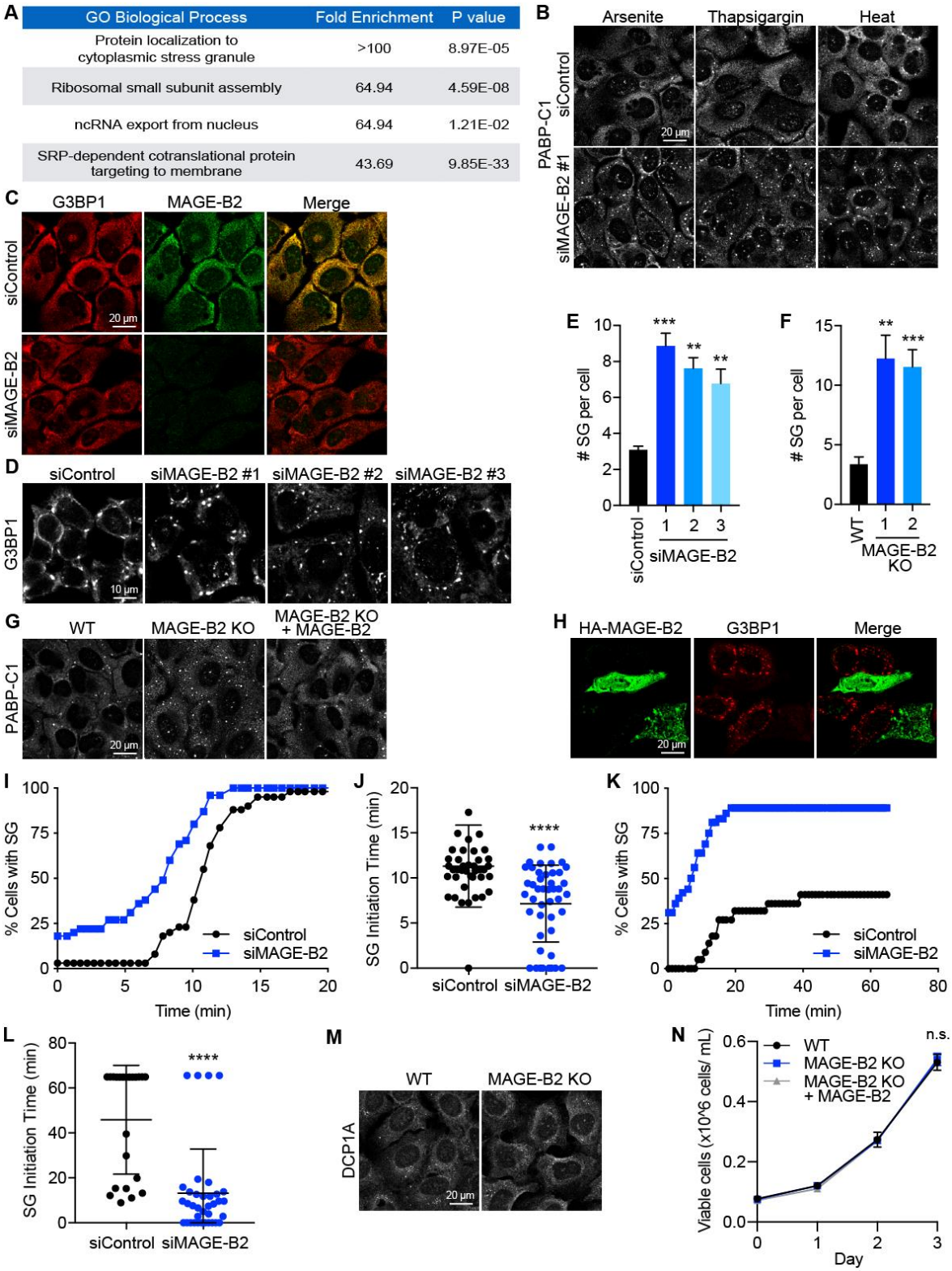

Figure 2-1. Depletion of MAGE-B2 enhances SG assembly

(A) Tandem affinity purification coupled to mass spectrometry. HEK293 cells stably expressing vector control or TAP-MAGE-B2 were subjected to tandem affinity purification followed by LC-MS/MS (n = 2). Gene ontology analysis of the identified proteins from mass spectrometry was performed using the PANTHER (protein annotation through evolutionary relationship) classification system according to biological process. The top enriched biological processes are ranked by fold enrichment over the expected value based on the reference list with raw *p* value determined by Fisher's exact test.

(B) MAGE-B2 knockdown increases SG in response to various stressors. U2OS cells were transfected with the indicated siRNAs from 72 hr, treated with 62 μM sodium arsenite, 1 μM thapsigargin, or 43 °C heat stress for 1hr, and immunostained for PABP-C1. Representative images are shown.

(C) MAGE-B2 knockdown does not cause spontaneous SG formation. U2OS cells were transfected with the indicated siRNAs for 72 hr and immunostained for G3BP1 and MAGE-B2. Representative images are shown.

(D and E) MAGE-B2 knockdown increases SG in HCT116 cells. HCT116 cells were transfected with the indicated siRNAs for 72 hr, treated with 62 μM sodium arsenite for 1 hr, and immunostained for G3BP1. Representative images (D) and quantification (n = 3) of SG numbers per cell (E) are shown. *P* values were determined by one-way ANOVA.

(F) WT or MAGE-B2 KO U2OS cells were treated with 62 μM sodium arsenite for 1 hr and immunostained for PABP-C1. Quantification (n = 3) of SG numbers per cell is shown. *P* values were determined by *t* test.

(G) WT, MAGE-B2 KO, or MAGE-B2-reconstituted KO U2OS cells were treated with 62 μM sodium arsenite for 1 hr and immunostained for PABP-C1. Representative images are shown.

(H) Overexpression of MAGE-B2 decreases SG. U2OS cells were transiently transfected with HA-MAGE-B2 for 48 hr, treated with 500 μM sodium arsenite for 1 hr, and immunostained for HA or G3BP1. Representative images are shown.

(I and J) Live-cell imaging of U2OS cells stably expressing G3BP1-GFP. 72 hr after transfection with the indicated siRNAs, cells were treated with 500 μM sodium arsenite to induce stress granule assembly. Quantification of the percentage of SG-containing cells over time (I) and SG initiation time for each cell (J) are shown. Data from one representative experiment of n = 3 biological replicates with at least 40 cells analyzed for each group. *P* value was determined by unpaired *t* test.

(K and L) Live-cell imaging of U2OS cell stably expressing G3BP1-GFP. 72 hr after transfection with the indicated siRNAs, cells were treated with 1 μM thapsigargin to induce SG assembly. Quantification of the percentage of SG-containing cells over time (K) and SG initiation time for each cell (K) are shown. Data from one representative experiment of n = 3 biological replicates with at least 20 cells analyzed for each group. *P* value was determined by unpaired *t* test.

(M) MAGE-B2 KO does not significantly affect P-body formation. WT or MAGE-B2 KO U2OS cells were immunostained for DCP1A. Representative images are shown.

(N) MAGE-B2 KO cells have similar growth rates to WT U2OS cells. WT, MAGE-B2 KO, or MAGE-B2-reconstituted KO U2OS cells were counted each day for 3 days after plating to determine relative growth rates. *P* value was determined by *t* test.

Data are mean ± SD. Asterisks indicate significant differences from the control (** = $p \leq 0.01$, *** = $p \leq 0.001$, **** = $p \leq 0.0001$, n.s. = not significant).

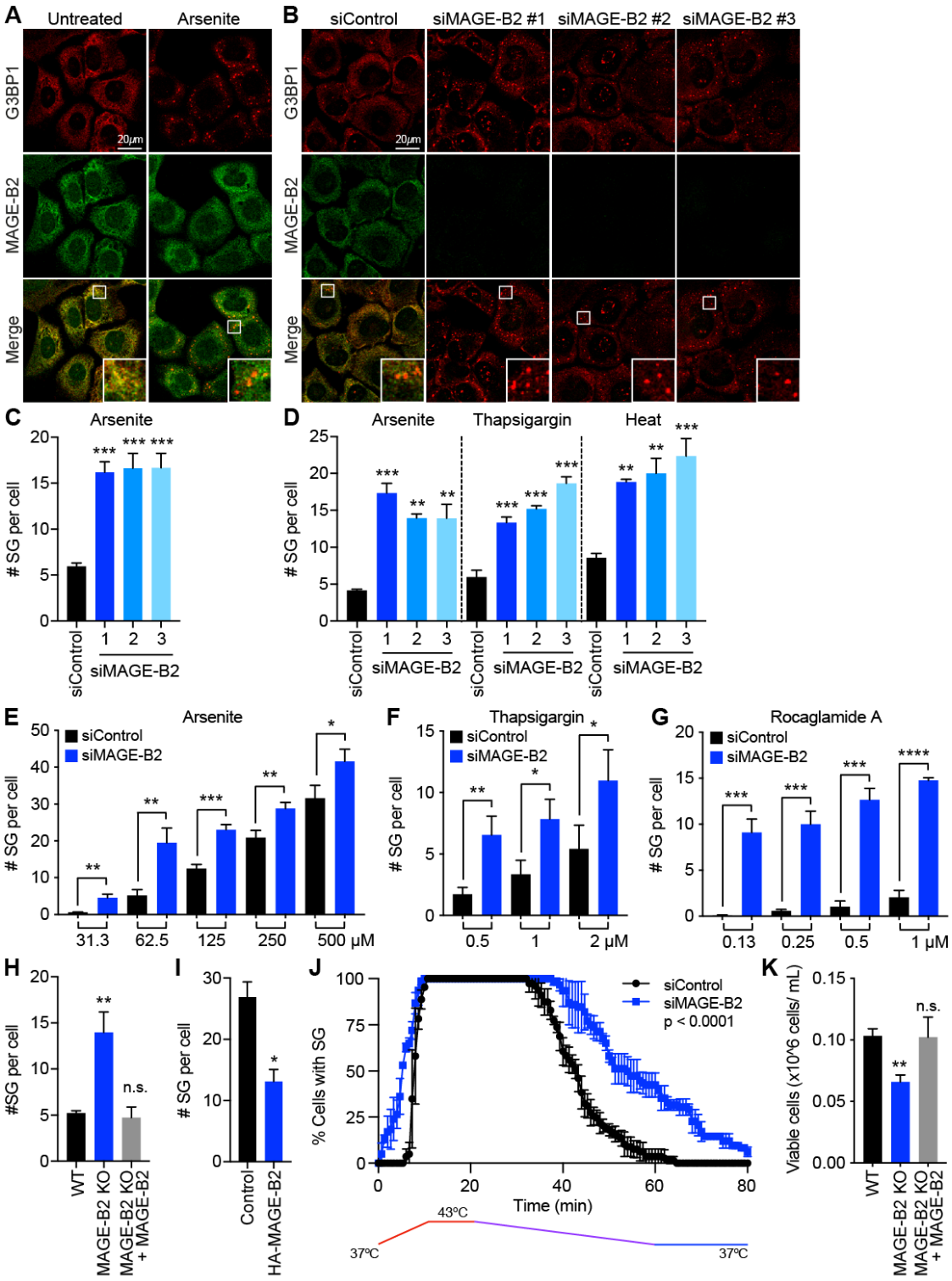

Figure 2-2. MAGE-B2 regulates SG dynamics

(A) MAGE-B2 does not localize to SG. U2OS cells were treated with or without 500 μM sodium arsenite for 1 hr, and immunostained for G3BP1 and MAGE-B2. Representative images are shown.

(B and C) MAGE-B2 knockdown increases SG. U2OS cells were transfected with the indicated siRNAs for 72 hr, treated with 62 μM sodium arsenite for 1 hr, and immunostained for G3BP1 and MAGE-B2. Representative images (B) and quantification (n = 3) of SG numbers per cell (C) are shown. *P* values were determined by one-way ANOVA.

(D) MAGE-B2 knockdown increases SG in response to various stressors. U2OS cells were transfected with the indicated siRNAs for 72 hr, treated with 62 μM sodium arsenite, 1 μM thapsigargin, or 43 °C heat stress for 1 hr, and immunostained for PABP-C1. Quantification (n = 3) of SG numbers per cell is shown. *P* values were determined by one-way ANOVA.

(E-G) MAGE-B2 knockdown increases SG in a dose-dependent manner. U2OS cells were transfected with the indicated siRNAs for 72 hr, treated with either 31 - 500 μM sodium arsenite (E), 0.5 - 2 μM thapsigargin (F), or 0.13 - 1 μM rocaglamide A (G) for 1 hr, and immunostained for G3BP1. Quantification (n = 3) of SG numbers per cell is shown. *P* values were determined by *t* test.

(H) WT, MAGE-B2 KO, or MAGE-B2-reconstituted KO U2OS cells were treated with 62 μM sodium arsenite for 1 hr and immunostained for PABP-C1. Quantification (n = 3) of SG numbers per cell is shown. *P* values were determined by *t* test.

(I) HA-MAGE-B2 overexpression reduces SG in U2OS cells treated with 500 μM sodium arsenite for 1 hr and immunostained for G3BP1. Quantification (n = 3) of SG numbers per cell is shown. *P* value was determined by *t* test.

(J) Live-cell imaging of U2OS cells stably expressing G3BP1-GFP. Cells were heat shocked at 43 °C to induce stress granule assembly and were subsequently recovered at 37 °C to measure stress granule disassembly. Quantification (n = 3) of the percentage of SG-containing cells over time is shown. P value was determined by two-way ANOVA.

(K) MAGE-B2 knockout cells are hypersensitive to chronic stress. WT, MAGE-B2 KO, or MAGE-B2-reconstituted KO U2OS cells were exposed to 4 μM sodium arsenite for 3 days before number of viable cells were counted (n = 3). *P* value was determined by *t* test.

Data are mean ± SD. Asterisks indicate significant differences from the control (* = $p \leq 0.05$, ** = $p \leq 0.01$, *** = $p \leq 0.001$, **** = $p \leq 0.0001$, n.s. = not significant).

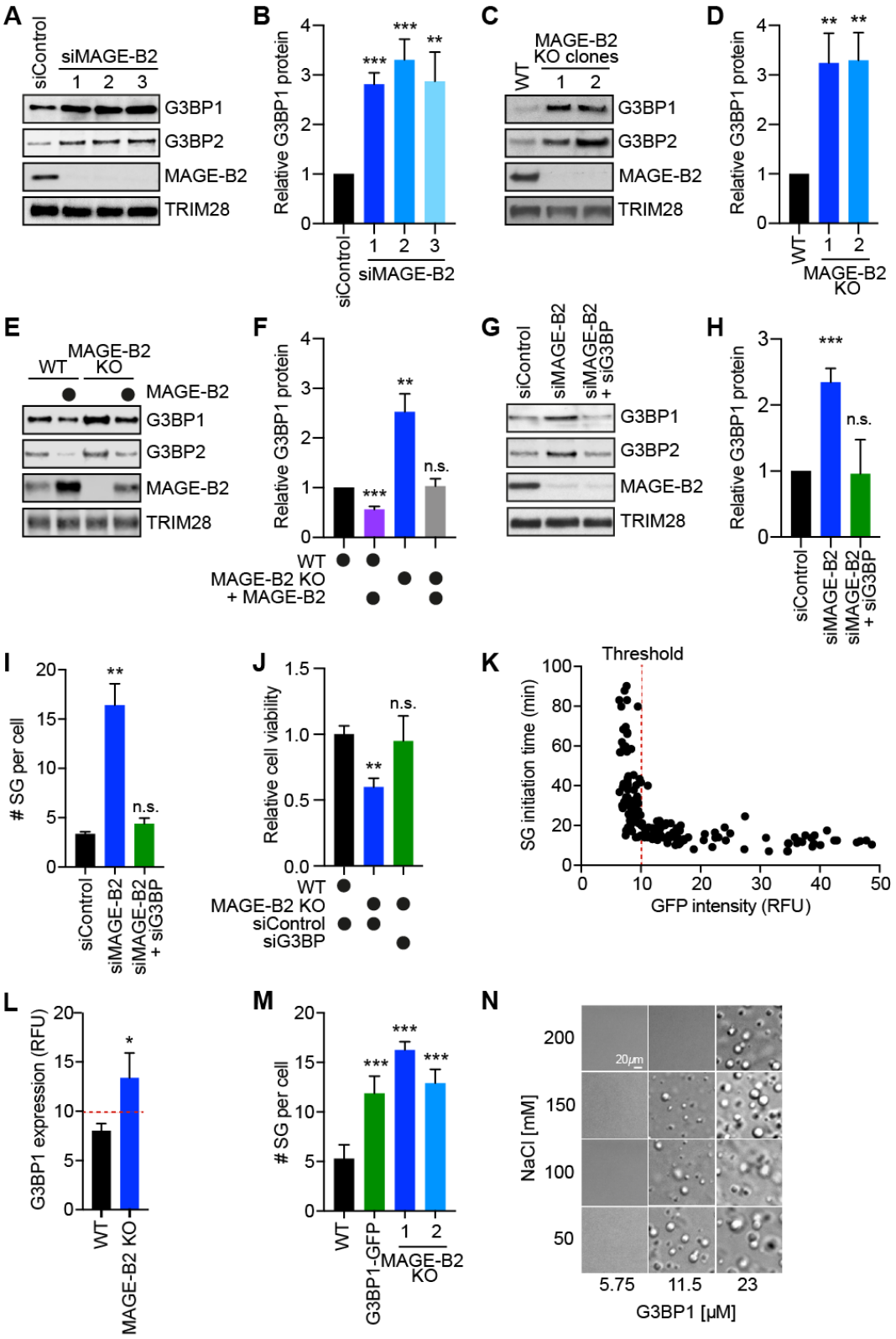

Figure 2-3. MAGE-B2 modulates SG formation through regulation of G3BP protein levels

(A and B) MAGE-B2 knockdown increases G3BP protein levels. U2OS cells were transfected with the indicated siRNAs for 72 hr and immunoblotted for the indicated proteins. Representative immunoblots (A) and quantification (n = 3) of relative G3BP1 protein levels (B) are shown. *P* values were determined by *t* test.

(C and D) MAGE-B2 KO increases G3BP protein levels. WT or MAGE-B2 KO U2OS cell lysates were immunoblotted for the indicated proteins. Representative immunoblots (C) and quantification (n = 3) of relative G3BP1 protein levels (D) are shown. *P* values were determined by *t* test.

(E and F) Overexpression of MAGE-B2 in WT U2OS cells reduces G3BP protein levels. Stable re-expression of MAGE-B2 in MAGE-B2 KO U2OS cells rescues G3BP protein levels. Cell lysates were immunoblotted for the indicated proteins. Representative immunoblots (E) and quantification (n = 3) of relative G3BP1 protein levels (F) are shown. *P* values were determined by *t* test.

(G-I) Increased G3BP protein levels in MAGE-B2-depleted cells are required for enhanced SG formation. U2OS cells were transfected with the indicated siRNAs for 72 hr and immunoblotted to confirm rescue of G3BP protein levels (G and H) or treated with 62 μM sodium arsenite for 1 hr and immunostained for SG quantification (I). Representative immunoblots (G), quantification (n = 3) of relative G3BP1 protein levels (H), and quantification (n = 3) of SG number per cell (I) are shown. *P* values were determined by *t* test.

(J) Depletion of G3BP in MAGE-B2 KO cells restores cell viability during prolonged stress. WT or MAGE-B2 KO U2OS cells were transfected with the indicated siRNAs for 72 hr and exposed to 4 μM sodium arsenite for 3 days before number of viable cells were counted (n = 3). *P* values were determined by *t* test.

(K) G3BP1 expression correlates with SG initiation time. G3BP KO U2OS cells were transiently transfected with varying levels of GFP-G3BP1. GFP-G3BP1 protein levels were determined at single-cell resolution by live-cell imaging before stress. Cells were then treated with 500 μM sodium arsenite to induce SG assembly and the time at which SG assembly initiated was quantified and correlated to GFP-G3BP1 protein levels (n = 3, total 76 cells analyzed). GFP-G3BP1 expression beyond a threshold (dotted red line) results in enhanced SG formation.

(L) MAGE-B2 KO increases G3BP1 protein levels beyond the threshold (dotted red line determined from Fig 2H) for enhanced SG formation. The relative amounts of endogenous G3BP1 in either WT or MAGE-B2 KO U2OS cells was determined in relation to GFP-G3BP1 in Figure 2-3K (n = 3). *P* value was determined by *t* test.

(M) Overexpression of G3BP1 is sufficient to increase SG formation similarly to MAGE-B2 KO. U2OS cells stably overexpressing G3BP1-GFP were treated with 62 μM sodium arsenite for 1 hr, immunostained for PABP-C1, and number of SG per cell was determined (n = 3). *P* values were determined by one-way ANOVA.

(N) *In vitro* liquid-liquid phase separation of G3BP1. The indicated concentrations of recombinant G3BP1 protein and 100 mg/mL Ficoll 400 were incubated at varying concentrations of NaCl and droplet formation was determined by microscopy. Representative images are shown.

Data are mean ± SD. Asterisks indicate significant differences from the control (* = $p \leq 0.05$, ** = $p \leq 0.01$, *** = $p \leq 0.001$, n.s. = not significant).

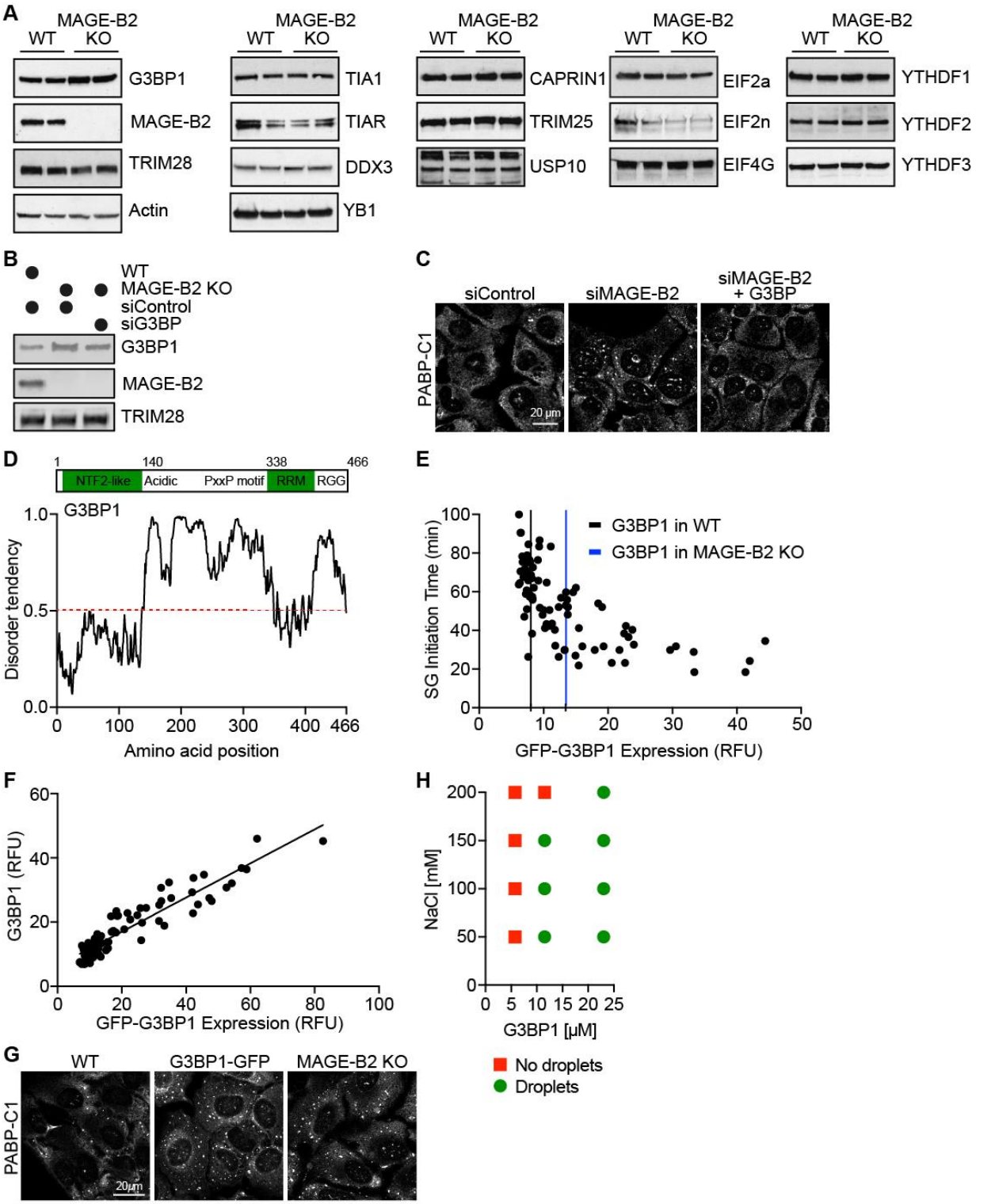

Figure 2-4. MAGE-B2 specifically regulates G3BP protein levels to alter SG dynamics

(A) MAGE-B2 regulates the protein levels of G3BP, but not that of other SG-associated proteins. WT or MAGE-B2 KO U2OS cell lysates were immunoblotted for the indicated proteins. Two biological replicate samples for each condition are shown.

(B) Rescue of G3BP protein levels in MAGE-B2 KO cells. WT or MAGE-B2 KO U2OS cells were transfected with the indicated siRNAs for 72 hr and immunoblotted for the indicated proteins.

(C) Increased G3BP protein levels in MAGE-B2-depleted cells are required for enhanced SG formation. U2OS cells were transfected with the indicated siRNAs for 72 hr, treated with 62 μM sodium arsenite for 1 hr, and immunostained for PABP-C1.

(D) G3BP1 is an intrinsically disordered protein. Domain map of G3BP1 protein and protein disorder prediction determined are shown.

(E) G3BP1 expression correlates with SG initiation time. G3BP KO U2OS cells were transiently transfected with varying levels of GFP-G3BP1. GFP-G3BP1 protein levels were determined at single-cell resolution by live-cell imaging before stress. Cells were then treated with 62 μM sodium arsenite to induce stress granule assembly (n = 3). The time at which SG assembly initiated was quantified and correlated to GFP-G3BP1 protein levels. Endogenous G3BP1 protein levels are indicated for WT or MAGE-B2 KO U2OS cells.

(F) Correlation between GFP-G3BP1 fluorescent intensity from GFP and immunofluorescent intensity from G3BP1 antibody staining. G3BP KO cells were transfected with GFP-G3BP1. 48 hr post-transfection, GFP intensity was determined at single-cell resolution by live-cell imaging. Cells were then immunostained for G3BP1 and fluorescence from the G3BP1 immunostaining was correlated to the previously measured GFP intensity on a cell-by-cell basis (n = 3, total 76 cells analyzed).

(G) Overexpression of G3BP1 is sufficient to increase SG formation similarly to MAGE-B2 KO. U2OS cells stably expressing G3BP1 were treated with 62 μM sodium arsenite for 1 hr and immunostained for PABP-C1. Representative images are shown.

(H) *In vitro* liquid-liquid phase separation of G3BP1. Protein/ NaCl concentration pairs scoring positive (green circles) or negative (red squares) for the appearance of droplets from one representative experiment of n = 3 replicates are shown.

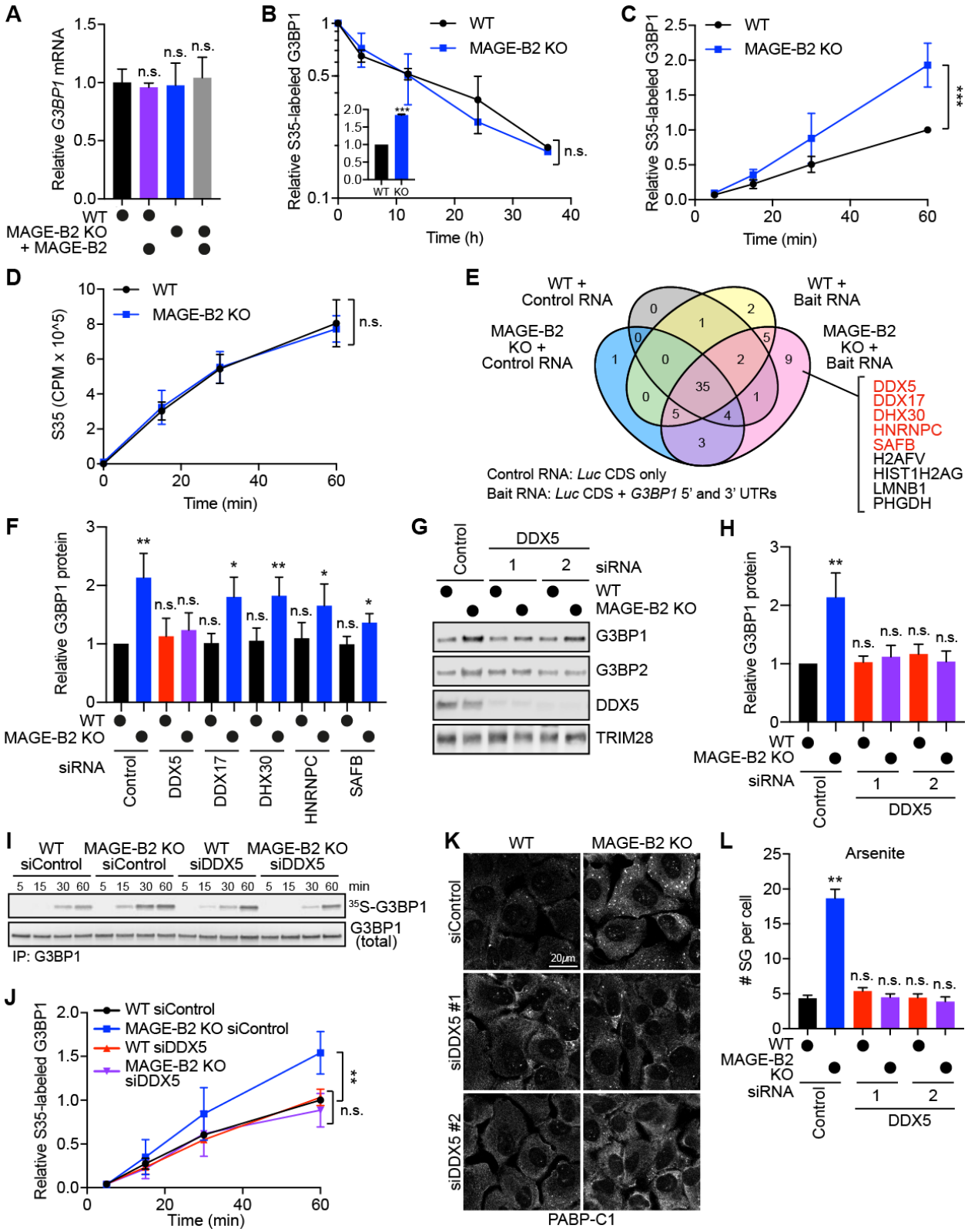

Figure 2-5. MAGE-B2 represses G3BP1 translation through inhibition of DDX5

(A) MAGE-B2 does not affect *G3BP1* mRNA levels. RT-qPCR analysis (n = 3) of *G3BP1* mRNA levels normalized to *18S* rRNA in the indicated U2OS cells. *P* values were determined by one-way ANOVA.

(B) MAGE-B2 does not affect G3BP1 protein degradation. G3BP1 protein half-life was measured (n = 3) in WT or MAGE-B2 KO U2OS cells by ^{35}S pulse-chase. Cells were pulse labeled with ^{35}S-Met/Cys for 1 hr (t = 0) and then chased in cold Met/Cys for the indicated times. ^{35}S-labeled G3BP1 was determined by immunoprecipitation, SDS-PAGE, and autoradiography. *P* value was determined by two-way ANOVA. The inset shows ^{35}S-labeled G3BP1 protein levels at t = 0 suggesting differences in G3BP1 translation. *P* value for t = 0 inset data was determined by unpaired *t* test.

(C) MAGE-B2 knockout enhances G3BP1 translation. WT or MAGE-B2 KO cells were incubated with ^{35}S-Met/Cys for the indicated times before G3BP1 was immunoprecipitated from cell lysates, separated by SDS-PAGE, and the newly synthesized G3BP1 was quantified (n = 3) by autoradiography. *P* value was determined by two-way ANOVA.

(D) MAGE-B2 does not affect global translation. Global translation was measured in WT or MAGE-B2 KO U2OS cells by ^{35}S-Met/Cys labeling for the indicated times and scintillation counting (n = 3). *P* value was determined by two-way ANOVA.

(E) Affinity pulldown of biotinylated RNA. Biotinylated control or bait transcripts (Luciferase CDS with *G3BP1* 5' and 3' UTRs) were pulled down from either WT or MAGE-B2 KO U2OS cells and subjected to mass spectrometry analysis. The Venn diagram lists the number of unique proteins for each sample. RNA-binding proteins that bound specifically to the bait transcript in MAGE-B2 KO cells are shown in red.

(F) DDX5 knockdown in MAGE-B2 KO cells rescues G3BP1 protein levels. RNA-binding proteins identified in Figure 3E were depleted in WT or MAGE-B2 KO U2OS cells by transfection with the indicated siRNAs for 72 hr to screen for potential involvement in MAGE-B2-mediated regulation of G3BP1. Cell lysates were immunoblotted and G3BP1 protein levels were quantified (n = 3).

(G and H) Validation of DDX5 knockdown by two independent siRNAs. WT or MAGE-B2 KO U2OS cells were transfected with the indicated siRNAs for 72 hr and immunoblotted for the indicated proteins. Representative immunoblots (G) and quantification (n = 3) of relative G3BP1 protein levels (H) are shown. *P* values were determined by *t* test.

(I and J) DDX5 knockdown in MAGE-B2 KO cells rescues G3BP1 translation. WT or MAGE-B2 KO cells were transfected with the indicated siRNAs for 72 hr before G3BP1 protein synthesis was measured by ^{35}S labeling as described in Figure 3B. Representative blots (I) and quantification (n = 3) of newly synthesized G3BP1 (J) are shown. *P* values were determined by two-way ANOVA.

(K and L) DDX5 knockdown in MAGE-B2 KO cells rescues SG formation. WT or MAGE-B2 KO U2OS cells were transfected with the indicated siRNAs for 72 hr, treated with 62 μM sodium arsenite for 1 hr, and immunostained for PABP-C1. Representative images (K) and quantification (n = 3) of SG number per cell (L) are shown. *P* values were determined by one-way ANOVA.

Data are mean ± SD. Asterisks indicate significant differences from the control (* = $p \leq 0.05$, ** = $p \leq 0.01$, *** = $p \leq 0.001$, n.s. = not significant).

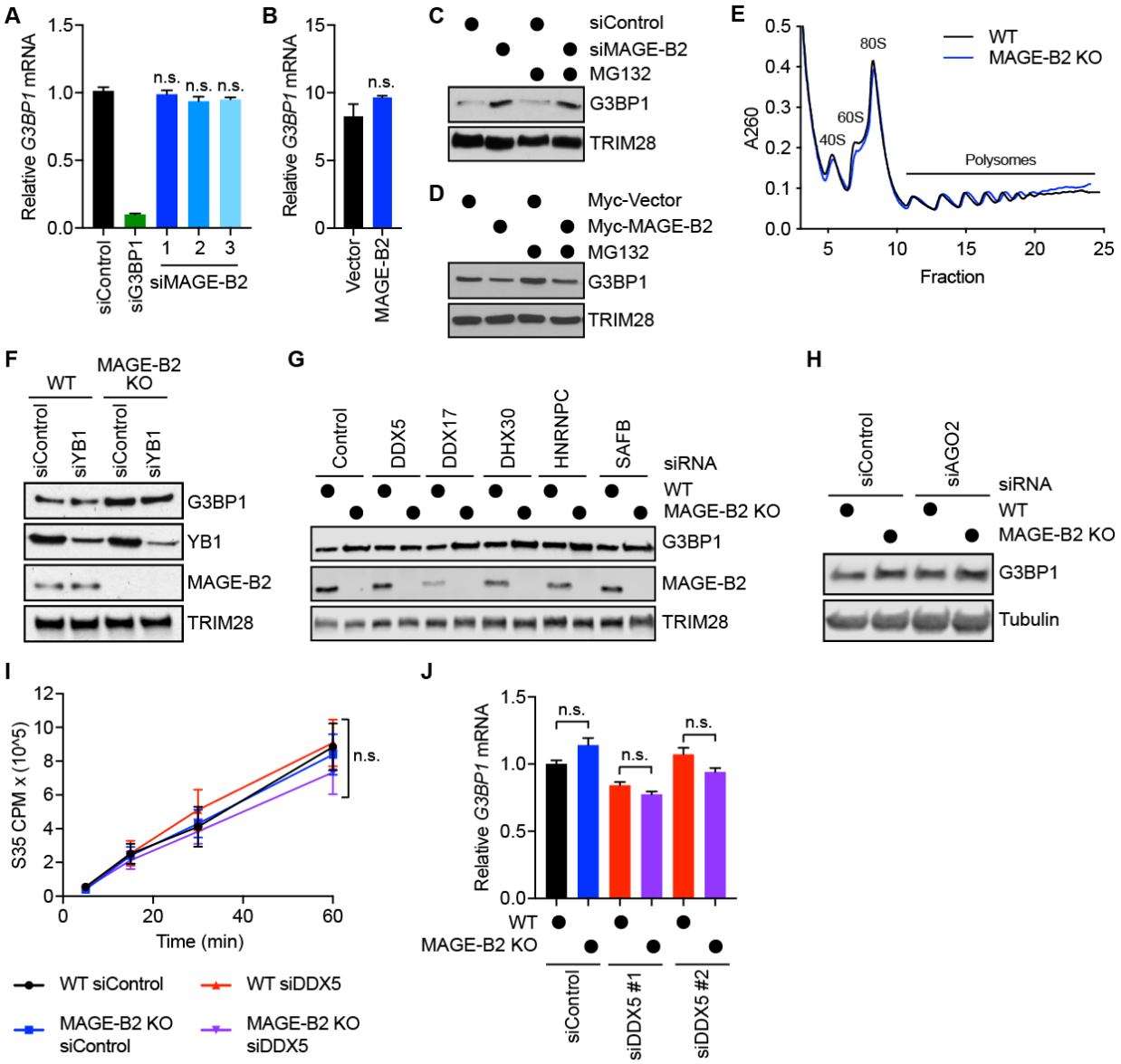

Figure 2-6. MAGE-B2 does not affect global translation, *G3BP* transcript levels, or protein stability

(A) Knockdown of MAGE-B2 does not affect *G3BP1* mRNA levels. RT-qPCR analysis of *G3BP1* mRNA levels normalized to *18S* rRNA in HCT116 cells transfected with the indicated siRNAs for 72 hr (n = 3). *P* values were determined by one-way ANOVA.

(B) Overexpression of MAGE-B2 does not affect *G3BP1* mRNA levels. RT-qPCR analysis of *G3BP1* mRNA levels normalized to *18S* rRNA in HeLa cells transiently transfected with either Myc-vector control or Myc-MAGE-B2 for 48 hr (n = 3). *P* value was determined by unpaired *t* test.

(C) Proteasomal inhibition does not affect G3BP1 protein levels. U2OS cells were transfected with the indicated siRNAs for 72 hr, treated with either DMSO or 10 μM MG132 for 6 hr, and immunoblotted for the indicated proteins.

(D) MAGE-B2 does not affect G3BP1 protein stability. HeLa cells were transfected with either Myc-vector control or Myc-MAGE-B2 for 48 hr, treated with either DMSO or 10 μM MG132 for 6 hr, and immunoblotted for the indicated proteins.

(E) MAGE-B2 KO does not affect global translation or polysome assembly. WT or MAGE-B2 KO U2OS cells were subjected to polysome fractionation by sucrose gradient. A260 nm was recorded during fraction collection. Data from one representative experiment of n = 4 biological replicates is shown.

(F) YB1 knockdown does not affect G3BP1 protein levels. WT or MAGE-B2 KO cells were transfected with control or YB1 siRNAs for 72 hr and immunoblotted for the indicated proteins.

(G) DDX5 knockdown in MAGE-B2 KO cells rescues G3BP1 protein levels. RNA-binding proteins identified in Figure 3E were depleted in WT or MAGE-B2 KO U2OS cells by transfection with the indicated siRNAs for 72 hr to screen for potential involvement in MAGE-B2-mediated regulation of G3BP1. Cell lysates were immunoblotted for the indicated proteins.

(H) AGO2 knockdown does not affect G3BP1 protein levels. WT or MAGE-B2 KO cells were transfected with control or AGO2 siRNAs for 72 hr and immunoblotted for the indicated proteins.

(I) DDX5 knockdown does not affect global translation. WT or MAGE-B2 KO U2OS cells were transfected with the indicated siRNAs for 72 hr before global translation was measured by ^{35}S-Met/Cys labeling for the indicated times and scintillation counting (n = 3). *P* values were determined by two-way ANOVA.

(J) DDX5 knockdown does not affect *G3BP1* mRNA levels. RT-qPCR analysis of *G3BP1* mRNA levels normalized to *18S* rRNA in WT or MAGE-B2 KO U2OS cells after transfection with the indicated siRNAs for 72 hr (n = 3). *P* values were determined by *t* test.

Data are mean ± SD. Asterisks indicate significant differences from the control (n.s. = not significant).

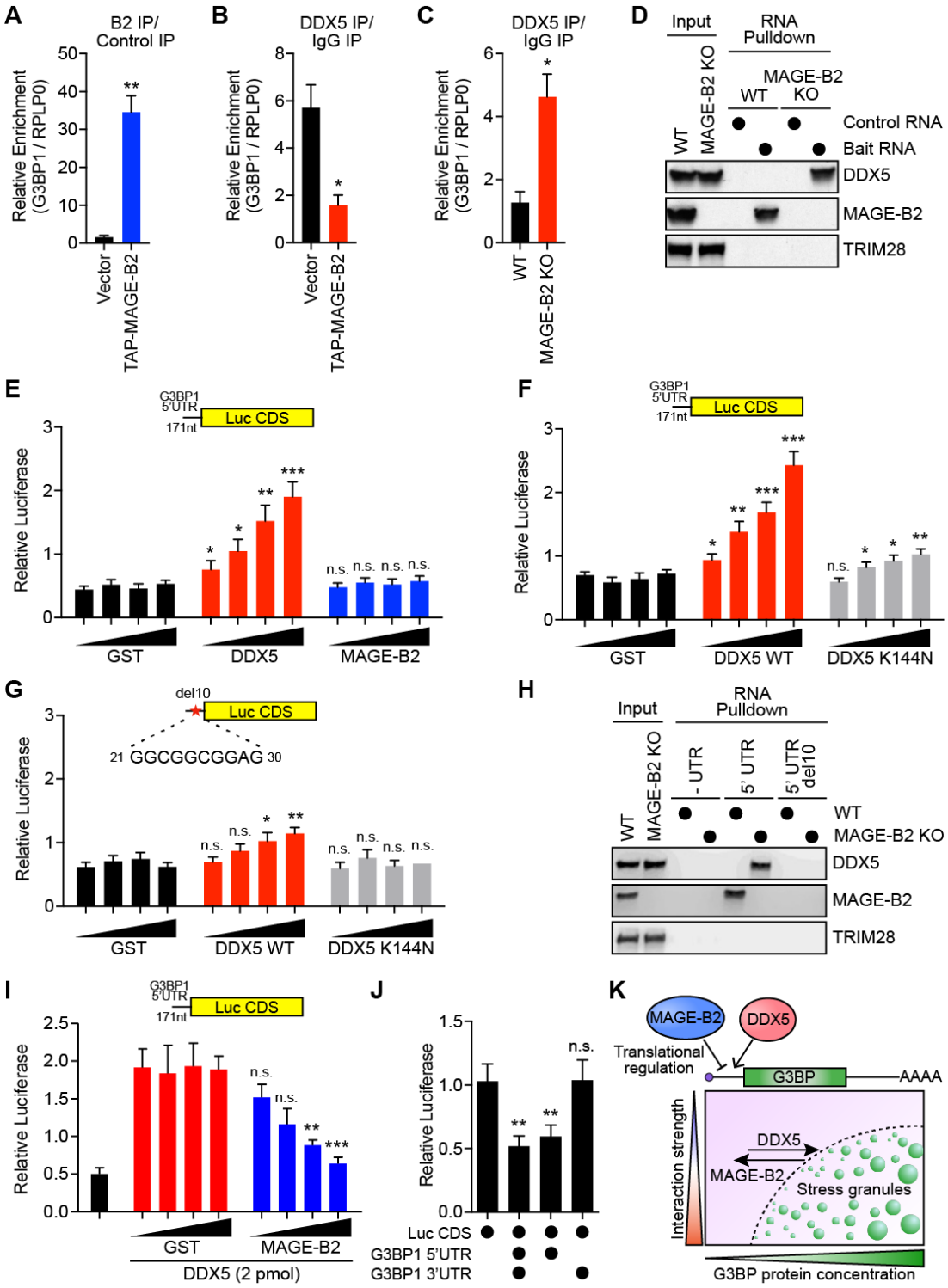

Figure 2-7. MAGE-B2 and DDX5 have opposing roles in the regulation of G3BP1 translation
(A) MAGE-B2 interacts with *G3BP1* mRNA by CLIP-qPCR. HEK293 cells stably expressing vector control or TAP-MAGE-B2 were subjected to 150 mJ/cm^2 of UVC (254 nm) before

immunoprecipitation of TAP-vector or TAP-MAGE-B2. *G3BP1* mRNA or *RPLP0* mRNA as a normalization control were then detected by RT-qPCR (n = 3). Relative amount of *G3BP1* mRNA in MAGE-B2 pulldown relative to control pulldown after *RPLP0* normalization is shown. *P* value was determined by *t* test.

(B) MAGE-B2 suppresses DDX5 interaction with *G3BP1* mRNA. CLIP-qPCR was performed as described above using HEK293 cells stably expressing vector control or TAP-MAGE-B2 to measure enrichment of *G3BP1* mRNA after DDX5 pulldown (n = 3). Relative levels of *G3BP1* mRNA in DDX5 pulldown relative to IgG control after *RPLP0* normalization is shown. *P* value was determined by *t* test.

(C) Loss of MAGE-B2 enhances DDX5 interaction with *G3BP1* mRNA. CLIP-qPCR was performed on WT or MAGE-B2 KO U2OS cells to measure enrichment of *G3BP1* mRNA for DDX5 (n = 3) as described above. *P* value was determined by *t* test.

(D) MAGE-B2 and DDX5 compete for binding to *G3BP1* mRNA. Biotinylated control (*Luc* CDS) or bait (*Luc* CDS with *G3BP1* 5' and 3' UTRs) transcripts were pulled down from either WT or MAGE-B2 KO U2OS cells and subjected to immunoblotting for DDX5, MAGE-B2, or TRIM28 as a negative control.

(E) DDX5 enhances G3BP1 translation *in vitro*. *In vitro* translation assays were performed using rabbit reticulocyte lysate with increasing amounts of recombinant GST (control), DDX5, or MAGE-B2 to measure translation of a luciferase reporter (n = 3) containing *G3BP1* 5' UTR. *P* values were determined by *t* test.

(F and G) DDX5 helicase activity is required for enhancing G3BP1 translation *in vitro*. *In vitro* translation assays were performed using increasing amounts of recombinant GST (control), DDX5 WT, or DDX5 K144N (helicase dead mutant) to measure translation of a luciferase reporter (n = 3) containing *G3BP1* 5' UTR (F) or *G3BP1* 5' UTR lacking the DDX5 binding motif (10 nucleotide deletion) (G). *P* values were determined by *t* test.

(H) Deletion of the DDX5 binding motif disrupts DDX5 and MAGE-B2 binding to *G3BP1* mRNA. Biotinylated *Luc* CDS (- UTR) transcripts containing *G3BP1* 5' UTR (5' UTR) or *G3BP1* 5' UTR lacking the DDX5 binding motif (5' UTR del10) were pulled down from either WT or MAGE-B2 KO U2OS cells and subjected to immunoblotted for DDX5, MAGE-B2, or TRIM28 as a negative control.

(I) *In vitro* translation assays reveal competition between DDX5 and MAGE-B2 for G3BP1 regulation via the 5' UTR. *In vitro* translation assays were performed using recombinant DDX5 and titrating increasing amounts of GST (control) or MAGE-B2 to measure translation (n = 3) of a luciferase reporter containing *G3BP1* 5' UTR. *P* values were determined by *t* test.

(J) Regulation of G3BP1 translation via the 5' UTR. Basal translation of the various luciferase reporters relative to control (Luc CDS) reveals that the presence of *G3BP1* 5' UTR suppresses translation (n = 3). *P* values were determined by one-way ANOVA.

(K) Model of the mechanism by which MAGE-B2 reduces G3BP and suppresses SG. MAGE-B2 inhibits G3BP translation by competing with the translational activator DDX5. This results in reduced G3BP protein levels, suppression of SG, and increased cellular stress threshold.

Data are mean ± SD. Asterisks indicate significant differences from the control (* = $p \leq 0.05$, ** = $p \leq 0.01$, *** = $p \leq 0.001$, n.s. = not significant).

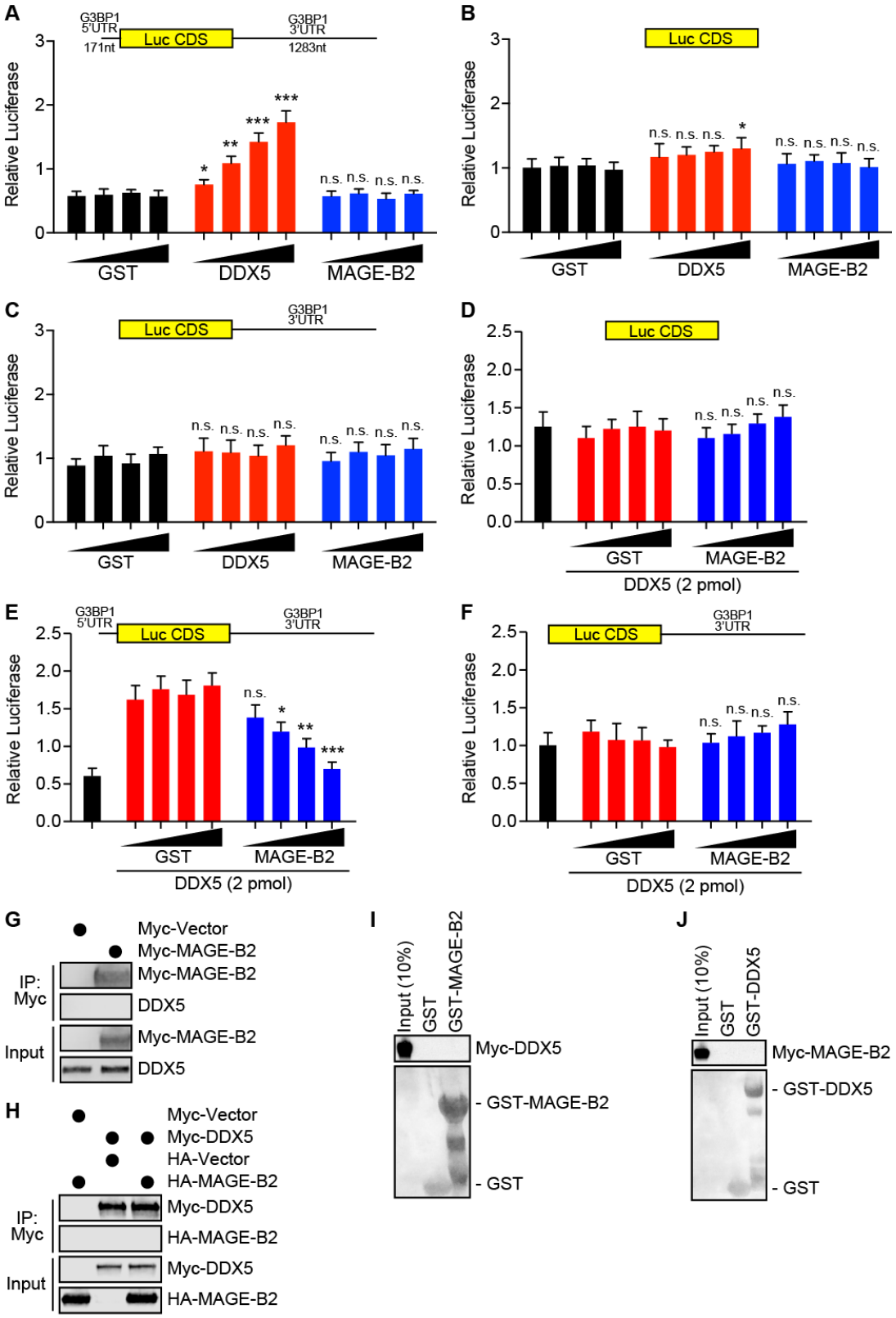

Figure 2-8. Regulation of G3BP1 translation occurs via the 5' UTR

(A-C) *G3BP1* 5' UTR is necessary for DDX5 to enhance G3BP1 translation *in vitro*. *In vitro* translation assays were performed (n = 3) using rabbit reticulocyte lysate with increasing amounts of recombinant GST (control), DDX5, or MAGE-B2 to measure translation of a luciferase reporter containing *G3BP1* 5' and 3' UTRs (A), control luciferase reporter lacking UTRs (B), or *G3BP1* 3' UTR (C).

(D-F) *In vitro* translation assays reveal competition between DDX5 and MAGE-B2 for G3BP1 regulation via the 5' UTR. *In vitro* translation assays were performed as in Figure 4I to measure translation of a control luciferase reporter (D), a luciferase reporter containing *G3BP1* 5' and 3' UTRs (E), or *G3BP1* 3' UTR (F) (n = 3).

(G and H) MAGE-B2 and DDX5 do not interact in cells. HeLa cells were transfected with the indicated constructs for 48 hr and immunoprecipitated with anti-Myc beads followed by immunoblotting for endogenous DDX5 (G) or overexpressed HA-MAGE-B2 (H).

(I and J) MAGE-B2 and DDX5 do not bind *in vitro*. Recombinant GST-MAGE-B2 (I) or GST-DDX5 (J) were incubated with *in vitro* translated Myc-DDX5 (I) or Myc-MAGE-B2 (J), pulled down by glutathione sepharose beads, eluted, separated by SDS-PAGE, and immunoblotted.

Data are mean ± SD. Asterisks indicate significant differences from the control (*p* values were determined by *t* test; * = $p \leq 0.05$, ** = $p \leq 0.01$, *** = $p \leq 0.001$, n.s. = not significant).

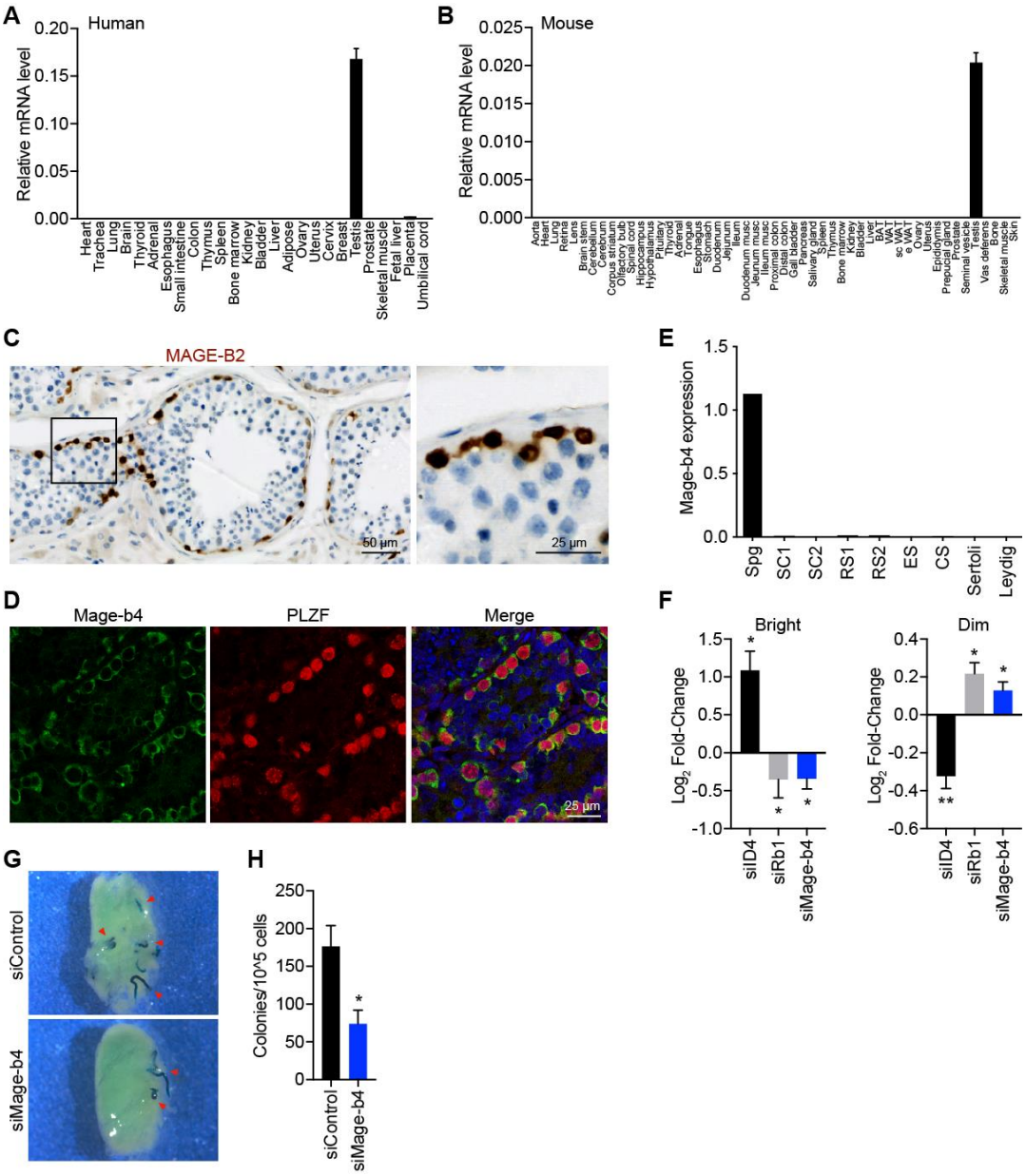

Figure 2-9. The mouse ortholog of human MAGE-B2 (Mage-b4) regulates stemness of testis spermatogonial stem cells

(A) Human *MAGE-B2* is expressed specifically in the testis. RT-qPCR analysis (n = 3) of normalized human *MAGE-B2* expression in the indicated tissues. Data are mean ± SD.

(B) Mouse *Mage-b4* is expressed specifically in the testis. RT-qPCR analysis (n = 3) of normalized mouse *Mage-b4* expression in the indicated tissues from BALB/C mice. Data are mean ± SD.

(C) Immunohistochemistry staining of human testis shows MAGE-B2 is expressed in spermatogonia.

(D) Mouse Mage-b4 is expressed in undifferentiated spermatogonia. Mouse testis were immunostained for Mage-b4 and PLZF and representative images are shown.

(E) Mouse Mage-b4 is enriched in spermatogonia. Analysis of previously described (Lukassen et al., 2018) single-cell RNA sequencing data derived from 8-week-old C57Bl/6J mice is shown. Spg = spermatogonia, SC = spermatocytes, RS = round spermatids, ES = elongating spermatids, CS = condensed/ condensing spermatids.

(F) Mage-b4 maintains ID4-EGFP^{bright} stem cells in primary cultures of undifferentiated spermatogonia. Primary spermatogonia cultures were treated with the indicated siRNAs for 6 days before flow cytometry analysis to determine the percentage of ID4-EGFP^{bright} and ID4-EGFP^{dim} (n = 3). Log_2 fold change of ID4-EGFP^{bright} (left) and ID4-EGFP^{dim} (right) is shown. Data are mean ± SEM.

(G and H) Mage-b4 is required for efficient repopulation of testis. Spermatogonial transplantation assays were performed by transfecting LacZ-expressing primary spermatogonia cells with the indicated siRNAs for 6 days and transplanting them into the testes of recipient males depleted of germ cells. Two months later the number of LacZ-positive donor-derived colonies of spermatogenesis in the testis was determined (n = 3). Representative images (G) and quantification (H) are shown. Data are mean ± SEM.

Asterisks indicate significant differences from the control (*p* values were determined by *t* test; * = $p \leq 0.05$, ** = $p \leq 0.01$).

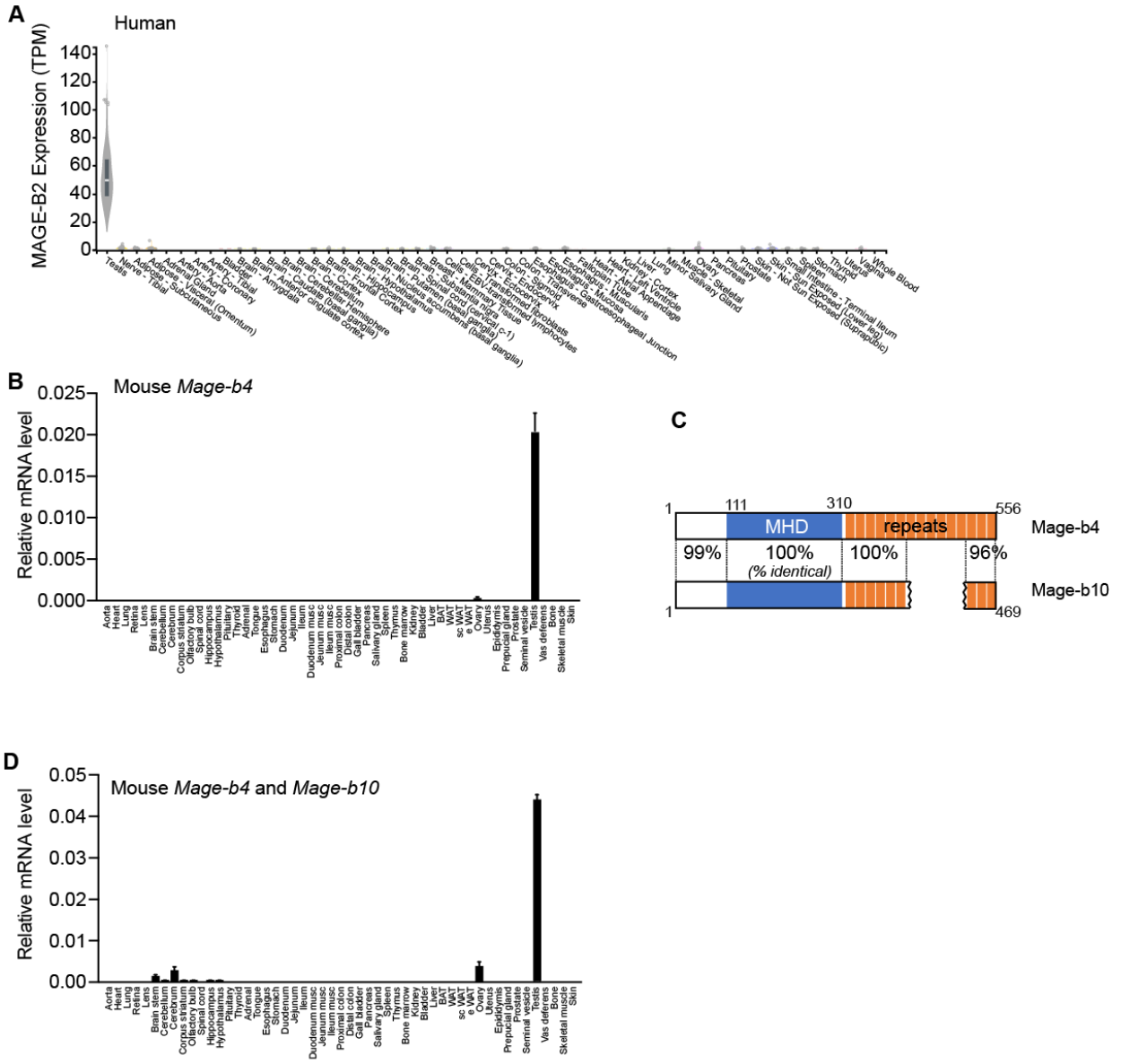

Figure 2-10. Mage-b4 and -b10 are enriched in the testis

(A) Human *MAGE-B2* is expressed specifically in the testis. Gene expression data based on TPM values from the Genome-Tissue Expression (GTEx) Portal.

(B) Mouse *Mage-b4* is expressed specifically testis. RT-qPCR analysis (n = 3) of normalized mouse *Mage-b4* expression in the indicated tissues from C57BL/6 mice. Data are mean ± SD.

(C) Domain map and sequence identities of mouse Mage-b4 (top) and mouse Mage-b10 (bottom).

(D) Mouse *Mage-b10* is highly enriched in the testis. RT-qPCR analysis (n = 3) of normalized mouse *Mage-b4* and *Mage-b10* expression in the indicated tissues from C57BL/6 mice. Note RT-qPCR primer detects both *Mage-b4* and *Mage-b10* paralogs. Data are mean ± SD.

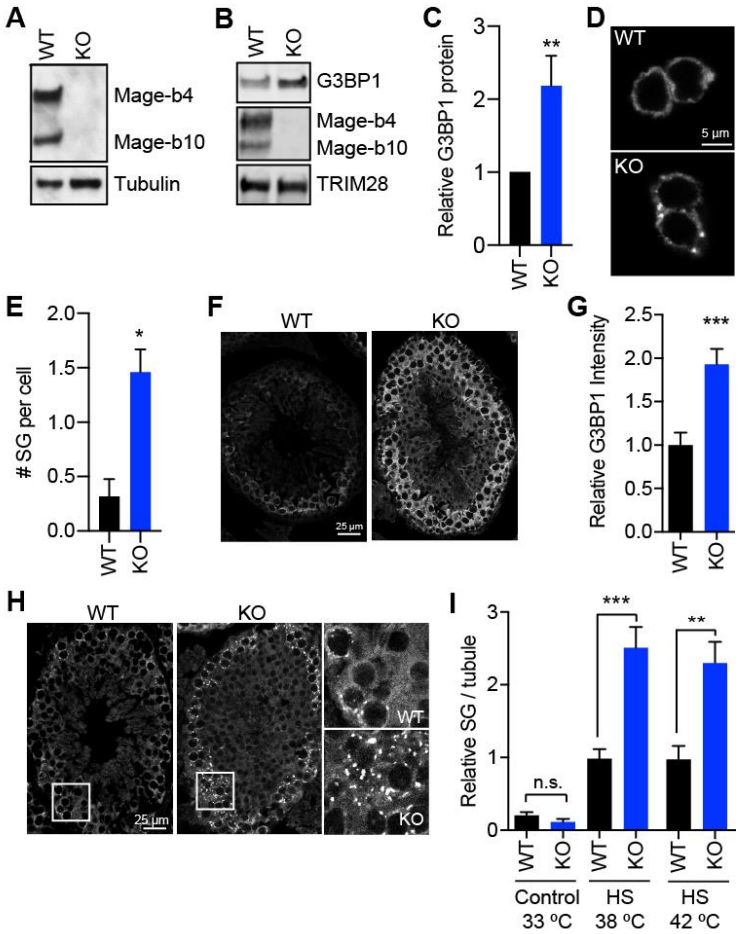

Figure 2-11. Mice deficient in the MAGE-B2 ortholog exhibit increased levels of G3BP1 protein and enhanced SG formation

(A) Mage-b4 and paralog Mage-b10 were knocked out by CRISPR/Cas9. Immunoblotting of testis lysates confirmed loss of Mage-b4/b10 protein.

(B and C) Primary cultures of undifferentiated spermatogonia from WT or Mage-b4 KO mice were immunoblotted for the indicated proteins. Representative immunoblots (B) and quantification (n = 3) of relative G3BP1 protein levels (C) are shown. *P* value was determined by *t* test.

(D and E) Primary cultures of undifferentiated spermatogonia from WT or Mage-b4 KO mice were treated with 250 µM sodium arsenite for 1 hr and immunostained for PABP-C1. Representative images (D) and quantification (n = 3) of SG number per cell (E) are shown. *P* value was determined by *t* test.

(F and G) Mage-b4 KO mice have increased levels of G3BP1 protein. Testes from WT or KO mice were sectioned and immunostained for G3BP1. Representative images (F) and quantification of relative G3BP1 intensity (G) are shown.

(H and I) Testes of WT or Mage-b4 KO mice were heat stressed (HS) for 15 min at 38 or 42 °C. Mice were immediately sacrificed, testes isolated and sectioned before G3BP1 immunostaining to detect stress granules. 10-20 seminiferous tubules were counted in testes of 4 mice per genotype totaling 80 tubules counted. Representative images (H) and quantification (I) are shown.

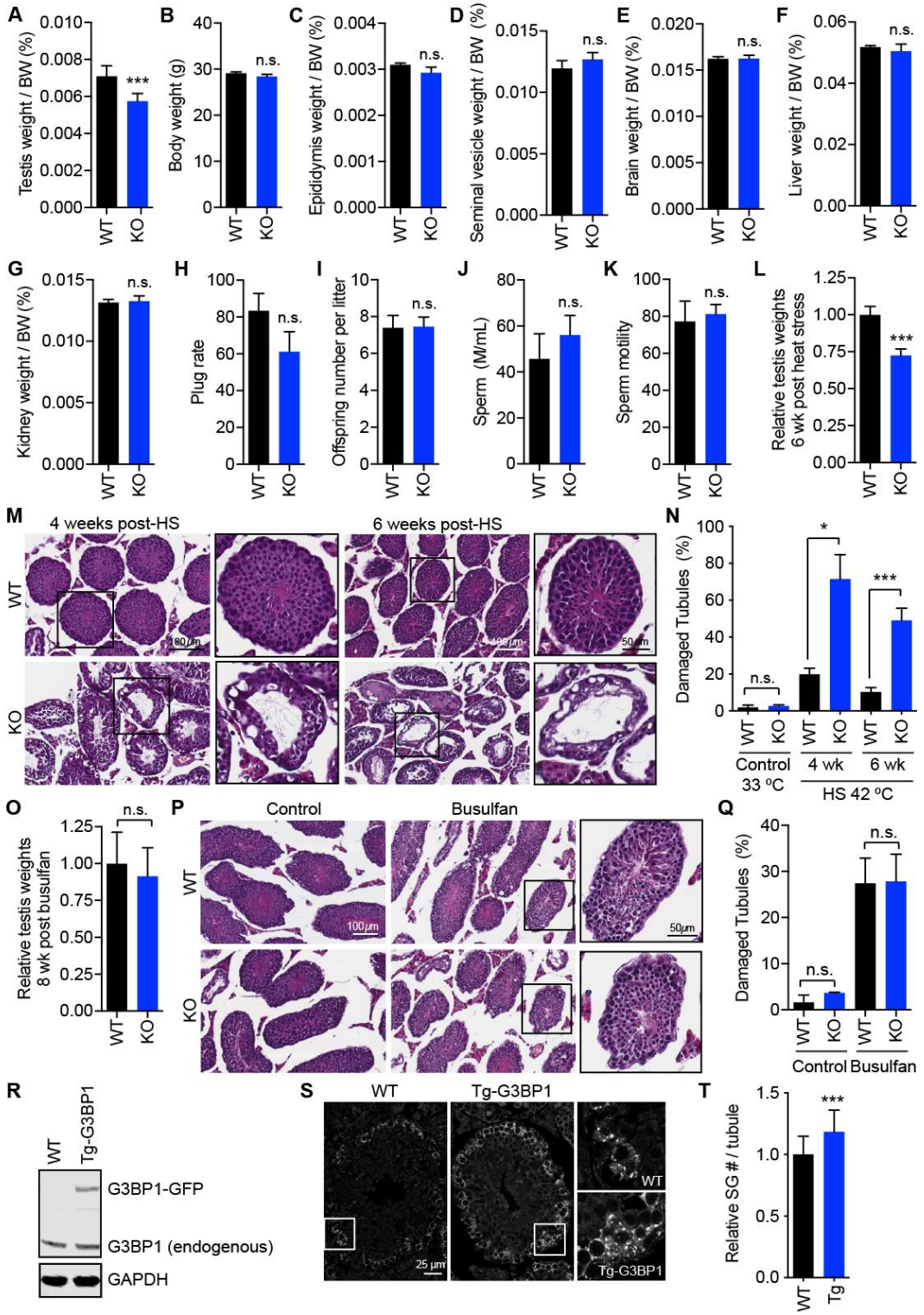

Figure 2-12. Characterization of Mage-b4 KO and transgenic G3BP1 mouse models

(A-G) General characterization of Mage-b4 KO mice. Testis weights (A), body weights (B), epididymis weights (C), seminal vesicle weights (D), brain weights (E), liver weights (F), and liver weights (G) are shown (n = 6 mice per genotype).

(H-K) Mage-b4 is not required for basal male fertility as shown by vaginal plug rates (H), number of pups born (I), sperm concentration (J), or sperm motility (K) compared to WT mice (n = 3-6 mice per genotype).

(L-N) Mage-b4 KO mice are hypersensitive to heat stress. WT or KO mice were heat shocked at 42 °C for 15 min and allowed to recover for 4 or 6 weeks as indicated. Testis weights were measured (n = 6 per genotype) and are reported relative to WT mice and normalized to unstressed mice from each genotype (L). Representative histology images (M) and quantification of damaged tubules (N) are shown (n = 6 control mice per genotype, n = 3-6 heat shocked mice per genotype per time point).

(O-Q) Mage-b4 KO mice are not hypersensitive to genotoxic stress. WT or KO mice were intraperitoneally injected with 20m mg/kg body weight of busulfan and allowed to recover for 8 weeks. Testis weights (O) were measured 8 weeks post-treatment and normalized to untreated mice (n = 4-6 busulfan-treated mice per genotype, n = 8-10 control mice per genotype). Representative images (P) and quantification of damaged tubules (Q) are shown (n = 2 control mice per genotype, n = 6 busulfan-treated mice per genotype).

(R) Immunblotting of brain lysates confirmed expression of the G3BP1-GFP transgene in Tg-G3BP1 mice.

(S and T) Testes of WT or Tg-G3BP1 mice were heat stressed at 42 °C for 15 min. Mice were immediately sacrificed, testes silated and section before G3BP1 immunostaining to detect stress granules. Representative images (S) and quantification (T) are shown (n = 23 seminiferous tubules from testes of 6 mice per genotype).

Data are mean ± SD. Asterisks indicate significant differences from the control (*p* values were determined by unpaired *t* test; * = $p \leq 0.05$, *** = $p \leq 0.001$, n.s. = not significant).

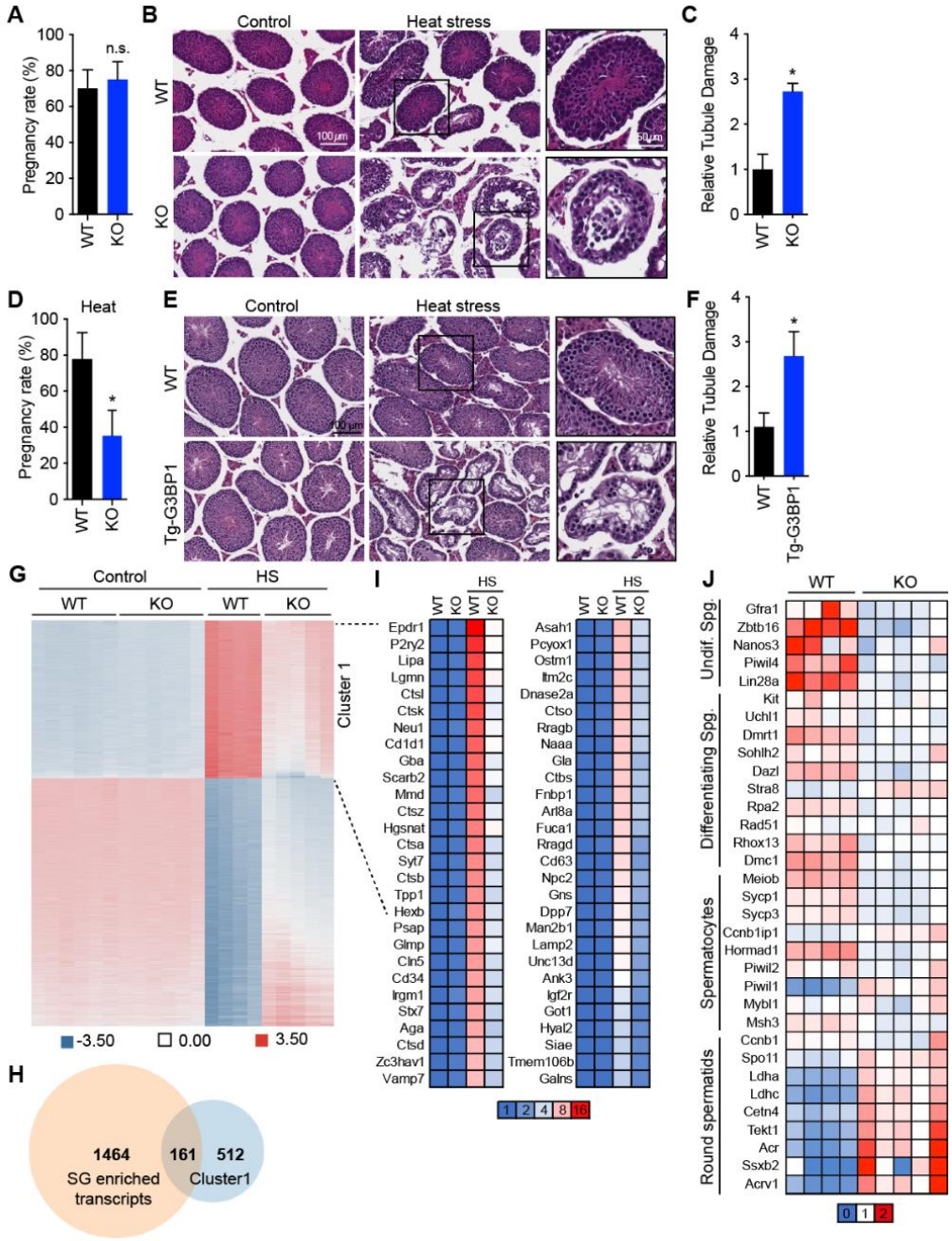

Figure 2-13. Knockout of the MAGE-B2 ortholog in mice results in hypersensitivity of the testis to heat stress

(A) Mage-b4 is not required for fertility under unstressed conditions. Pregnancy rates were determined by breeding WT or KO male mice to virgin WT females (n = 20 mating trails across 12 mice per genotype).

(B and C) Mage-b4 KO mice are hypersensitive to heat stress. WT or KO mice were control treated at 33 °C or heat stressed at 42 °C for 15 min and allowed to recover for 2 weeks. Representative

histology images (B) and quantification of relative tubule damage (C) are shown (n = 6 mice per genotype, n = 3-6 heat stressed mice per genotype per time point).
(D) Mage-b4 KO mice are less fertile after heat stress. WT or KO mice were heat shocked at 42 °C for 15 min and allowed to recover for 6 weeks (n = 9 per genotype). P value was determined by Chi-square analysis.
(E and F) G3BP1-GFP transgenic mice are hypersensitive to heat stress. WT or Tg-G3BP1 mice were control treated at 33 °C or heat stressed at 42 °C for 15 min and allowed to recover for 2 weeks. Representative histology images (E) and quantification of relative tubule damage (F) are shown (n = 6 control mice per genotype).
(G) Heat map of differentially expressed transcripts upon heat stress. WT or Mage-b4 KO mice were control treated at 33 °C or heat stressed at 42 °C for 20 min and allowed to recover for 72 hr before testes were harvested for RNA isolation and RNA-sequencing analysis (n = 6 control mice per genotype, n = 4-5 heat stressed mice per genotype).
(H) Cluster 1 is significantly (χ^2, $p<0.000001$) enriched for transcripts previously identified to be enriched in SG (Jain et al., 2016; Khong et al., 2017; Markmiller et al., 2018; Namkoong et al., 2018; Souquere et al., 2009; Wheeler et al., 2016). Venn diagram shows number of transcripts overlapping.
(I) Heatmap of genes involved in the lysosomal pathway. Differentially expressed transcripts in Cluster 1 were subjected to gene ontology analysis and found to be enriched for genes associated with the lysosomal pathway.
(J) Mage-b4 KO mice exhibit reduced levels of early spermatogenesis markers after heat stress. Gene expression of select spermatogenesis markers was analyzed relative to median expression. Undif. Spg. = Undifferentiated spermatogonia.
Data are mean ± SD. Asterisks indicate significant differences from the control (*p* values were determined by unpaired *t* test; * = $p \leq 0.05$, n.s. = not significant).

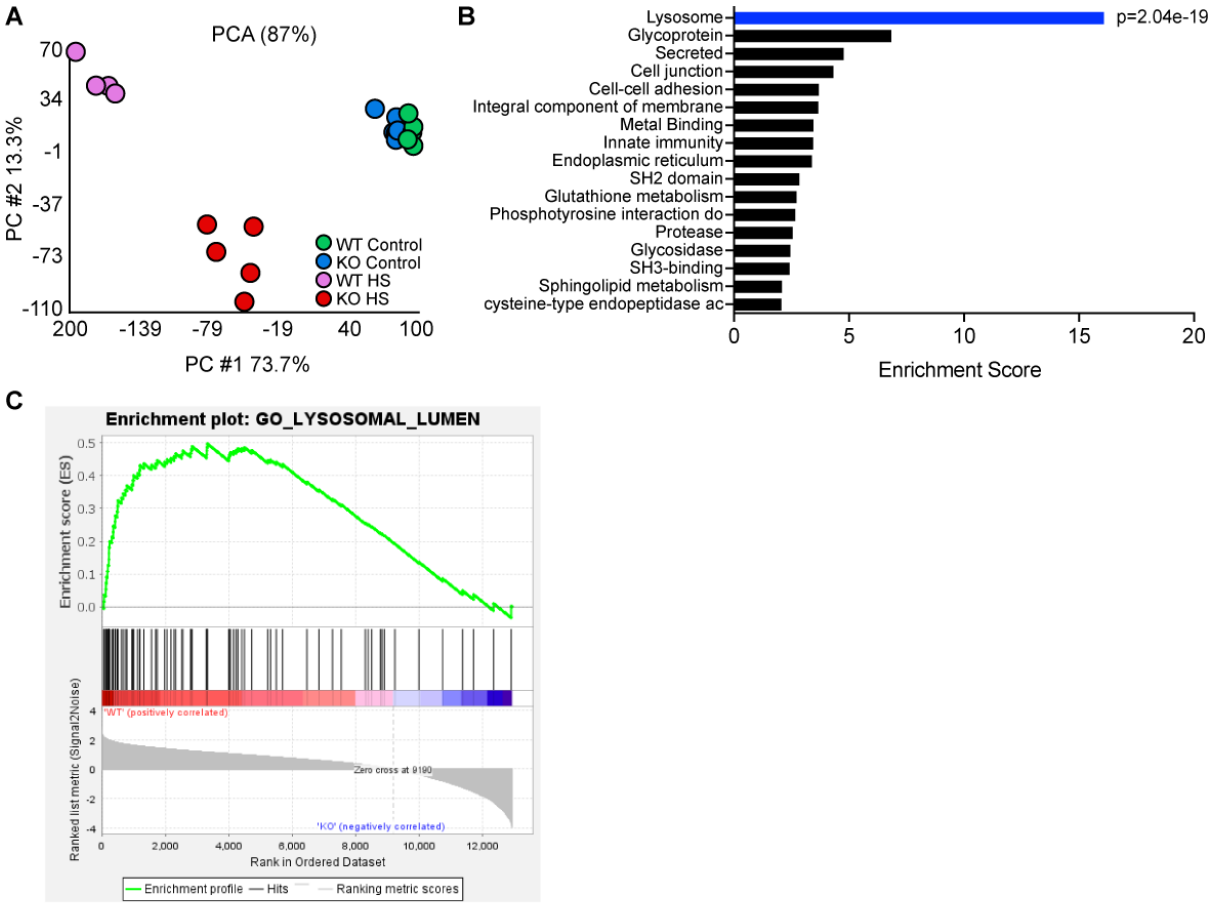

Figure 2-14. Differential gene expression between WT and Mage-b4 KO mice after heat stress

(A) Gene expression variances between samples are displayed as principal component analysis (PCA).

(B) Gene ontology analysis of differentially expressed genes in Cluster 1.

(C) Gene set enrichment analysis (GSEA) revealed significant enrichment of lysosomal lumen genes in Cluster 1.

CHAPTER THREE
Conclusions and Future Directions

MAGE-B2 IS A CANCER-TESTIS ANTIGEN

MAGE-B2, like other type I MAGE CTAs, is primarily expressed in the testis and is aberrantly expressed in various cancers where it has been implicated in tumor growth and progression. More specifically, MAGE-B2 overexpression promoted cell proliferation in transformed oral keratinocytes, while MAGE-B2 depletion reduced proliferation in osteosarcoma cell lines (Pattani et al., 2012; Peche et al., 2015). Moreover, subcutaneous injection of mouse melanoma cell lines expressing human MAGE-B2 enhanced tumor xenograft growth in mice (Peche et al., 2015). Interestingly, MAGE-B2 is thought to be activated early during carcinogenesis and has also been shown to be expressed in the cancer stem cell-like side population derived from colon adenocarcinoma cells (Yamada et al., 2013). Despite the mounting evidence indicative of MAGE-B2's oncogenic potential, little is known about its molecular function. However, this thesis reveals a theme analogous to MAGE-A function—stress tolerance (Fon Tacer et al., 2019).

REGULATION OF STRESS TOLERANCE

We determined that MAGE-B2 enhances the cellular stress threshold by suppressing stress granule (SG) assembly. SG are conserved ribonucleoprotein membraneless organelles that form in response to a variety of stress stimuli (Protter and Parker, 2016; Van Treeck and Parker, 2018). Upon exposure to stress, translation stalls, polysomes disassemble, and a number of

proteins and mRNAs condense into cytoplasmic SG (Anderson et al., 2015; Kedersha and Anderson, 2002). Recent studies have demonstrated that the collective behavior of protein-protein, protein-RNA, and RNA-RNA interactions allow for the assembly of droplet-like structures via liquid-liquid phase separation (LLPS) (Banani et al., 2016; Van Treeck and Parker, 2018). Although the specific proteins and mRNAs that localize to SG have been shown to be stress-dependent, G3BP1 and its paralog G3BP2 (collectively referred to as G3BP) are uniquely critical for SG core assembly, where overexpression of G3BP induces spontaneous SG formation and deletion ablates SG in response to sodium arsenite (Jain et al., 2016; Kedersha et al., 2016; Khong et al., 2017; Markmiller et al., 2018; Namkoong et al., 2018; Reineke et al., 2012; Souquere et al., 2009; Wheeler et al., 2016; Zhang et al., 2019). While the exact molecular features that drive SG formation are still being elucidated, G3BP is predicted to promote LLPS of SG due to its ability to bind RNA and form higher order oligomers.

We sought to determine the molecular function of this understudied MAGE and found that MAGE-B2 regulates SG dynamics, such that depletion of MAGE-B2 led to increased SG formation and overexpression of MAGE-B2 had the opposite effect. Contrary to a previous report from Peche et al. (Peche et al., 2015), we found that MAGE-B2 depletion in U2OS osteosarcoma cells had no affect on cell proliferation; however, upon exposure to prolonged low dose oxidative stress by sodium arsenite, MAGE-B2 knockout cells exhibited reduced cell viability that could be rescued by re-expression of MAGE-B2. Intriguingly, although Peche and colleagues reported that MAGE-B2 depletion in U2OS cells resulted in reduced cell proliferation quantified by optical density and colony formation, BrdU incorporation was not

affected. Yet, treatment with the ribotoxic agent actinomycin D at a low dose led to reduced BrdU incorporation in MAGE-B2-depleted U2OS cells (Peche et al., 2015). Together, these findings suggest that MAGE-B2 increases cellular stress tolerance.

Further investigation into the mechanism by which MAGE-B2 alters SG assembly revealed that MAGE-B2 reduces G3BP protein levels. Given that *in vitro* LLPS is highly dependent on protein concentration, we hypothesized that cellular G3BP protein levels would dictate the set point for SG assembly and the cellular stress tolerance. Indeed, we found that MAGE-B2-mediated regulation of G3BP protein levels was responsible for altering SG formation and cell viability under prolonged stress.

In a surprising deviation from prototypical MAGE-RING ubiquitin ligases, we demonstrated that MAGE-B2 functions as an RNA-binding protein that directly binds the *G3BP* transcript to inhibit its translation. In addition, we found that MAGE-B2 binding to the 5'UTR of *G3BP* displaces the translational activator DDX5, also referred to as p68. Furthermore, depletion of DDX5 in MAGE-B2 knockout cells rescued both G3BP translation and SG formation, thereby indicating a competitive model by which MAGE-B2 and DDX5 fine-tune G3BP concentration to regulate SG dynamics.

To examine MAGE-B2 function in terms of normal physiological conditions, we characterized the expression of human MAGE-B2 and its mouse orthologs, Mage-b4 and Mage-b10 (simply referred to as Mage-b4 due to sequence identity). Both human and mouse genes exhibited testis-specific expression and enrichment in undifferentiated spermatogonia including spermatogonial stem cells (SSC). These findings were consistent with previous reports that showed preferential expression of MAGE-B2 and Mage-b4 in spermatogonia and

suggested a potential role in germ cell differentiation (Fon Tacer et al., 2019; Guo et al., 2018; Jung et al., 2019; Osterlund et al., 2000; Sohni et al., 2019; Xia et al., 2020). To test this hypothesis, we depleted Mage-b4 from *in vitro* primary cultures of undifferentiated spermatogonia from Id4-eGFP reporter mice or *in vivo* spermatogonial transplantation assays and demonstrated that Mage-b4 plays a key role in SSC function and maintenance.

Spermatogenesis is a highly coordinated developmental process that requires proper SSC maintenance for continuous sperm production. Most mammals maintain testes in scrotum outside the body, thereby sustaining spermatogenesis at temperatures significantly lower than the core body temperature (Widlak and Vydra, 2017). It is well-established that exposure of the testes to elevated temperatures disrupts the highly thermo-sensitive process of spermatogenesis and results in germ cell apoptosis, compromised sperm quality, and increased risk of infertility (Reid et al., 1981; Rockett et al., 2001; Yin et al., 1997). Given that MAGE-B2 inhibition of SG formation was important for increasing the cellular threshold against stress, we hypothesized that Mage-b4 might also protect the male germline from stress. Generation of Mage-b4 knockout mice revealed enhanced SG formation within the SSCs in response to stress *in vitro* and *in vivo*. In addition, Mage-b4 knockout mice were exposed to heat stress followed by a recovery period of up to 6 weeks to allow enough time for two rounds of spermatogenesis. While unstressed Mage-b4 knockout mice showed no defects in fertility compared to wildtype mice, heat stressed knockout mice had reduced fertility and increased damage within the seminiferous tubules. Together, these data suggest that Mage-b4 evolved to protect male germline cells from stress and preserve spermatogenesis.

A previous study from Peche et al. demonstrated that MAGE-B2 enhances E2F activity (Peche et al., 2015). E2F genes are transcriptional regulators of cell-cycle progression and virtually all cancers exhibit high E2F activity (Kent and Leone, 2019). Elevated E2F target expression in tumors is thought to induce aberrant cell proliferation and increase cell cycle-generated genomic errors. Because Necdin was previously shown to target and inhibit E2F function, the authors tested whether MAGE-B2 also shares this function (Kuwako et al., 2004; Taniura et al., 1998). They found that depletion of MAGE-B2 reduced transcript levels of known cell cycle-associated E2F target genes such as MCM6, CyclinD1, and CDK1; whereas, MAGE-B2 overexpression enhanced E2F reporter activity. Further analysis revealed that MAGE-B2 binds the E2F1 repressor HDAC1, thereby reducing the inhibitory E2F1-HDAC1 interaction. Therefore, whether MAGE-B2-mediated activation of E2F contributes to stress tolerance warrants further investigation.

MAGE-B2 AND AUTOIMMUNE DISEASES

Interestingly, while MAGE function is typically assessed in the context of spermatogenesis or tumorigenesis, MAGE-B2 was originally identified in pediatric patients with systemic lupus erythematosus (SLE) where MAGE-B2 protein and autoantibodies can be found (Hoftman et al., 2008). SLE is a chronic autoimmune disease that causes widespread inflammation and tissue damage in affected organs (OMIM 152700). While the pathogenic role of MAGE-B2 in SLE remains unknown, the presence of MAGE-B2 protein and autoantibodies in patients with active lupus nephritis and the ability of MAGE-B2 to stimulate an immune response when it

is presented by the MHC suggest a potential role in immune activation (Barnea et al., 2002; Fleischhauer et al., 1998; Mizukami et al., 2005; Novellino et al., 2005). Just as DNA hypomethylation is a ubiquitous feature of carcinogenesis, genome-wide methylation abnormalities are seen in patients with SLE (Ballestar et al., 2006; Richardson, 2003; Timp and Feinberg, 2013). Therefore, it is plausible that disrupted DNA methylation allows for aberrant MAGE-B2 expression and the presentation of normally hidden antigens to provoke an autoimmune response and inflammation associated with SLE pathology.

Since its identification in SLE, MAGE-B2 autoantibodies have also been detected in patients with autoimmune polyendocrine syndrome type 1 (APS1), a monogenic autoimmune disorder that is caused by loss-of-function mutations in the Autoimmune regulator (AIRE) gene (Finnish-German, 1997; Landegren et al., 2016; Nagamine et al., 1997). AIRE encodes a transcription factor that plays an essential role in promoting self-tolerance in the thymus by driving promiscuous expression of tissue-restricted antigens (Anderson et al., 2002; Liston et al., 2003). This AIRE-driven antigen display allows naïve T-cells to be exposed to tissue-specific antigens and subsequent elimination of autoreactive T-cells. In patients with APS1, defective AIRE allows autoreactive T cells to survive, thereby creating an autoimmune response. Intriguingly, infertility is a common manifestation of APS1 in both male and female patients; however, whether MAGE-B2 antigens play a role in APS1 infertility remains unknown. Further investigation by Conteduca et al. identified two identified two variant alleles of the rs1800522 AIRE SNP and demonstrated differential modulation of MAGE-B2-specific T cell survival and mouse *in vivo* susceptibility to melanoma; however, whether this finding translates to cancer predisposition in humans is yet to be determined (Conteduca et al., 2016).

FINAL CONCLUSIONS

This work begins with a general overview of MAGEs to provide context for our subsequent investigation of MAGE-B2 function. Our studies revealed that MAGE-B2 enhances stress tolerance by reducing SG in spermatogonia and cancer cells. Interestingly, these findings support a growing notion that MAGEs recently evolved in eutherians to allow for rapid adaptation against a diverse range of stressors. However, unlike previously characterized MAGEs, MAGE-B2 functions as an RBP to repress translation of the key SG nucleator G3BP. By discovering this mechanistic deviation from prototypical MRLs, we not only characterize the first RNA-binding MAGE, but also broaden the potential functional roles of other MAGE proteins, particularly those in the MAGE-B subfamily.

BIBLIOGRAPHY

Alberti, S. (2017). Phase separation in biology. Curr Biol *27*, R1097-R1102.

Alberti, S., Mateju, D., Mediani, L., and Carra, S. (2017). Granulostasis: Protein Quality Control of RNP Granules. Front Mol Neurosci *10*, 84.

Anderson, M.S., Venanzi, E.S., Klein, L., Chen, Z., Berzins, S.P., Turley, S.J., von Boehmer, H., Bronson, R., Dierich, A., Benoist, C., *et al.* (2002). Projection of an immunological self shadow within the thymus by the aire protein. Science (New York, N.Y.) *298*, 1395-1401.

Anderson, P., Kedersha, N., and Ivanov, P. (2015). Stress granules, P-bodies and cancer. Biochim Biophys Acta *1849*, 861-870.

Andrieu, D., Watrin, F., Niinobe, M., Yoshikawa, K., Muscatelli, F., and Fernandez, P.A. (2003). Expression of the Prader-Willi gene Necdin during mouse nervous system development correlates with neuronal differentiation and p75NTR expression. Gene Expr Patterns *3*, 761-765.

Arimoto, K., Fukuda, H., Imajoh-Ohmi, S., Saito, H., and Takekawa, M. (2008). Formation of stress granules inhibits apoptosis by suppressing stress-responsive MAPK pathways. Nat Cell Biol *10*, 1324-1332.

Askew, E.B., Bai, S., Blackwelder, A.J., and Wilson, E.M. (2010). Transcriptional synergy between melanoma antigen gene protein-A11 (MAGE-11) and p300 in androgen receptor signaling. The Journal of biological chemistry *285*, 21824-21836.

Askew, E.B., Bai, S., Hnat, A.T., Minges, J.T., and Wilson, E.M. (2009). Melanoma antigen gene protein-A11 (MAGE-11) F-box links the androgen receptor NH2-terminal transactivation domain to p160 coactivators. The Journal of biological chemistry *284*, 34793-34808.

Atanackovic, D., Altorki, N.K., Stockert, E., Williamson, B., Jungbluth, A.A., Ritter, E., Santiago, D., Ferrara, C.A., Matsuo, M., Selvakumar, A., *et al.* (2004). Vaccine-induced CD4+ T cell responses to MAGE-3 protein in lung cancer patients. J Immunol *172*, 3289-3296.

Atanackovic, D., Hildebrandt, Y., Jadczak, A., Cao, Y., Luetkens, T., Meyer, S., Kobold, S., Bartels, K., Pabst, C., Lajmi, N., *et al.* (2010). Cancer-testis antigens MAGE-C1/CT7 and MAGE-A3 promote the survival of multiple myeloma cells. Haematologica *95*, 785-793.

Ayyoub, M., Scarlata, C.M., Hamai, A., Pignon, P., and Valmori, D. (2014). Expression of MAGE-A3/6 in primary breast cancer is associated with hormone receptor negative status, high histologic grade, and poor survival. J Immunother *37*, 73-76.

Bai, S., He, B., and Wilson, E.M. (2005). Melanoma antigen gene protein MAGE-11 regulates androgen receptor function by modulating the interdomain interaction. Mol Cell Biol *25*, 1238-1257.

Bai, S., and Wilson, E.M. (2008). Epidermal-growth-factor-dependent phosphorylation and ubiquitinylation of MAGE-11 regulates its interaction with the androgen receptor. Mol Cell Biol *28*, 1947-1963.

Balafoutas, D., zur Hausen, A., Mayer, S., Hirschfeld, M., Jaeger, M., Denschlag, D., Gitsch, G., Jungbluth, A., and Stickeler, E. (2013). Cancer testis antigens and NY-BR-1 expression in primary breast cancer: prognostic and therapeutic implications. BMC cancer *13*, 271.

Ballestar, E., Esteller, M., and Richardson, B.C. (2006). The epigenetic face of systemic lupus erythematosus. J Immunol *176*, 7143-7147.

Banani, S.F., Rice, A.M., Peeples, W.B., Lin, Y., Jain, S., Parker, R., and Rosen, M.K. (2016). Compositional Control of Phase-Separated Cellular Bodies. Cell *166*, 651-663.

Bao, L., Dunham, K., and Lucas, K. (2011). MAGE-A1, MAGE-A3, and NY-ESO-1 can be upregulated on neuroblastoma cells to facilitate cytotoxic T lymphocyte-mediated tumor cell killing. Cancer Immunol Immunother *60*, 1299-1307.

Barker, P.A., and Salehi, A. (2002). The MAGE proteins: emerging roles in cell cycle progression, apoptosis, and neurogenetic disease. Journal of neuroscience research *67*, 705-712.

Barnea, E., Beer, I., Patoka, R., Ziv, T., Kessler, O., Tzehoval, E., Eisenbach, L., Zavazava, N., and Admon, A. (2002). Analysis of endogenous peptides bound by soluble MHC class I molecules: a novel approach for identifying tumor-specific antigens. Eur J Immunol *32*, 213-222.

Barrow, C., Browning, J., MacGregor, D., Davis, I.D., Sturrock, S., Jungbluth, A.A., and Cebon, J. (2006). Tumor antigen expression in melanoma varies according to antigen and stage. Clinical cancer research : an official journal of the American Association for Cancer Research *12*, 764-771.

Bart, J., Groen, H.J., van der Graaf, W.T., Hollema, H., Hendrikse, N.H., Vaalburg, W., Sleijfer, D.T., and de Vries, E.G. (2002). An oncological view on the blood-testis barrier. Lancet Oncol *3*, 357-363.

Becker, J.C., Gillitzer, R., and Brocker, E.B. (1994). A member of the melanoma antigen-encoding gene (MAGE) family is expressed in human skin during wound healing. Int J Cancer *58*, 346-348.

Bertrand, M., Huijbers, I., Chomez, P., and De Backer, O. (2004). Comparative expression analysis of the MAGED genes during embryogenesis and brain development. Dev Dyn *230*, 325-334.

Bhatia, N., Yang, B., Xiao, T.Z., Peters, N., Hoffmann, M.F., and Longley, B.J. (2011). Identification of novel small molecules that inhibit protein-protein interactions between MAGE and KAP-1. Arch Biochem Biophys *508*, 217-221.

Bischof, J.M., Stewart, C.L., and Wevrick, R. (2007). Inactivation of the mouse Magel2 gene results in growth abnormalities similar to Prader-Willi syndrome. Hum Mol Genet *16*, 2713-2719.

Bonifacino, J.S. (2001). Metabolic labeling with amino acids. Curr Protoc Protein Sci *Chapter 3*, Unit 3 7.

Borden, K.L. (2000). RING domains: master builders of molecular scaffolds? Journal of molecular biology *295*, 1103-1112.

Brasseur, F., Rimoldi, D., Liénard, D., Lethé, B., Carrel, S., Arienti, F., Suter, L., Vanwijck, R., Bourlond, A., and Humblet, Y. (1995). Expression of MAGE genes in primary and metastatic cutaneous melanoma. International journal of cancer. Journal international du cancer *63*, 375-380.

Brichard, V.G., and Lejeune, D. (2007). GSK's antigen-specific cancer immunotherapy programme: pilot results leading to Phase III clinical development. Vaccine *25 Suppl 2*, B61-71.

Brinster, R.L., and Zimmermann, J.W. (1994). Spermatogenesis following male germ-cell transplantation. Proc Natl Acad Sci U S A *91*, 11298-11302.

Caballero, O.L., and Chen, Y.T. (2009). Cancer/testis (CT) antigens: potential targets for immunotherapy. Cancer Sci *100*, 2014-2021.

Camfferman, D., McEvoy, R.D., O'Donoghue, F., and Lushington, K. (2008). Prader Willi Syndrome and excessive daytime sleepiness. Sleep Med Rev *12*, 65-75.

Cassidy, S.B., Schwartz, S., Miller, J.L., and Driscoll, D.J. (2012). Prader-Willi syndrome. Genet Med *14*, 10-26.

Chan, F., Oatley, M.J., Kaucher, A.V., Yang, Q.E., Bieberich, C.J., Shashikant, C.S., and Oatley, J.M. (2014). Functional and molecular features of the Id4+ germline stem cell population in mouse testes. Genes Dev *28*, 1351-1362.

Chelly, J., and Mandel, J.L. (2001). Monogenic causes of X-linked mental retardation. Nat Rev Genet *2*, 669-680.

Chen, H.Z., Tsai, S.Y., and Leone, G. (2009). Emerging roles of E2Fs in cancer: an exit from cell cycle control. Nat Rev Cancer *9*, 785-797.

Chen, X., Wang, L., Liu, J., Huang, L., Yang, L., Gao, Q. ... Zhang, Y. (2017). Expression and prognostic relevance of MAGE-A3 and MAGE-C2 in non-small cell lung cancer. Oncology Letters *13*, 1609-1628.

Chi, P., Allis, C.D., and Wang, G.G. (2010). Covalent histone modifications--miswritten, misinterpreted and mis-erased in human cancers. Nat Rev Cancer *10*, 457-469.

Chibuk, T.K., Bischof, J.M., and Wevrick, R. (2001). A necdin/MAGE-like gene in the chromosome 15 autism susceptibility region: expression, imprinting, and mapping of the human and mouse orthologues. BMC Genet *2*, 22.

Chomez, P., De Backer, O., Bertrand, M., De Plaen, E., Boon, T., and Lucas, S. (2001). An overview of the MAGE gene family with the identification of all human members of the family. Cancer Res *61*, 5544-5551.

Chomez, P., Williams, R., De Backer, O., Boon, T., and Vennstrom, B. (1996). The SMAGE gene family is expressed in post-meiotic spermatids during mouse germ cell differentiation. Immunogenetics *43*, 97-100.

Clotman, F., De Backer, O., De Plaen, E., Boon, T., and Picard, J. (2000). Cell- and stage-specific expression of mage genes during mouse spermatogenesis. Mamm Genome *11*, 696-699.

Conteduca, G., Fenoglio, D., Parodi, A., Battaglia, F., Kalli, F., Negrini, S., Tardito, S., Ferrera, F., Salis, A., Millo, E., *et al.* (2016). AIRE polymorphism, melanoma antigen-specific T cell immunity, and susceptibility to melanoma. Oncotarget *7*, 60872-60884.

Cook, E.H., Jr., Lindgren, V., Leventhal, B.L., Courchesne, R., Lincoln, A., Shulman, C., Lord, C., and Courchesne, E. (1997). Autism or atypical autism in maternally but not paternally derived proximal 15q duplication. Am J Hum Genet *60*, 928-934.

Dabovic, B., Zanaria, E., Bardoni, B., Lisa, A., Bordignon, C., Russo, V., Matessi, C., Traversari, C., and Camerino, G. (1995). A family of rapidly evolving genes from the sex reversal critical region in Xp21. Mamm Genome *6*, 571-580.

Dardenne, E., Polay Espinoza, M., Fattet, L., Germann, S., Lambert, M.P., Neil, H., Zonta, E., Mortada, H., Gratadou, L., Deygas, M., *et al.* (2014). RNA helicases DDX5 and DDX17 dynamically orchestrate transcription, miRNA, and splicing programs in cell differentiation. Cell Rep *7*, 1900-1913.

Daudi, S., Eng, K.H., Mhawech-Fauceglia, P., Morrison, C., Miliotto, A., Beck, A., Matsuzaki, J., Tsuji, T., Groman, A., Gnjatic, S., *et al.* (2014). Expression and immune responses to MAGE antigens predict survival in epithelial ovarian cancer. PLoS One *9*, e104099.

De Backer, O., Verheyden, A.M., Martin, B., Godelaine, D., De Plaen, E., Brasseur, R., Avner, P., and Boon, T. (1995). Structure, chromosomal location, and expression pattern of three mouse genes homologous to the human MAGE genes. Genomics *28*, 74-83.

de Bot, S.T., Vermeer, S., Buijsman, W., Heister, A., Voorendt, M., Verrips, A., Scheffer, H., Kremer, H.P., van de Warrenburg, B.P., and Kamsteeg, E.J. (2013). Pure adult-onset spastic paraplegia caused by a novel mutation in the KIAA0196 (SPG8) gene. J Neurol *260*, 1765-1769.

De Plaen, E., Arden, K., Traversari, C., Gaforio, J.J., Szikora, J.P., De Smet, C., Brasseur, F., van der Bruggen, P., Lethe, B., Lurquin, C., *et al.* (1994). Structure, chromosomal localization, and expression of 12 genes of the MAGE family. Immunogenetics *40*, 360-369.

de Rooij, D.G. (2017). The nature and dynamics of spermatogonial stem cells. Development *144*, 3022-3030.

De Smet, C., Courtois, S.J., Faraoni, I., Lurquin, C., Szikora, J.P., De Backer, O., and Boon, T. (1995). Involvement of two Ets binding sites in the transcriptional activation of the MAGE1 gene. Immunogenetics *42*, 282-290.

De Smet, C., De Backer, O., Faraoni, I., Lurquin, C., Brasseur, F., and Boon, T. (1996). The activation of human gene MAGE-1 in tumor cells is correlated with genome-wide demethylation. Proceedings of the National Academy of Sciences of the United States of America *93*, 7149-7153.

de Smith, A.J., Purmann, C., Walters, R.G., Ellis, R.J., Holder, S.E., Van Haelst, M.M., Brady, A.F., Fairbrother, U.L., Dattani, M., Keogh, J.M., *et al.* (2009). A deletion of the HBII-85 class of small nucleolar RNAs (snoRNAs) is associated with hyperphagia, obesity and hypogonadism. Hum Mol Genet *18*, 3257-3265.

Derivery, E., Sousa, C., Gautier, J.J., Lombard, B., Loew, D., and Gautreau, A. (2009). The Arp2/3 activator WASH controls the fission of endosomes through a large multiprotein complex. Dev Cell *17*, 712-723.

Devos, J., Weselake, S.V., and Wevrick, R. (2011). Magel2, a Prader-Willi syndrome candidate gene, modulates the activities of circadian rhythm proteins in cultured cells. J Circadian Rhythms *9*, 12.

Dobra, I., Pankivskyi, S., Samsonova, A., Pastre, D., and Hamon, L. (2018). Relation Between Stress Granules and Cytoplasmic Protein Aggregates Linked to Neurodegenerative Diseases. Curr Neurol Neurosci Rep *18*, 107.

Dombret, C., Nguyen, T., Schakman, O., Michaud, J.L., Hardin-Pouzet, H., Bertrand, M.J., and De Backer, O. (2012). Loss of Maged1 results in obesity, deficits of social interactions, impaired sexual behavior and severe alteration of mature oxytocin production in the hypothalamus. Hum Mol Genet *21*, 4703-4717.

Donnelly, B.F., Needham, P.G., Snyder, A.C., Roy, A., Khadem, S., Brodsky, J.L., and Subramanya, A.R. (2013). Hsp70 and Hsp90 multichaperone complexes sequentially regulate thiazide-sensitive cotransporter endoplasmic reticulum-associated degradation and biogenesis. The Journal of biological chemistry *288*, 13124-13135.

Dorleijn, D.M., Cohen-Overbeek, T.E., Groenendaal, F., Bruinse, H.W., and Stoutenbeek, P. (2009). Idiopathic polyhydramnios and postnatal findings. J Matern Fetal Neonatal Med *22*, 315-320.

Doyle, J.M., Gao, J., Wang, J., Yang, M., and Potts, P.R. (2010). MAGE-RING protein complexes comprise a family of E3 ubiquitin ligases. Molecular cell *39*, 963-974.

Duker, A.L., Ballif, B.C., Bawle, E.V., Person, R.E., Mahadevan, S., Alliman, S., Thompson, R., Traylor, R., Bejjani, B.A., Shaffer, L.G., *et al.* (2010). Paternally inherited microdeletion at 15q11.2 confirms a significant role for the SNORD116 C/D box snoRNA cluster in Prader-Willi syndrome. Eur J Hum Genet *18*, 1196-1201.

Dykens, E.M., Lee, E., and Roof, E. (2011). Prader-Willi syndrome and autism spectrum disorders: an evolving story. J Neurodev Disord *3*, 225-237.

Feng, Y., Gao, J., and Yang, M. (2011). When MAGE meets RING: insights into biological functions of MAGE proteins. Protein Cell *2*, 7-12.

Figley, M.D., Bieri, G., Kolaitis, R.M., Taylor, J.P., and Gitler, A.D. (2014). Profilin 1 associates with stress granules and ALS-linked mutations alter stress granule dynamics. J Neurosci *34*, 8083-8097.

Filho, P.A., Lopez-Albaitero, A., Xi, L., Gooding, W., Godfrey, T., and Ferris, R.L. (2009). Quantitative expression and immunogenicity of MAGE-3 and -6 in upper aerodigestive tract cancer. Int J Cancer *125*, 1912-1920.

Finnish-German, A.C. (1997). An autoimmune disease, APECED, caused by mutations in a novel gene featuring two PHD-type zinc-finger domains. Nat Genet *17*, 399-403.

Fiszer, D., and Kurpisz, M. (1998). Major histocompatibility complex expression on human, male germ cells: a review. Am J Reprod Immunol *40*, 172-176.

Fleischhauer, K., Gattinoni, L., Dalerba, P., Lauvau, G., Zanaria, E., Dabovic, B., van Endert, P.M., Bordignon, C., and Traversari, C. (1998). The DAM gene family encodes a new group of tumor-specific antigens recognized by human leukocyte antigen A2-restricted cytotoxic T lymphocytes. Cancer Res *58*, 2969-2972.

Fon Tacer, K., Montoya, M.C., Oatley, M.J., Lord, T., Oatley, J.M., Klein, J., Ravichandran, R., Tillman, H., Kim, M., Connelly, J.P., *et al.* (2019). MAGE cancer-testis antigens protect the mammalian germline under environmental stress. Sci Adv *5*, eaav4832.

Fountain, M.D., Aten, E., Cho, M.T., Juusola, J., Walkiewicz, M.A., Ray, J.W., Xia, F., Yang, Y., Graham, B.H., Bacino, C.A., *et al.* (2016). The phenotypic spectrum of Schaaf-Yang syndrome: 18 new affected individuals from 14 families. Genet Med.

Fountain, M.D., Jr., and Schaaf, C.P. (2015). MAGEL2 and Oxytocin-Implications in Prader-Willi Syndrome and Beyond. Biol Psychiatry *78*, 78-80.

Gerard, M., Hernandez, L., Wevrick, R., and Stewart, C.L. (1999). Disruption of the mouse necdin gene results in early post-natal lethality. Nat Genet *23*, 199-202.

Gilbert, S.F. (2000). Developmental Biology. In Spermatogenesis (Sunderland MA, Sinauer Associates).

Gjerstorff, M.F., Harkness, L., Kassem, M., Frandsen, U., Nielsen, O., Lutterodt, M., Mollgard, K., and Ditzel, H.J. (2008). Distinct GAGE and MAGE-A expression during early human development indicate specific roles in lineage differentiation. Hum Reprod *23*, 2194-2201.

Gjerstorff, M.F., Kock, K., Nielsen, O., and Ditzel, H.J. (2007). MAGE-A1, GAGE and NY-ESO-1 cancer/testis antigen expression during human gonadal development. Hum Reprod *22*, 953-960.

Gomez, T.S., and Billadeau, D.D. (2009). A FAM21-containing WASH complex regulates retromer-dependent sorting. Dev Cell *17*, 699-711.

Grossberger, R., Gieffers, C., Zachariae, W., Podtelejnikov, A.V., Schleiffer, A., Nasmyth, K., Mann, M., and Peters, J.M. (1999). Characterization of the DOC1/APC10 subunit of the yeast and the human anaphase-promoting complex. The Journal of biological chemistry *274*, 14500-14507.

Gu, X., Fu, M., Ge, Z., Zhan, F., Ding, Y., Ni, H., Zhang, W., Zhu, Y., Tang, X., Xiong, L., *et al.* (2014). High expression of MAGE-A9 correlates with unfavorable survival in hepatocellular carcinoma. Sci Rep *4*, 6625.

Guerineau, M., Kriz, Z., Kozakova, L., Bednarova, K., Janos, P., and Palecek, J. (2012). Analysis of the Nse3/MAGE-binding domain of the Nse4/EID family proteins. PLoS One *7*, e35813.

Guo, J., Grow, E.J., Mlcochova, H., Maher, G.J., Lindskog, C., Nie, X., Guo, Y., Takei, Y., Yun, J., Cai, L., *et al.* (2018). The adult human testis transcriptional cell atlas. Cell Res *28*, 1141-1157.

Gure, A.O., Chua, R., Williamson, B., Gonen, M., Ferrera, C.A., Gnjatic, S., Ritter, G., Simpson, A.J., Chen, Y.T., Old, L.J., *et al.* (2005). Cancer-testis genes are coordinately expressed and are markers of poor outcome in non-small cell lung cancer. Clinical cancer research : an official journal of the American Association for Cancer Research *11*, 8055-8062.

Hackman, P., Sarparanta, J., Lehtinen, S., Vihola, A., Evila, A., Jonson, P.H., Luque, H., Kere, J., Screen, M., Chinnery, P.F., *et al.* (2013). Welander distal myopathy is caused by a mutation in the RNA-binding protein TIA1. Ann Neurol *73*, 500-509.

Hagiwara, Y., Sieverling, L., Hanif, F., Anton, J., Dickinson, E.R., Bui, T.T., Andreeva, A., Barran, P.E., Cota, E., and Nikolova, P.V. (2016). Consequences of point mutations in melanoma-associated antigen 4 (MAGE-A4) protein: Insights from structural and biophysical studies. Sci Rep *6*, 25182.

Han, L., Jiang, B., Wu, H., Zhang, S., and Lu, X. (2014). Expression and prognostic value of MAGE-A9 in laryngeal squamous cell carcinoma. Int J Clin Exp Pathol *7*, 6734-6742.

Hao, J., Song, X., Wang, J., Guo, C., Li, Y., Li, B., Zhang, Y., and Yin, Y. (2015a). Cancer-testis antigen MAGE-C2 binds Rbx1 and inhibits ubiquitin ligase-mediated turnover of cyclin E. Oncotarget *6*, 42028-42039.

Hao, Y.H., Doyle, J.M., Ramanathan, S., Gomez, T.S., Jia, D., Xu, M., Chen, Z.J., Billadeau, D.D., Rosen, M.K., and Potts, P.R. (2013). Regulation of WASH-dependent actin polymerization and protein trafficking by ubiquitination. Cell *152*, 1051-1064.

Hao, Y.H., Fountain, M.D., Jr., Fon Tacer, K., Xia, F., Bi, W., Kang, S.H., Patel, A., Rosenfeld, J.A., Le Caignec, C., Isidor, B., *et al.* (2015b). USP7 Acts as a Molecular Rheostat to Promote WASH-Dependent Endosomal Protein Recycling and Is Mutated in a Human Neurodevelopmental Disorder. Molecular cell *59*, 956-969.

Hardie, D.G., Ross, F.A., and Hawley, S.A. (2012). AMPK: a nutrient and energy sensor that maintains energy homeostasis. Nature reviews. Molecular cell biology *13*, 251-262.

Hartmann, S., Brisam, M., Rauthe, S., Driemel, O., Brands, R.C., Rosenwald, A., Kubler, A.C., and Muller-Richter, U.D. (2016). Contrary melanoma-associated antigen-A expression at the tumor front and center: A comparative analysis of stage I and IV head and neck squamous cell carcinoma. Oncol Lett *12*, 2942-2947.

Hayashi, Y., Matsuyama, K., Takagi, K., Sugiura, H., and Yoshikawa, K. (1995). Arrest of cell growth by necdin, a nuclear protein expressed in postmitotic neurons. Biochemical and biophysical research communications *213*, 317-324.

Hellings, J.A., and Warnock, J.K. (1994). Self-injurious behavior and serotonin in Prader-Willi syndrome. Psychopharmacol Bull *30*, 245-250.

Helsel, A.R., Oatley, M.J., and Oatley, J.M. (2017a). Glycolysis-Optimized Conditions Enhance Maintenance of Regenerative Integrity in Mouse Spermatogonial Stem Cells during Long-Term Culture. Stem Cell Reports *8*, 1430-1441.

Helsel, A.R., Yang, Q.E., Oatley, M.J., Lord, T., Sablitzky, F., and Oatley, J.M. (2017b). ID4 levels dictate the stem cell state in mouse spermatogonia. Development *144*, 624-634.

Hoch-Kraft, P., White, R., Tenzer, S., Kramer-Albers, E.M., Trotter, J., and Gonsior, C. (2018). Dual role of the RNA helicase DDX5 in post-transcriptional regulation of myelin basic protein in oligodendrocytes. J Cell Sci *131*.

Hofmann, O., Caballero, O.L., Stevenson, B.J., Chen, Y.T., Cohen, T., Chua, R., Maher, C.A., Panji, S., Schaefer, U., Kruger, A., *et al.* (2008). Genome-wide analysis of cancer/testis gene expression. Proceedings of the National Academy of Sciences of the United States of America *105*, 20422-20427.

Hoftman, A.D., Tai, L.Q., Tze, S., Seligson, D., Gatti, R.A., and McCurdy, D.K. (2008). MAGE-B2 autoantibody: a new biomarker for pediatric systemic lupus erythematosus. J Rheumatol *35*, 2430-2438.

Holm, V.A., Cassidy, S.B., Butler, M.G., Hanchett, J.M., Greenswag, L.R., Whitman, B.Y., and Greenberg, F. (1993). Prader-Willi syndrome: consensus diagnostic criteria. Pediatrics *91*, 398-402.

Hou, S., Sang, M., Zhao, L., Hou, R., and Shan, B. (2016a). The expression of MAGE-C1 and MAGE-C2 in breast cancer and their clinical significance. Am J Surg *211*, 142-151.

Hou, S., Xian, L., Shi, P., Li, C., Lin, Z., and Gao, X. (2016b). The Magea gene cluster regulates male germ cell apoptosis without affecting the fertility in mice. Sci Rep *6*, 26735.

Hudson, J.J., Bednarova, K., Kozakova, L., Liao, C., Guerineau, M., Colnaghi, R., Vidot, S., Marek, J., Bathula, S.R., Lehmann, A.R., *et al.* (2011). Interactions between the Nse3 and Nse4 components of the SMC5-6 complex identify evolutionarily conserved interactions between MAGE and EID Families. PLoS One *6*, e17270.

Jager, E., and Knuth, A. (2012). The discovery of cancer/testis antigens by autologous typing with T cell clones and the evolution of cancer vaccines. Cancer Immun *12*, 6.

Jain, S., Wheeler, J.R., Walters, R.W., Agrawal, A., Barsic, A., and Parker, R. (2016). ATPase-Modulated Stress Granules Contain a Diverse Proteome and Substructure. Cell *164*, 487-498.

Jang, S.J., Soria, J.C., Wang, L., Hassan, K.A., Morice, R.C., Walsh, G.L., Hong, W.K., and Mao, L. (2001). Activation of melanoma antigen tumor antigens occurs early in lung carcinogenesis. Cancer Res *61*, 7959-7963.

Jeck, N., Schlingmann, K.P., Reinalter, S.C., Komhoff, M., Peters, M., Waldegger, S., and Seyberth, H.W. (2005). Salt handling in the distal nephron: lessons learned from inherited human disorders. Am J Physiol Regul Integr Comp Physiol *288*, R782-795.

Jung, M., Wells, D., Rusch, J., Ahmad, S., Marchini, J., Myers, S.R., and Conrad, D.F. (2019). Unified single-cell analysis of testis gene regulation and pathology in five mouse strains. Elife *8*.

Jungbluth, A.A., Busam, K.J., Kolb, D., Iversen, K., Coplan, K., Chen, Y.T., Spagnoli, G.C., and Old, L.J. (2000). Expression of MAGE-antigens in normal tissues and cancer. Int J Cancer *85*, 460-465.

Jungbluth, A.A., Chen, Y.T., Busam, K.J., Coplan, K., Kolb, D., Iversen, K., Williamson, B., Van Landeghem, F.K., Stockert, E., and Old, L.J. (2002). CT7 (MAGE-C1) antigen expression in normal and neoplastic tissues. Int J Cancer *99*, 839-845.

Kalejs, M., and Erenpreisa, J. (2005). Cancer/testis antigens and gametogenesis: a review and "brain-storming" session. Cancer Cell Int *5*, 4.

Kamaludin, A.A., Smolarchuk, C., Bischof, J.M., Eggert, R., Greer, J.J., Ren, J., Lee, J.J., Yokota, T., Berry, F.B., and Wevrick, R. (2016). Muscle dysfunction caused by loss of Magel2 in a mouse model of Prader-Willi and Schaaf-Yang syndromes. Hum Mol Genet.

Kanber, D., Giltay, J., Wieczorek, D., Zogel, C., Hochstenbach, R., Caliebe, A., Kuechler, A., Horsthemke, B., and Buiting, K. (2009). A paternal deletion of MKRN3, MAGEL2 and NDN does not result in Prader-Willi syndrome. Eur J Hum Genet *17*, 582-590.

Karamysheva, Z.N., Tikhonova, E.B., Grozdanov, P.N., Huffman, J.C., Baca, K.R., Karamyshev, A., Denison, R.B., MacDonald, C.C., Zhang, K., and Karamyshev, A.L. (2018). Polysome Profiling in Leishmania, Human Cells and Mouse Testis. J Vis Exp.

Karpf, A.R., Bai, S., James, S.R., Mohler, J.L., and Wilson, E.M. (2009). Increased expression of androgen receptor coregulator MAGE-11 in prostate cancer by DNA hypomethylation and cyclic AMP. Mol Cancer Res *7*, 523-535.

Karpf, A.R., Lasek, A.W., Ririe, T.O., Hanks, A.N., Grossman, D., and Jones, D.A. (2004). Limited gene activation in tumor and normal epithelial cells treated with the DNA methyltransferase inhibitor 5-aza-2'-deoxycytidine. Mol Pharmacol *65*, 18-27.

Kato, M., Han, T.W., Xie, S., Shi, K., Du, X., Wu, L.C., Mirzaei, H., Goldsmith, E.J., Longgood, J., Pei, J., *et al.* (2012). Cell-free formation of RNA granules: low complexity sequence domains form dynamic fibers within hydrogels. Cell *149*, 753-767.

Katsura, Y., and Satta, Y. (2011). Evolutionary history of the cancer immunity antigen MAGE gene family. PLoS One *6*, e20365.

Kaushik, S., and Cuervo, A.M. (2018). The coming of age of chaperone-mediated autophagy. Nature reviews. Molecular cell biology *19*, 365-381.

Kedersha, N., and Anderson, P. (2002). Stress granules: sites of mRNA triage that regulate mRNA stability and translatability. Biochemical Society transactions *30*, 963-969.

Kedersha, N., Panas, M.D., Achorn, C.A., Lyons, S., Tisdale, S., Hickman, T., Thomas, M., Lieberman, J., McInerney, G.M., Ivanov, P., *et al.* (2016). G3BP-Caprin1-USP10 complexes mediate stress granule condensation and associate with 40S subunits. J Cell Biol *212*, 845-860.

Kent, L.N., and Leone, G. (2019). The broken cycle: E2F dysfunction in cancer. Nat Rev Cancer *19*, 326-338.

Khong, A., Matheny, T., Jain, S., Mitchell, S.F., Wheeler, J.R., and Parker, R. (2017). The Stress Granule Transcriptome Reveals Principles of mRNA Accumulation in Stress Granules. Molecular cell *68*, 808-820 e805.

Kim, H.J., Kim, N.C., Wang, Y.D., Scarborough, E.A., Moore, J., Diaz, Z., MacLea, K.S., Freibaum, B., Li, S., Molliex, A., *et al.* (2013). Mutations in prion-like domains in hnRNPA2B1 and hnRNPA1 cause multisystem proteinopathy and ALS. Nature *495*, 467-473.

Kondo, T., Zhu, X., Asa, S.L., and Ezzat, S. (2007). The cancer/testis antigen melanoma-associated antigen-A3/A6 is a novel target of fibroblast growth factor receptor 2-IIIb through histone H3 modifications in thyroid cancer. Clinical cancer research : an official journal of the American Association for Cancer Research *13*, 4713-4720.

Kozakova, L., Vondrova, L., Stejskal, K., Charalabous, P., Kolesar, P., Lehmann, A.R., Uldrijan, S., Sanderson, C.M., Zdrahal, Z., and Palecek, J.J. (2015). The melanoma-associated antigen 1 (MAGEA1) protein stimulates the E3 ubiquitin-ligase activity of TRIM31 within a TRIM31-MAGEA1-NSE4 complex. Cell Cycle *14*, 920-930.

Kozlov, S.V., Bogenpohl, J.W., Howell, M.P., Wevrick, R., Panda, S., Hogenesch, J.B., Muglia, L.J., Van Gelder, R.N., Herzog, E.D., and Stewart, C.L. (2007). The imprinted gene Magel2 regulates normal circadian output. Nat Genet *39*, 1266-1272.

Krausz, C., Giachini, C., Lo Giacco, D., Daguin, F., Chianese, C., Ars, E., Ruiz-Castane, E., Forti, G., and Rossi, E. (2012). High resolution X chromosome-specific array-CGH detects new CNVs in infertile males. PLoS One *7*, e44887.

Krishnadas, D.K., Shusterman, S., Bai, F., Diller, L., Sullivan, J.E., Cheerva, A.C., George, R.E., and Lucas, K.G. (2015). A phase I trial combining decitabine/dendritic cell vaccine targeting MAGE-A1, MAGE-A3 and NY-ESO-1 for children with relapsed or therapy-refractory neuroblastoma and sarcoma. Cancer Immunol Immunother *64*, 1251-1260.

Kruit, W.H., Suciu, S., Dreno, B., Mortier, L., Robert, C., Chiarion-Sileni, V., Maio, M., Testori, A., Dorval, T., Grob, J.J., *et al.* (2013). Selection of immunostimulant AS15 for active immunization with MAGE-A3 protein: results of a randomized phase II study of the European Organisation for Research and Treatment of Cancer Melanoma Group in Metastatic Melanoma. J Clin Oncol *31*, 2413-2420.

Kus-Liskiewicz, M., Polanska, J., Korfanty, J., Olbryt, M., Vydra, N., Toma, A., and Widlak, W. (2013). Impact of heat shock transcription factor 1 on global gene expression profiles in cells which induce either cytoprotective or pro-apoptotic response following hyperthermia. BMC Genomics *14*, 456.

Kuwako, K., Taniura, H., and Yoshikawa, K. (2004). Necdin-related MAGE proteins differentially interact with the E2F1 transcription factor and the p75 neurotrophin receptor. The Journal of biological chemistry *279*, 1703-1712.

Laghmani, K., Beck, B.B., Yang, S.S., Seaayfan, E., Wenzel, A., Reusch, B., Vitzthum, H., Priem, D., Demaretz, S., Bergmann, K., *et al.* (2016). Polyhydramnios, Transient Antenatal Bartter's Syndrome, and MAGED2 Mutations. N Engl J Med *374*, 1853-1863.

Landegren, N., Sharon, D., Freyhult, E., Hallgren, A., Eriksson, D., Edqvist, P.H., Bensing, S., Wahlberg, J., Nelson, L.M., Gustafsson, J., *et al.* (2016). Proteome-wide survey of the autoimmune target repertoire in autoimmune polyendocrine syndrome type 1. Sci Rep *6*, 20104.

Lee, A.K., and Potts, P.R. (2017). A Comprehensive Guide to the MAGE Family of Ubiquitin Ligases. J Mol Biol *429*, 1114-1142.

Lee, S., Kozlov, S., Hernandez, L., Chamberlain, S.J., Brannan, C.I., Stewart, C.L., and Wevrick, R. (2000). Expression and imprinting of MAGEL2 suggest a role in Prader-willi syndrome and the homologous murine imprinting phenotype. Hum Mol Genet *9*, 1813-1819.

Lee, Y.J., Wang, Q., and Rio, D.C. (2018). Coordinate regulation of alternative pre-mRNA splicing events by the human RNA chaperone proteins hnRNPA1 and DDX5. Genes Dev *32*, 1060-1074.

Li, B., Qian, X.P., Pang, X.W., Zou, W.Z., Wang, Y.P., Wu, H.Y., and Chen, W.F. (2003). HCA587 antigen expression in normal tissues and cancers: correlation with tumor differentiation in hepatocellular carcinoma. Lab Invest *83*, 1185-1192.

Linette, G.P., Stadtmauer, E.A., Maus, M.V., Rapoport, A.P., Levine, B.L., Emery, L., Litzky, L., Bagg, A., Carreno, B.M., Cimino, P.J., *et al.* (2013). Cardiovascular toxicity and titin cross-reactivity of affinity-enhanced T cells in myeloma and melanoma. Blood *122*, 863-871.

Lipkowitz, S., and Weissman, A.M. (2011). RINGs of good and evil: RING finger ubiquitin ligases at the crossroads of tumour suppression and oncogenesis. Nat Rev Cancer *11*, 629-643.

Liston, A., Lesage, S., Wilson, J., Peltonen, L., and Goodnow, C.C. (2003). Aire regulates negative selection of organ-specific T cells. Nat Immunol *4*, 350-354.

Liu, W., Cheng, S., Asa, S.L., and Ezzat, S. (2008). The melanoma-associated antigen A3 mediates fibronectin-controlled cancer progression and metastasis. Cancer Res *68*, 8104-8112.

Liu, Y., Zhu, M., Lin, L., Fan, X., Piao, Z., and Jiang, X. (2014). Deficiency of Trim27 protects dopaminergic neurons from apoptosis in the neurotoxin model of Parkinson's disease. Brain Res *1588*, 17-24.

Lopez-Sanchez, N., Gonzalez-Fernandez, Z., Niinobe, M., Yoshikawa, K., and Frade, J.M. (2007). Single mage gene in the chicken genome encodes CMage, a protein with functional similarities to mammalian type II Mage proteins. Physiological genomics *30*, 156-171.

Lorick, K.L., Jensen, J.P., Fang, S., Ong, A.M., Hatakeyama, S., and Weissman, A.M. (1999). RING fingers mediate ubiquitin-conjugating enzyme (E2)-dependent ubiquitination. Proceedings of the National Academy of Sciences of the United States of America *96*, 11364-11369.

Loriot, A., De Plaen, E., Boon, T., and De Smet, C. (2006). Transient down-regulation of DNMT1 methyltransferase leads to activation and stable hypomethylation of MAGE-A1 in melanoma cells. The Journal of biological chemistry *281*, 10118-10126.

Lucas, S., Brasseur, F., and Boon, T. (1999). A new MAGE gene with ubiquitous expression does not code for known MAGE antigens recognized by T cells. Cancer Res *59*, 4100-4103.

Lucas, S., De Plaen, E., and Boon, T. (2000). MAGE-B5, MAGE-B6, MAGE-C2, and MAGE-C3: four new members of the MAGE family with tumor-specific expression. Int J Cancer *87*, 55-60.

Lucas, S., De Smet, C., Arden, K.C., Viars, C.S., Lethe, B., Lurquin, C., and Boon, T. (1998). Identification of a new MAGE gene with tumor-specific expression by representational difference analysis. Cancer Res *58*, 743-752.

Lukassen, S., Bosch, E., Ekici, A.B., and Winterpacht, A. (2018). Single-cell RNA sequencing of adult mouse testes. Sci Data *5*, 180192.

Lurquin, C., De Smet, C., Brasseur, F., Muscatelli, F., Martelange, V., De Plaen, E., Brasseur, R., Monaco, A.P., and Boon, T. (1997). Two members of the human MAGEB gene family located in Xp21.3 are expressed in tumors of various histological origins. Genomics *46*, 397-408.

Mackenzie, I.R., Nicholson, A.M., Sarkar, M., Messing, J., Purice, M.D., Pottier, C., Annu, K., Baker, M., Perkerson, R.B., Kurti, A., *et al.* (2017). TIA1 Mutations in Amyotrophic Lateral Sclerosis and Frontotemporal Dementia Promote Phase Separation and Alter Stress Granule Dynamics. Neuron *95*, 808-816 e809.

Magann, E.F., Chauhan, S.P., Doherty, D.A., Lutgendorf, M.A., Magann, M.I., and Morrison, J.C. (2007). A review of idiopathic hydramnios and pregnancy outcomes. Obstet Gynecol Surv *62*, 795-802.

Marcar, L., Ihrig, B., Hourihan, J., Bray, S.E., Quinlan, P.R., Jordan, L.B., Thompson, A.M., Hupp, T.R., and Meek, D.W. (2015). MAGE-A Cancer/Testis Antigens Inhibit MDM2 Ubiquitylation Function and Promote Increased Levels of MDM4. PLoS One *10*, e0127713.

Marcar, L., Maclaine, N.J., Hupp, T.R., and Meek, D.W. (2010). Mage-A cancer/testis antigens inhibit p53 function by blocking its interaction with chromatin. Cancer Res *70*, 10362-10370.

Marchand, M., Punt, C.J., Aamdal, S., Escudier, B., Kruit, W.H., Keilholz, U., Hakansson, L., van Baren, N., Humblet, Y., Mulders, P., *et al.* (2003). Immunisation of metastatic cancer patients with MAGE-3 protein combined with adjuvant SBAS-2: a clinical report. Eur J Cancer *39*, 70-77.

Marchand, M., van Baren, N., Weynants, P., Brichard, V., Dreno, B., Tessier, M.H., Rankin, E., Parmiani, G., Arienti, F., Humblet, Y., *et al.* (1999). Tumor regressions observed in patients with metastatic melanoma treated with an antigenic peptide encoded by gene MAGE-3 and presented by HLA-A1. Int J Cancer *80*, 219-230.

Markmiller, S., Soltanieh, S., Server, K.L., Mak, R., Jin, W., Fang, M.Y., Luo, E.C., Krach, F., Yang, D., Sen, A., *et al.* (2018). Context-Dependent and Disease-Specific Diversity in Protein Interactions within Stress Granules. Cell *172*, 590-604 e513.

Martin, S., Zekri, L., Metz, A., Maurice, T., Chebli, K., Vignes, M., and Tazi, J. (2013). Deficiency of G3BP1, the stress granules assembly factor, results in abnormal synaptic plasticity and calcium homeostasis in neurons. J Neurochem *125*, 175-184.

Maruyama, K., Usami, M., Aizawa, T., and Yoshikawa, K. (1991). A novel brain-specific mRNA encoding nuclear protein (necdin) expressed in neurally differentiated embryonal carcinoma cells. Biochemical and biophysical research communications *178*, 291-296.

Matsumoto, K., Taniura, H., Uetsuki, T., and Yoshikawa, K. (2001). Necdin acts as a transcriptional repressor that interacts with multiple guanosine clusters. Gene *272*, 173-179.

McCurdy, D.K., Tai, L.Q., Imfeld, K.L., Schwartz, M., Zaldivar, F., and Berman, M.A. (2002). Expression of melanoma antigen gene by cells from inflamed joints in juvenile rheumatoid arthritis. J Rheumatol *29*, 2219-2224.

McCurdy, D.K., Tai, L.Q., Nguyen, J., Wang, Z., Yang, H.M., Udar, N., Naiem, F., Concannon, P., and Gatti, R.A. (1998). MAGE Xp-2: a member of the MAGE gene family isolated from an expression library using systemic lupus erythematosus sera. Mol Genet Metab *63*, 3-13.

Mejlachowicz, D., Nolent, F., Maluenda, J., Ranjatoelina-Randrianaivo, H., Giuliano, F., Gut, I., Sternberg, D., Laquerriere, A., and Melki, J. (2015). Truncating Mutations of MAGEL2, a Gene within the Prader-Willi Locus, Are Responsible for Severe Arthrogryposis. Am J Hum Genet *97*, 616-620.

Mercer, R.E., Kwolek, E.M., Bischof, J.M., van Eede, M., Henkelman, R.M., and Wevrick, R. (2009). Regionally reduced brain volume, altered serotonin neurochemistry, and abnormal behavior in mice null for the circadian rhythm output gene Magel2. Am J Med Genet B Neuropsychiatr Genet *150B*, 1085-1099.

Mercer, R.E., and Wevrick, R. (2009). Loss of magel2, a candidate gene for features of Prader-Willi syndrome, impairs reproductive function in mice. PLoS One *4*, e4291.

Mizukami, M., Hanagiri, T., Baba, T., Fukuyama, T., Nagata, Y., So, T., Ichiki, Y., Sugaya, M., Yasuda, M., Takenoyama, M., *et al.* (2005). Identification of tumor associated antigens recognized by IgG from tumor-infiltrating B cells of lung cancer: correlation between Ab titer of the patient's sera and the clinical course. Cancer Sci *96*, 882-888.

Mollgard, K., Jespersen, A., Lutterodt, M.C., Yding Andersen, C., Hoyer, P.E., and Byskov, A.G. (2010). Human primordial germ cells migrate along nerve fibers and Schwann

cells from the dorsal hind gut mesentery to the gonadal ridge. Mol Hum Reprod *16*, 621-631.

Molliex, A., Temirov, J., Lee, J., Coughlin, M., Kanagaraj, A.P., Kim, H.J., Mittag, T., and Taylor, J.P. (2015). Phase separation by low complexity domains promotes stress granule assembly and drives pathological fibrillization. Cell *163*, 123-133.

Monte, M., Simonatto, M., Peche, L.Y., Bublik, D.R., Gobessi, S., Pierotti, M.A., Rodolfo, M., and Schneider, C. (2006). MAGE-A tumor antigens target p53 transactivation function through histone deacetylase recruitment and confer resistance to chemotherapeutic agents. Proceedings of the National Academy of Sciences of the United States of America *103*, 11160-11165.

Morgan, R.A., Dudley, M.E., Wunderlich, J.R., Hughes, M.S., Yang, J.C., Sherry, R.M., Royal, R.E., Topalian, S.L., Kammula, U.S., Restifo, N.P., *et al.* (2006). Cancer regression in patients after transfer of genetically engineered lymphocytes. Science (New York, N.Y.) *314*, 126-129.

Mouri, A., Sasaki, A., Watanabe, K., Sogawa, C., Kitayama, S., Mamiya, T., Miyamoto, Y., Yamada, K., Noda, Y., and Nabeshima, T. (2012). MAGE-D1 regulates expression of depression-like behavior through serotonin transporter ubiquitylation. J Neurosci *32*, 4562-4580.

Muscatelli, F., Abrous, D.N., Massacrier, A., Boccaccio, I., Le Moal, M., Cau, P., and Cremer, H. (2000). Disruption of the mouse Necdin gene results in hypothalamic and behavioral alterations reminiscent of the human Prader-Willi syndrome. Hum Mol Genet *9*, 3101-3110.

Muscatelli, F., Walker, A.P., De Plaen, E., Stafford, A.N., and Monaco, A.P. (1995). Isolation and characterization of a MAGE gene family in the Xp21.3 region. Proceedings of the National Academy of Sciences of the United States of America *92*, 4987-4991.

Nagamine, K., Peterson, P., Scott, H.S., Kudoh, J., Minoshima, S., Heino, M., Krohn, K.J., Lalioti, M.D., Mullis, P.E., Antonarakis, S.E., *et al.* (1997). Positional cloning of the APECED gene. Nat Genet *17*, 393-398.

Nakamura, M., Okinaga, S., and Arai, K. (1984). Metabolism of round spermatids: evidence that lactate is preferred substrate. Am J Physiol *247*, E234-242.

Namkoong, S., Ho, A., Woo, Y.M., Kwak, H., and Lee, J.H. (2018). Systematic Characterization of Stress-Induced RNA Granulation. Mol Cell *70*, 175-187 e178.

Nedelsky, N.B., and Taylor, J.P. (2019). Bridging biophysics and neurology: aberrant phase transitions in neurodegenerative disease. Nat Rev Neurol *15*, 272-286.

Nestle, F.O., Alijagic, S., Gilliet, M., Sun, Y., Grabbe, S., Dummer, R., Burg, G., and Schadendorf, D. (1998). Vaccination of melanoma patients with peptide- or tumor lysate-pulsed dendritic cells. Nature medicine *4*, 328-332.

Newman, J.A., Cooper, C.D., Roos, A.K., Aitkenhead, H., Oppermann, U.C., Cho, H.J., Osman, R., and Gileadi, O. (2016). Structures of Two Melanoma-Associated Antigens Suggest Allosteric Regulation of Effector Binding. PLoS One *11*, e0148762.

Niinobe, M., Koyama, K., and Yoshikawa, K. (2000). Cellular and subcellular localization of necdin in fetal and adult mouse brain. Dev Neurosci *22*, 310-319.

Nishimura, I., Shimizu, S., Sakoda, J.Y., and Yoshikawa, K. (2007). Expression of Drosophila MAGE gene encoding a necdin homologous protein in postembryonic neurogenesis. Gene Expr Patterns *7*, 244-251.

Noh, S.T., Lee, H.S., Lim, S.J., Kim, S.W., Chang, H.K., Oh, J., Jeon, C.H., Park, J.W., and Lee, K.D. (2016). MAGE-A1-6 expression in patients with head and neck squamous cell carcinoma: impact on clinical patterns and oncologic outcomes. Int J Clin Oncol *21*, 875-882.

Novellino, L., Castelli, C., and Parmiani, G. (2005). A listing of human tumor antigens recognized by T cells: March 2004 update. Cancer Immunol Immunother *54*, 187-207.

Oatley, J.M., and Brinster, R.L. (2006). Spermatogonial stem cells. Methods Enzymol *419*, 259-282.

Oatley, M.J., Kaucher, A.V., Racicot, K.E., and Oatley, J.M. (2011). Inhibitor of DNA binding 4 is expressed selectively by single spermatogonia in the male germline and regulates the self-renewal of spermatogonial stem cells in mice. Biol Reprod *85*, 347-356.

Osterlund, C., Tohonen, V., Forslund, K.O., and Nordqvist, K. (2000). Mage-b4, a novel melanoma antigen (MAGE) gene specifically expressed during germ cell differentiation. Cancer Res *60*, 1054-1061.

Panda, A.C., Martindale, J.L., and Gorospe, M. (2016). Affinity Pulldown of Biotinylated RNA for Detection of Protein-RNA Complexes. Bio Protoc *6*.

Pastuszak, A.W.C., C.; Bekheirniac, M.; Lamb, D.J. (2015). Melanoma antigen protein MAGEC1 mutation identified in familial non-obstructive azoospermia In 71st Annual Meeting of the American Society for Reproductive Medicine, p. e80.

Patel, A., Lee, H.O., Jawerth, L., Maharana, S., Jahnel, M., Hein, M.Y., Stoynov, S., Mahamid, J., Saha, S., Franzmann, T.M., *et al.* (2015). A Liquid-to-Solid Phase

Transition of the ALS Protein FUS Accelerated by Disease Mutation. Cell *162*, 1066-1077.

Pattani, K.M., Soudry, E., Glazer, C.A., Ochs, M.F., Wang, H., Schussel, J., Sun, W., Hennessey, P., Mydlarz, W., Loyo, M., *et al.* (2012). MAGEB2 is activated by promoter demethylation in head and neck squamous cell carcinoma. PLoS One *7*, e45534.

Pebernard, S., Perry, J.J., Tainer, J.A., and Boddy, M.N. (2008). Nse1 RING-like domain supports functions of the Smc5-Smc6 holocomplex in genome stability. Mol Biol Cell *19*, 4099-4109.

Peche, L.Y., Ladelfa, M.F., Toledo, M.F., Mano, M., Laiseca, J.E., Schneider, C., and Monte, M. (2015). Human MageB2 Protein Expression Enhances E2F Transcriptional Activity, Cell Proliferation, and Resistance to Ribotoxic Stress. The Journal of biological chemistry *290*, 29652-29662.

Petroski, M.D., and Deshaies, R.J. (2005). Function and regulation of cullin-RING ubiquitin ligases. Nature reviews. Molecular cell biology *6*, 9-20.

Pineda, C.T., and Potts, P.R. (2015). Oncogenic MAGEA-TRIM28 ubiquitin ligase downregulates autophagy by ubiquitinating and degrading AMPK in cancer. Autophagy *11*, 844-846.

Pineda, C.T., Ramanathan, S., Fon Tacer, K., Weon, J.L., Potts, M.B., Ou, Y.H., White, M.A., and Potts, P.R. (2015). Degradation of AMPK by a cancer-specific ubiquitin ligase. Cell *160*, 715-728.

Potts, P.R. (2009). The Yin and Yang of the MMS21-SMC5/6 SUMO ligase complex in homologous recombination. DNA Repair (Amst) *8*, 499-506.

Potts, P.R., Porteus, M.H., and Yu, H. (2006). Human SMC5/6 complex promotes sister chromatid homologous recombination by recruiting the SMC1/3 cohesin complex to double-strand breaks. The EMBO journal *25*, 3377-3388.

Potts, P.R., and Yu, H. (2005). Human MMS21/NSE2 is a SUMO ligase required for DNA repair. Mol Cell Biol *25*, 7021-7032.

Potts, P.R., and Yu, H. (2007). The SMC5/6 complex maintains telomere length in ALT cancer cells through SUMOylation of telomere-binding proteins. Nat Struct Mol Biol *14*, 581-590.

Powers, C.J., McLeskey, S.W., and Wellstein, A. (2000). Fibroblast growth factors, their receptors and signaling. Endocr Relat Cancer *7*, 165-197.

Prader, A.L., A.; Willi, H. (1956). Ein Syndrom von Adipositas, Kleinwuchs, Kryptorchismus und Oligophrenie nach myatonieartigem Zustand im Neugeborenenalter. Schweiz Med Wochenschr *86*, 1260-1261.

Protter, D.S.W., and Parker, R. (2016). Principles and Properties of Stress Granules. Trends Cell Biol *26*, 668-679.

Puthenveedu, M.A., Lauffer, B., Temkin, P., Vistein, R., Carlton, P., Thorn, K., Taunton, J., Weiner, O.D., Parton, R.G., and von Zastrow, M. (2010). Sequence-dependent sorting of recycling proteins by actin-stabilized endosomal microdomains. Cell *143*, 761-773.

Raben, N., and Puertollano, R. (2016). TFEB and TFE3: Linking Lysosomes to Cellular Adaptation to Stress. Annu Rev Cell Dev Biol *32*, 255-278.

Ramaswami, M., Taylor, J.P., and Parker, R. (2013). Altered ribostasis: RNA-protein granules in degenerative disorders. Cell *154*, 727-736.

Reid, B.O., Mason, K.A., Withers, H.R., and West, J. (1981). Effects of hyperthermia and radiation on mouse testis stem cells. Cancer Res *41*, 4453-4457.

Reinalter, S., Devlieger, H., and Proesmans, W. (1998). Neonatal Bartter syndrome: spontaneous resolution of all signs and symptoms. Pediatr Nephrol *12*, 186-188.

Reineke, L.C., Dougherty, J.D., Pierre, P., and Lloyd, R.E. (2012). Large G3BP-induced granules trigger eIF2alpha phosphorylation. Mol Biol Cell *23*, 3499-3510.

Reineke, L.C., and Neilson, J.R. (2019). Differences between acute and chronic stress granules, and how these differences may impact function in human disease. Biochem Pharmacol *162*, 123-131.

Ren, J., Lee, S., Pagliardini, S., Gerard, M., Stewart, C.L., Greer, J.J., and Wevrick, R. (2003). Absence of Ndn, encoding the Prader-Willi syndrome-deleted gene necdin, results in congenital deficiency of central respiratory drive in neonatal mice. J Neurosci *23*, 1569-1573.

Reya, T., Morrison, S.J., Clarke, M.F., and Weissman, I.L. (2001). Stem cells, cancer, and cancer stem cells. Nature *414*, 105-111.

Richardson, B. (2003). DNA methylation and autoimmune disease. Clin Immunol *109*, 72-79.

Rockett, J.C., Mapp, F.L., Garges, J.B., Luft, J.C., Mori, C., and Dix, D.J. (2001). Effects of hyperthermia on spermatogenesis, apoptosis, gene expression, and fertility in adult male mice. Biol Reprod *65*, 229-239.

Rogner, U.C., Wilke, K., Steck, E., Korn, B., and Poustka, A. (1995). The melanoma antigen gene (MAGE) family is clustered in the chromosomal band Xq28. Genomics *29*, 725-731.

Ropers, F., Derivery, E., Hu, H., Garshasbi, M., Karbasiyan, M., Herold, M., Nurnberg, G., Ullmann, R., Gautreau, A., Sperling, K., *et al.* (2011). Identification of a novel candidate gene for non-syndromic autosomal recessive intellectual disability: the WASH complex member SWIP. Hum Mol Genet *20*, 2585-2590.

Ross, M.T., Grafham, D.V., Coffey, A.J., Scherer, S., McLay, K., Muzny, D., Platzer, M., Howell, G.R., Burrows, C., Bird, C.P., *et al.* (2005). The DNA sequence of the human X chromosome. Nature *434*, 325-337.

Sahoo, T., del Gaudio, D., German, J.R., Shinawi, M., Peters, S.U., Person, R.E., Garnica, A., Cheung, S.W., and Beaudet, A.L. (2008). Prader-Willi phenotype caused by paternal deficiency for the HBII-85 C/D box small nucleolar RNA cluster. Nat Genet *40*, 719-721.

Saiag, P., Gutzmer, R., Ascierto, P.A., Maio, M., Grob, J.J., Murawa, P., Dreno, B., Ross, M., Weber, J., Hauschild, A., *et al.* (2016). Prospective assessment of a gene signature potentially predictive of clinical benefit in metastatic melanoma patients following MAGE-A3 immunotherapeutic (PREDICT). Ann Oncol *27*, 1947-1953.

Sang, M., Gu, L., Liu, F., Lian, Y., Yin, D., Fan, X., Ding, C., Huang, W., Liu, S., and Shan, B. (2016). Prognostic Significance of MAGE-A11 in Esophageal Squamous Cell Carcinoma and Identification of Related Genes Based on DNA Microarray. Archives of medical research *47*, 151-161.

Sasaki, A., Masuda, Y., Iwai, K., Ikeda, K., and Watanabe, K. (2002). A RING finger protein Praja1 regulates Dlx5-dependent transcription through its ubiquitin ligase activity for the Dlx/Msx-interacting MAGE/Necdin family protein, Dlxin-1. The Journal of biological chemistry *277*, 22541-22546.

Schaaf, C.P., Gonzalez-Garay, M.L., Xia, F., Potocki, L., Gripp, K.W., Zhang, B., Peters, B.A., McElwain, M.A., Drmanac, R., Beaudet, A.L., *et al.* (2013). Truncating mutations of MAGEL2 cause Prader-Willi phenotypes and autism. Nat Genet *45*, 1405-1408.

Schaller, F., Watrin, F., Sturny, R., Massacrier, A., Szepetowski, P., and Muscatelli, F. (2010). A single postnatal injection of oxytocin rescues the lethal feeding behaviour in mouse newborns deficient for the imprinted Magel2 gene. Hum Mol Genet *19*, 4895-4905.

Seaman, M.N., Gautreau, A., and Billadeau, D.D. (2013). Retromer-mediated endosomal protein sorting: all WASHed up! Trends Cell Biol *23*, 522-528.

Serrano, A., Garcia, A., Abril, E., Garrido, F., and Ruiz-Cabello, F. (1996). Methylated CpG points identified within MAGE-1 promoter are involved in gene repression. Int J Cancer *68*, 464-470.

Serrano, A., Tanzarella, S., Lionello, I., Mendez, R., Traversari, C., Ruiz-Cabello, F., and Garrido, F. (2001). Rexpression of HLA class I antigens and restoration of antigen-specific CTL response in melanoma cells following 5-aza-2'-deoxycytidine treatment. Int J Cancer *94*, 243-251.

Seyberth, H.W., Rascher, W., Schweer, H., Kuhl, P.G., Mehls, O., and Scharer, K. (1985). Congenital hypokalemia with hypercalciuria in preterm infants: a hyperprostaglandinuric tubular syndrome different from Bartter syndrome. J Pediatr *107*, 694-701.

Sharma, P., and Allison, J.P. (2015). The future of immune checkpoint therapy. Science (New York, N.Y.) *348*, 56-61.

Sigalotti, L., Altomonte, M., Colizzi, F., Degan, M., Rupolo, M., Zagonel, V., Pinto, A., Gattei, V., and Maio, M. (2003). 5-Aza-2'-deoxycytidine (decitabine) treatment of hematopoietic malignancies: a multimechanism therapeutic approach? Blood *101*, 4644-4646; discussion 4645-4646.

Sigalotti, L., Coral, S., Nardi, G., Spessotto, A., Cortini, E., Cattarossi, I., Colizzi, F., Altomonte, M., and Maio, M. (2002). Promoter methylation controls the expression of MAGE2, 3 and 4 genes in human cutaneous melanoma. J Immunother *25*, 16-26.

Sigalotti, L., Covre, A., Zabierowski, S., Himes, B., Colizzi, F., Natali, P.G., Herlyn, M., and Maio, M. (2008). Cancer testis antigens in human melanoma stem cells: expression, distribution, and methylation status. J Cell Physiol *215*, 287-291.

Smith, I.M., Glazer, C.A., Mithani, S.K., Ochs, M.F., Sun, W., Bhan, S., Vostrov, A., Abdullaev, Z., Lobanenkov, V., Gray, A., *et al.* (2009). Coordinated activation of candidate proto-oncogenes and cancer testes antigens via promoter demethylation in head and neck cancer and lung cancer. PLoS One *4*, e4961.

Sohni, A., Tan, K., Song, H.W., Burow, D., de Rooij, D.G., Laurent, L., Hsieh, T.C., Rabah, R., Hammoud, S.S., Vicini, E., *et al.* (2019). The Neonatal and Adult Human Testis Defined at the Single-Cell Level. Cell Rep *26*, 1501-1517 e1504.

Sonenberg, N., and Hinnebusch, A.G. (2009). Regulation of translation initiation in eukaryotes: mechanisms and biological targets. Cell *136*, 731-745.

Song, X., Hao, J., Wang, J., Guo, C., Wang, Y., He, Q., Tang, H., Qin, X., Li, Y., Zhang, Y., *et al.* (2016). The cancer/testis antigen MAGEC2 promotes amoeboid invasion of tumor cells by enhancing STAT3 signaling. Oncogene.

Souquere, S., Mollet, S., Kress, M., Dautry, F., Pierron, G., and Weil, D. (2009). Unravelling the ultrastructure of stress granules and associated P-bodies in human cells. J Cell Sci *122*, 3619-3626.

St Pourcain, B., Whitehouse, A.J., Ang, W.Q., Warrington, N.M., Glessner, J.T., Wang, K., Timpson, N.J., Evans, D.M., Kemp, J.P., Ring, S.M., *et al.* (2013). Common variation contributes to the genetic architecture of social communication traits. Mol Autism *4*, 34.

Studier, F.W. (2014). Stable expression clones and auto-induction for protein production in E. coli. Methods Mol Biol *1091*, 17-32.

Su, S., Chen, X., Geng, J., Minges, J.T., Grossman, G., and Wilson, E.M. (2017). Melanoma antigen-A11 regulates substrate-specificity of Skp2-mediated protein degradation. Mol Cell Endocrinol *439*, 1-9.

Su, S., Minges, J.T., Grossman, G., Blackwelder, A.J., Mohler, J.L., and Wilson, E.M. (2013). Proto-oncogene activity of melanoma antigen-A11 (MAGE-A11) regulates retinoblastoma-related p107 and E2F1 proteins. The Journal of biological chemistry *288*, 24809-24824.

Suyama, T., Ohashi, H., Nagai, H., Hatano, S., Asano, H., Murate, T., Saito, H., and Kinoshita, T. (2002). The MAGE-A1 gene expression is not determined solely by methylation status of the promoter region in hematological malignancies. Leuk Res *26*, 1113-1118.

Tachibana, M., Sugimoto, K., Nozaki, M., Ueda, J., Ohta, T., Ohki, M., Fukuda, M., Takeda, N., Niida, H., Kato, H., *et al.* (2002). G9a histone methyltransferase plays a dominant role in euchromatic histone H3 lysine 9 methylation and is essential for early embryogenesis. Genes Dev *16*, 1779-1791.

Tajima, K., Obata, Y., Tamaki, H., Yoshida, M., Chen, Y.T., Scanlan, M.J., Old, L.J., Kuwano, H., Takahashi, T., Takahashi, T., *et al.* (2003). Expression of cancer/testis (CT) antigens in lung cancer. Lung Cancer *42*, 23-33.

Takahashi, K., Shichijo, S., Noguchi, M., Hirohata, M., and Itoh, K. (1995). Identification of MAGE-1 and MAGE-4 proteins in spermatogonia and primary spermatocytes of testis. Cancer Res *55*, 3478-3482.

Taniura, H., Taniguchi, N., Hara, M., and Yoshikawa, K. (1998). Necdin, a postmitotic neuron-specific growth suppressor, interacts with viral transforming proteins and cellular transcription factor E2F1. The Journal of biological chemistry *273*, 720-728.

Taylor, E.M., Copsey, A.C., Hudson, J.J., Vidot, S., and Lehmann, A.R. (2008). Identification of the proteins, including MAGEG1, that make up the human SMC5-6 protein complex. Mol Cell Biol *28*, 1197-1206.

Teuber, J., Mueller, B., Fukabori, R., Lang, D., Albrecht, A., and Stork, O. (2013). The ubiquitin ligase Praja1 reduces NRAGE expression and inhibits neuronal differentiation of PC12 cells. PLoS One *8*, e63067.

Thurner, B., Haendle, I., Roder, C., Dieckmann, D., Keikavoussi, P., Jonuleit, H., Bender, A., Maczek, C., Schreiner, D., von den Driesch, P., *et al.* (1999). Vaccination with mage-3A1 peptide-pulsed mature, monocyte-derived dendritic cells expands specific cytotoxic T cells and induces regression of some metastases in advanced stage IV melanoma. J Exp Med *190*, 1669-1678.

Timp, W., and Feinberg, A.P. (2013). Cancer as a dysregulated epigenome allowing cellular growth advantage at the expense of the host. Nat Rev Cancer *13*, 497-510.

Trendel, J., Schwarzl, T., Horos, R., Prakash, A., Bateman, A., Hentze, M.W., and Krijgsveld, J. (2019). The Human RNA-Binding Proteome and Its Dynamics during Translational Arrest. Cell *176*, 391-403 e319.

Tyagi, P., and Mirakhur, B. (2009). MAGRIT: the largest-ever phase III lung cancer trial aims to establish a novel tumor-specific approach to therapy. Clin Lung Cancer *10*, 371-374.

Valdmanis, P.N., Meijer, I.A., Reynolds, A., Lei, A., MacLeod, P., Schlesinger, D., Zatz, M., Reid, E., Dion, P.A., Drapeau, P., *et al.* (2007). Mutations in the KIAA0196 gene at the SPG8 locus cause hereditary spastic paraplegia. Am J Hum Genet *80*, 152-161.

van der Bruggen, P., Traversari, C., Chomez, P., Lurquin, C., De Plaen, E., Van den Eynde, B., Knuth, A., and Boon, T. (1991). A gene encoding an antigen recognized by cytolytic T lymphocytes on a human melanoma. Science (New York, N.Y.) *254*, 1643-1647.

van der Crabben, S.N., Hennus, M.P., McGregor, G.A., Ritter, D.I., Nagamani, S.C., Wells, O.S., Harakalova, M., Chinn, I.K., Alt, A., Vondrova, L., *et al.* (2016). Destabilized SMC5/6 complex leads to chromosome breakage syndrome with severe lung disease. J Clin Invest *126*, 2881-2892.

Van Treeck, B., and Parker, R. (2018). Emerging Roles for Intermolecular RNA-RNA Interactions in RNP Assemblies. Cell *174*, 791-802.

Vansteenkiste, J., Zielinski, M., Linder, A., Dahabreh, J., Gonzalez, E.E., Malinowski, W., Lopez-Brea, M., Vanakesa, T., Jassem, J., Kalofonos, H., *et al.* (2013). Adjuvant MAGE-A3 immunotherapy in resected non-small-cell lung cancer: phase II randomized study results. J Clin Oncol *31*, 2396-2403.

Vansteenkiste, J.F., Cho, B.C., Vanakesa, T., De Pas, T., Zielinski, M., Kim, M.S., Jassem, J., Yoshimura, M., Dahabreh, J., Nakayama, H., *et al.* (2016). Efficacy of the MAGE-A3 cancer immunotherapeutic as adjuvant therapy in patients with resected MAGE-

A3-positive non-small-cell lung cancer (MAGRIT): a randomised, double-blind, placebo-controlled, phase 3 trial. Lancet Oncol *17*, 822-835.

Vardarajan, B.N., Bruesegem, S.Y., Harbour, M.E., Inzelberg, R., Friedland, R., St George-Hyslop, P., Seaman, M.N., and Farrer, L.A. (2012). Identification of Alzheimer disease-associated variants in genes that regulate retromer function. Neurobiol Aging *33*, 2231 e2215-2231 e2230.

Verhoeven, W.M., and Tuinier, S. (2006). Prader-Willi syndrome: atypical psychoses and motor dysfunctions. Int Rev Neurobiol *72*, 119-130.

Warburton, P.E., Giordano, J., Cheung, F., Gelfand, Y., and Benson, G. (2004). Inverted repeat structure of the human genome: the X-chromosome contains a preponderance of large, highly homologous inverted repeats that contain testes genes. Genome Res *14*, 1861-1869.

Warnock, J.K., and Kestenbaum, T. (1992). Pharmacologic treatment of severe skin-picking behaviors in Prader-Willi syndrome. Two case reports. Arch Dermatol *128*, 1623-1625.

Weber, J., Salgaller, M., Samid, D., Johnson, B., Herlyn, M., Lassam, N., Treisman, J., and Rosenberg, S.A. (1994). Expression of the MAGE-1 tumor antigen is up-regulated by the demethylating agent 5-aza-2'-deoxycytidine. Cancer Res *54*, 1766-1771.

Weon, J.L., and Potts, P.R. (2015). The MAGE protein family and cancer. Curr Opin Cell Biol *37*, 1-8.

Wheeler, J.R., Matheny, T., Jain, S., Abrisch, R., and Parker, R. (2016). Distinct stages in stress granule assembly and disassembly. Elife *5*.

Widlak, W., and Vydra, N. (2017). The Role of Heat Shock Factors in Mammalian Spermatogenesis. Adv Anat Embryol Cell Biol *222*, 45-65.

Wienand, K., and Shires, K. (2015). The use of MAGE C1 and flow cytometry to determine the malignant cell type in multiple myeloma. PLoS One *10*, e0120734.

Wilkinson, L.S., Davies, W., and Isles, A.R. (2007). Genomic imprinting effects on brain development and function. Nat Rev Neurosci *8*, 832-843.

Wilson, E.M. (2010). Androgen receptor molecular biology and potential targets in prostate cancer. Ther Adv Urol *2*, 105-117.

Wischnewski, F., Pantel, K., and Schwarzenbach, H. (2006). Promoter demethylation and histone acetylation mediate gene expression of MAGE-A1, -A2, -A3, and -A12 in human cancer cells. Mol Cancer Res *4*, 339-349.

Wu, J., Wang, J., and Shen, W. (2017). Identification of MAGEA12 as a prognostic outlier gene in gastric cancers. Neoplasma *64*.

Xia, B., Yan, Y., Baron, M., Wagner, F., Barkley, D., Chiodin, M., Kim, S.Y., Keefe, D.L., Alukal, J.P., Boeke, J.D., *et al.* (2020). Widespread Transcriptional Scanning in the Testis Modulates Gene Evolution Rates. Cell *180*, 248-262 e221.

Xiao, T.Z., Bhatia, N., Urrutia, R., Lomberk, G.A., Simpson, A., and Longley, B.J. (2011). MAGE I transcription factors regulate KAP1 and KRAB domain zinc finger transcription factor mediated gene repression. PLoS One *6*, e23747.

Xiao, T.Z., Suh, Y., and Longley, B.J. (2014). MAGE proteins regulate KRAB zinc finger transcription factors and KAP1 E3 ligase activity. Arch Biochem Biophys *563*, 136-144.

Xu, X., Tang, X., Lu, M., Tang, Q., Zhang, H., Zhu, H., Xu, N., Zhang, D., Xiong, L., Mao, Y., *et al.* (2014). Overexpression of MAGE-A9 predicts unfavorable outcome in breast cancer. Exp Mol Pathol *97*, 579-584.

Xu, Y., Wang, C., Zhang, Y., Jia, L., and Huang, J. (2015). Overexpression of MAGE-A9 Is Predictive of Poor Prognosis in Epithelial Ovarian Cancer. Sci Rep *5*, 12104.

Yamada, R., Takahashi, A., Torigoe, T., Morita, R., Tamura, Y., Tsukahara, T., Kanaseki, T., Kubo, T., Watarai, K., Kondo, T., *et al.* (2013). Preferential expression of cancer/testis genes in cancer stem-like cells: proposal of a novel sub-category, cancer/testis/stem gene. Tissue Antigens *81*, 428-434.

Yang, B., O'Herrin, S., Wu, J., Reagan-Shaw, S., Ma, Y., Nihal, M., and Longley, B.J. (2007a). Select cancer testes antigens of the MAGE-A, -B, and -C families are expressed in mast cell lines and promote cell viability in vitro and in vivo. J Invest Dermatol *127*, 267-275.

Yang, B., O'Herrin, S.M., Wu, J., Reagan-Shaw, S., Ma, Y., Bhat, K.M., Gravekamp, C., Setaluri, V., Peters, N., Hoffmann, F.M., *et al.* (2007b). MAGE-A, mMage-b, and MAGE-C proteins form complexes with KAP1 and suppress p53-dependent apoptosis in MAGE-positive cell lines. Cancer research *67*, 9954-9962.

Yang, B., Wu, J., Maddodi, N., Ma, Y., Setaluri, V., and Longley, B.J. (2007c). Epigenetic control of MAGE gene expression by the KIT tyrosine kinase. J Invest Dermatol *127*, 2123-2128.

Yang, F., Zhou, X., Miao, X., Zhang, T., Hang, X., Tie, R., Liu, N., Tian, F., Wang, F., and Yuan, J. (2014). MAGEC2, an epithelial-mesenchymal transition inducer, is associated with breast cancer metastasis. Breast Cancer Res Treat *145*, 23-32.

Yang, Q.E., Gwost, I., Oatley, M.J., and Oatley, J.M. (2013). Retinoblastoma protein (RB1) controls fate determination in stem cells and progenitors of the mouse male germline. Biol Reprod *89*, 113.

Yao, J., Caballero, O.L., Yung, W.K., Weinstein, J.N., Riggins, G.J., Strausberg, R.L., and Zhao, Q. (2014). Tumor subtype-specific cancer-testis antigens as potential biomarkers and immunotherapeutic targets for cancers. Cancer Immunol Res *2*, 371-379.

Ye, Q., Shen, Y., Wang, X., Yang, J., Miao, F., Shen, C., and Zhang, J. (2010). Hypermethylation of HLA class I gene is associated with HLA class I down-regulation in human gastric cancer. Tissue Antigens *75*, 30-39.

Yin, B., Zeng, Y., Liu, G., Wang, X., Wang, P., and Song, Y. (2014). MAGE-A3 is highly expressed in a cancer stem cell-like side population of bladder cancer cells. Int J Clin Exp Pathol *7*, 2934-2941.

Yin, Y., Hawkins, K.L., DeWolf, W.C., and Morgentaler, A. (1997). Heat stress causes testicular germ cell apoptosis in adult mice. J Androl *18*, 159-165.

Yoon, J.H., and Gorospe, M. (2016). Cross-Linking Immunoprecipitation and qPCR (CLIP-qPCR) Analysis to Map Interactions Between Long Noncoding RNAs and RNA-Binding Proteins. Methods Mol Biol *1402*, 11-17.

Yu, H., Peters, J.M., King, R.W., Page, A.M., Hieter, P., and Kirschner, M.W. (1998). Identification of a cullin homology region in a subunit of the anaphase-promoting complex. Science (New York, N.Y.) *279*, 1219-1222.

Zachariae, W., Shevchenko, A., Andrews, P.D., Ciosk, R., Galova, M., Stark, M.J., Mann, M., and Nasmyth, K. (1998). Mass spectrometric analysis of the anaphase-promoting complex from yeast: identification of a subunit related to cullins. Science (New York, N.Y.) *279*, 1216-1219.

Zamuner, F.T., Karia, B.T., de Oliveira, C.Z., Santos, C.R., Carvalho, A.L., and Vettore, A.L. (2015). A Comprehensive Expression Analysis of Cancer Testis Antigens in Head and Neck Squamous Cell Carcinoma Revels MAGEA3/6 as a Marker for Recurrence. Mol Cancer Ther *14*, 828-834.

Zanella, S., Watrin, F., Mebarek, S., Marly, F., Roussel, M., Gire, C., Diene, G., Tauber, M., Muscatelli, F., and Hilaire, G. (2008). Necdin plays a role in the serotonergic modulation of the mouse respiratory network: implication for Prader-Willi syndrome. J Neurosci *28*, 1745-1755.

Zhan, W., Zhang, Z., Zhang, Y., Ma, J., Wu, T., Gu, Y., Li, Y., and Yang, J. (2016). Prognostic value of MAGE-A9 expression in patients with colorectal cancer. Clinics and research in hepatology and gastroenterology *40*, 239-245.

Zhang, K., Daigle, J.G., Cunningham, K.M., Coyne, A.N., Ruan, K., Grima, J.C., Bowen, K.E., Wadhwa, H., Yang, P., Rigo, F., *et al.* (2018). Stress Granule Assembly Disrupts Nucleocytoplasmic Transport. Cell *173*, 958-971 e917.

Zhang, P., Fan, B., Yang, P., Temirov, J., Messing, J., Kim, H.J., and Taylor, J.P. (2019). Chronic optogenetic induction of stress granules is cytotoxic and reveals the evolution of ALS-FTD pathology. Elife *8*.

Zhang, S., Zhai, X., Wang, G., Feng, J., Zhu, H., Xu, L., Mao, G., and Huang, J. (2015). High expression of MAGE-A9 in tumor and stromal cells of non-small cell lung cancer was correlated with patient poor survival. Int J Clin Exp Pathol *8*, 541-550.

Zhao, Q., Caballero, O.L., Simpson, A.J., and Strausberg, R.L. (2012). Differential evolution of MAGE genes based on expression pattern and selection pressure. PLoS One *7*, e48240.

Zheng, N., Schulman, B.A., Song, L., Miller, J.J., Jeffrey, P.D., Wang, P., Chu, C., Koepp, D.M., Elledge, S.J., Pagano, M., *et al.* (2002). Structure of the Cul1-Rbx1-Skp1-F boxSkp2 SCF ubiquitin ligase complex. Nature *416*, 703-709.

Zhou, Z., Kawabe, H., Suzuki, A., Shinmyozu, K., and Saga, Y. (2017). NEDD4 controls spermatogonial stem cell homeostasis and stress response by regulating messenger ribonucleoprotein complexes. Nat Commun *8*, 15662.

Zhu, X., Asa, S.L., and Ezzat, S. (2008). Fibroblast growth factor 2 and estrogen control the balance of histone 3 modifications targeting MAGE-A3 in pituitary neoplasia. Clinical cancer research : an official journal of the American Association for Cancer Research *14*, 1984-1996.